

The Impact of Deafness:
Maturation of Synaptic and Biophysical Properties
in an Auditory Brainstem Nucleus

Inaugural-Dissertation

to obtain the academic degree

Doctor rerum naturalium (Dr. rer. nat.)

submitted to the Department of Biology, Chemistry and Pharmacy
of Freie Universität Berlin

by

Franziska Caspari

from Berlin, Germany

2018

Supervisor: Prof. Dr. Ursula Koch

Second expert appraiser. Dr. Daniela Vallentin

Date of the oral defense: January 31st 2019

Für Franz und Luise

1 Contents

1	Contents.....	7
2	Abstract	11
3	Zusammenfassung	13
4	Introduction	15
4.1	The outer ear.....	16
4.2	The middle ear.....	16
4.3	The inner ear.....	16
4.4	The central auditory pathway	19
4.5	Ventral nucleus of the lateral lemniscus.....	22
4.6	Large calyx-like synapses in the auditory brainstem.....	23
4.7	Development of intrinsic neuronal properties in the auditory brainstem	25
4.8	Synaptic development in the auditory brainstem	26
4.9	Biophysical background of electrophysiological measurements.....	27
4.9.1	Passive membrane properties	27
4.9.2	Active membrane properties.....	29
4.9.3	I_h – HCN-channel mediated current	30
4.9.4	AMPA and NMDA receptors	31
4.9.5	Presynaptic and postsynaptic properties.....	32
4.10	Deafness	36
4.11	Deaf mouse models and the impact of deafness on central auditory structures	36
4.11.1	Deafwaddler	36
4.11.2	DFN.....	37
4.11.2.1	dn/dn.....	37
4.11.2.2	DFNB9	38
4.12	Hypothesis.....	40
4.13	Aim of this study	40
4.14	Scientific relevance	41
5	Material and methods	43
5.1	Animals	43
5.2	Breeding	43
5.2.1	C57Bl/6	43
5.2.3	OTOF.....	44

5.3	Genotyping.....	45
5.4	Solutions	46
5.4	Brain Slice preparation	46
5.5	Patch-clamp electrophysiology and data acquisition	47
5.6	Data acquisition	48
5.7	Data analysis	49
5.7.1	Membrane properties	49
5.7.2	I_h measurements	50
5.7.3	Postsynaptic currents after single stimulations	50
5.7.4	Miniature EPSCs.....	50
5.7.5	Short-term plasticity.....	51
5.8	Statistics	52
5.9	Immunohistochemistry	52
5.10	Confocal microscopy	54
6	Results.....	55
6.1	Part 1 – Characterization of the VNLL.....	56
6.1.1	Intrinsic properties differ between neurons of the dorsal and the ventral parts of the VNLL	56
6.1.2	VNLL neurons have large hyperpolarization-activated currents (I_h) compared to ventral VNLL neurons	60
6.1.3	Lateral vVNLL neurons have extremely large excitatory postsynaptic currents... ..	60
6.1.4	Inhibitory postsynaptic currents are similar in all vVNLL neurons.....	64
6.1.5	Synaptic short-term plasticity of excitatory and inhibitory inputs is similar in vVNLL and dVNLL neurons	65
6.1.6	Neurons in the dorsal and ventral VNLL are all inhibitory	67
6.2	Part 2 – Development of the calyx-like synapse in the VNLL	69
6.2.1	NMDA-current components of vVNLL neurons undergo a significant reduction during development.....	69
6.2.2	Calyx-like excitatory inputs develop in the vVNLL around hearing onset in mice	72
6.3	Part 3 – The impact of deafness on the intrinsic and neuronal development in the VNLL.....	75
6.3.1	Spiking patterns of vVNLL neurons change to an exclusive onset-type firing late during development.....	75
6.3.2	Otoferlin WT mice undergo the same developmental reduction of excitatory synaptic inputs as found in C57Bl/6 animals.....	79
6.3.3	mEPSC become significantly briefer during development	81
6.3.4	Degree of short-term depression is reduced during development.....	83
6.3.5	VGluT1 is a consistent vesicular glutamate transporter in synapses innervating vVNLL neurons	86

6.3.6	Does congenital deafness affect the proper development of vVNLL neurons?	88
6.3.7	Deafness impairs the typical development of spiking patterns and intrinsic neuronal properties	88
6.3.8	Deafness impairs synaptic refinement	91
6.3.9	Hyperactivity of vVNLL synapses in deaf mice	93
6.3.10	Depletion of the readily releasable pool remains unaffected in vVNLL synapses of deaf mice	95
6.3.11	VGluT1 and calretinin distribution is similar in deaf and hearing mice	97
7	Discussion	99
7.1	Characterization of the VNLL	99
7.1.1	The ventral part of the VNLL contains a cluster of neurons with calyx-like synaptic inputs	100
7.1.2	Neurons in the dorsal part of the VNLL have two different firing patterns and large I_h	101
7.1.3	Dorsal and ventral VNLL neurons are inhibitory	102
7.1.4	Functional heterogeneity of VNLL neurons for sound processing	102
7.2	Development of neuronal and synaptic features in the ventrolateral VNLL	104
7.2.1	Neurons of the vVNLL become more homogeneous during development	105
7.2.2	Low-voltage-activated potassium channels might trigger fast and precise onset firing	106
7.2.3	Synaptic refinement of calyx-like inputs in the vVNLL occurs much later around hearing onset than of the calyces of Held in the MNTB	108
7.2.4	Strain-specific synaptic refinement of excitatory inputs to the vVNLL	109
7.2.5	Downregulation of NMDA receptor-mediated currents is accompanied by postsynaptic AMPA receptor acceleration	110
7.2.6	Short-term depression is reduced in neurons of mature mice	113
7.2.7	Assumption I: Only presynaptic factors contribute to short-term depression	113
7.2.8	Assumption II: Both pre- and postsynaptic factors contribute to short-term depression	114
7.2.9	AMPA receptor subunit switch might be responsible for reduction of short-term depression	115
7.3	Deafness impairs the typical neuronal and synaptic development	116
7.3.1	Auditory-evoked activity is essential for a typical neuronal and synaptic development	117
7.3.2	Spontaneous activity is not involved in synaptic refinement of vVNLL synapses	118
7.3.3	Sound-evoked experience is necessary for determining firing patterns through ion channel modulation	120
7.4	Concluding remarks and outlook	121
8	References	123

9	Abbreviations	147
10	List of figures	149
11	List of tables.....	151
12	Publication	153
13	Acknowledgements.....	155
14	Declaration of originality.....	157
15	Curriculum vitæ	159

2 Abstract

The ventral nucleus of the lateral lemniscus (VNLL) is a monaural brainstem nucleus of the ascending auditory pathway that may play a critical role in the analysis of temporal sound patterns. Its underlying intrinsic and synaptic properties have not been systematically studied in a ventrodorsal orientation in mice.

Using *in vitro* electrophysiological recordings from acute brain slices of mice and immunohistochemistry, we aimed to discover the margins of the VNLL and the neuronal and synaptic characteristics of the neurons lying within. We demonstrate that the biophysical membrane properties and excitatory input characteristics differ between dorsal and ventral VNLL neurons. Neurons in the ventral VNLL displayed an onset-type firing pattern and little hyperpolarization-activated current (I_h), and, in the ventrolateral VNLL (vVNLL), received calyx-like inputs that were similar to calyx of Held synapses in the medial nucleus of the trapezoid body (MNTB). Neurons of the dorsal part received several and weak input fibers that were slower than in the vVNLL, while displaying either onset- or sustained-type firing patterns with large I_h . Using a mouse model that expresses channelrhodopsin under the promotor of the vesicular GABA transporter (VGAT) suggests that dorsal and ventral neurons are inhibitory, since they were all depolarized by light stimulation. The diverse membrane and input properties in dorsal and ventral VNLL neurons suggest differential roles of these neurons in sound processing.

Furthermore, we were interested in discovering when the excitatory calyx-like inputs in the vVNLL develop. Before hearing onset, neurons of the vVNLL received generally more than one excitatory input, which refined shortly after hearing onset. Additionally, NMDA receptor-mediated currents were almost completely reduced after hearing onset, resulting in fast and large postsynaptic current responses mediated by AMPA receptors. Next, we wanted to elucidate whether sound-evoked activity is essential for the observed synaptic refinement. Therefore, we used a congenitally deaf mouse that lacks otoferlin and compared it with young and mature hearing mice. Otoferlin is found in inner hair cells, among other places, and mediates exocytosis of neurotransmitters. We demonstrate that KO mice have an impaired firing behavior. While neurons displayed either an onset-type or sustained-type firing in KO and young WT animals, mature WT mice had only onset-firing neurons. Additionally, synaptic refinement was also altered and showed great similarities to young WT mice. Neurons of mature WT mice received on average one large calyx-like synapse, whereas neurons of KO and young WT mice received up to five excitatory inputs. Fiber stimulations of the inputs in KO mice evoked smaller and slower postsynaptic currents than in mature WT mice. However, establishment of the readily releasable pool was unaffected by deafness. Our results suggest that sensory experience is necessary for a typical maturation of biophysical properties and the calyx-like input to the vVNLL. Consequently, our results encourage the use of cochlear implants in patients with an otoferlin-related deafness, since it may be possible that the synaptic and biophysical impairment can be reduced by providing sound-evoked activity to the auditory brainstem.

3 Zusammenfassung

Der ventrale Nukleus des lateralen Lemniskus‘ (VNLL) ist ein monauraler Hirnstammkern der aufsteigenden auditorischen Hörbahn, welcher eine entscheidende Rolle bei der Analyse zeitlicher Schallmuster spielen könnte. Seine zugrundeliegenden intrinsischen und synaptischen Eigenschaften wurden bisher nicht systematisch in ventrodorsaler Orientierung untersucht.

Mittels elektrophysiologischer *in vitro* Untersuchungen an akuten Hirnschnitten von Mäusen und Immunhistochemie sollten die Grenzen des VNLL und seine neuronalen und synaptischen Eigenschaften untersucht werden. Wir zeigen, dass die biophysikalischen Membraneigenschaften und die exzitatorischen Eingangseigenschaften zwischen dorsalen und ventralen VNLL Neuronen unterschiedlich sind. Neurone im ventralen VNLL zeigten ein Feuermuster vom Onset-Typ (ein Aktionspotential zu Beginn), kleine hyperpolarisationsaktivierte Ströme (I_h) und, im ventrolateralen VNLL (vVNLL), Kalyx-ähnliche Eingänge, die den Kalyx von Held-Synapsen im medialen Nukleus des trapezoiden Körpers (engl. MNTB) ähnelten. Neurone des dorsalen Teils wurden von mehreren und schwächeren Eingängen innerviert, die langsamer als im vVNLL waren, und eines von zwei Feuermustern zeigten, ein Aktionspotential zu Beginn oder anhaltende Aktionspotentiale über die gesamte Dauer mit jeweils großem I_h . Die Verwendung eines Mausmodells, das Channelrhodopsin unter dem Promotor des vesikulären GABA-Transporters (VGAT) exprimiert, zeigte, dass dorsale und ventrale Neurone inhibitorisch sind, da sie alle durch Licht-Stimulation depolarisiert wurden. Die unterschiedlichen Membran- und Eingangseigenschaften in dorsalen und ventralen VNLL-Neuronen lassen unterschiedliche Rollen dieser Neurone für die Schallverarbeitung vermuten.

Darüber hinaus waren wir daran interessiert, wann sich die exzitatorischen Kalyx-ähnlichen Eingänge im vVNLL entwickeln. Vor Hörbeginn erhielten diese Neurone des vVNLL im Allgemeinen mehr als einen exzitatorischen Eingang, die kurz nach Hörbeginn reduziert wurden. Zusätzlich wurden die NMDA Rezeptor-vermittelten Ströme nach Hörbeginn fast vollständig reduziert, was zu schnellen und großen postsynaptischen Stromantworten führte, die durch AMPA Rezeptoren vermittelt wurden. Als nächstes wollten wir herausfinden, ob Hörerfahrung essentiell für die Reduktion synaptischer Eingänge ist. Dafür verwendeten wir eine kongenitale taube Maus, die einen Mangel an Otoferlin hat, und verglichen sie mit jungen und reifen hörenden Mäusen. Otoferlin wird u.a. in inneren Haarzellen gefunden und vermittelt die Exozytose von Neurotransmitter. Wir zeigen, dass KO Mäuse ein verändertes Feuerverhalten hatten. Während eine Strominjektion bei Neuronen von KO- und jungen WT-Tieren entweder ein oder mehrere Aktionspotentiale hervorriefen, hatten reife WT-Mäuse nur Neuronen, die zu Beginn ein Aktionspotential feuern. Zusätzlich wurde auch die synaptische Entwicklung verändert und zeigte große Ähnlichkeiten zu jungen WT Mäusen. Neurone von reifen WT-Mäusen erhielten durchschnittlich eine große Kalyx-ähnliche Synapse, während Neurone von KO- und jungen WT-Mäusen bis zu fünf exzitatorische Eingänge bekamen. Faserstimulationen dieser Eingänge riefen im Vergleich zu reifen WT-Mäusen kleinere und langsamere postsynaptische Ströme in KO-Mäusen hervor. Die Größe des readily releasable pool (sofort bereitgestelltes Reservoir an transmittergefüllten Vesikeln) wurde jedoch durch Taubheit nicht beeinflusst. Unsere Ergebnisse

weisen darauf, dass sensorische Erfahrung für eine typische Reifung biophysikalischer Eigenschaften und Entwicklung Kalyx-ähnlicher Eingänge im vVNLL notwendig ist. Folglich bestärken unsere Ergebnisse die Verwendung von Cochlea-Implantaten bei Patienten mit einer Otoferlin-bedingten Taubheit, da es möglich wäre, dass die synaptischen und biophysikalischen Beeinträchtigungen durch die Bereitstellung von akustisch evozierter Aktivität an den auditorischen Hirnstamm reduziert werden können.

4 Introduction

Hearing is the physiological ability to perceive and localize the origins of sounds for navigation, communication, finding food and avoiding predators (Schacter et al. 2011). Hence, through evolution, hearing has become immensely important for individuals to survive.

Most invertebrates, apart from arthropods (Schwartzkopff 1977) and cephalopods (Samson et al. 2016), live a mute life, whereas vertebrates usually have well-developed hearing. The first acoustic organs developed during the Devonian period 380 million years ago (Manley and Köppl 1998). Humans perceive sound frequencies from 20 Hz to 20 kHz (Moore 2012), whereas elephants are capable of perceiving infrasonics (Payne et al. 1986; Poole et al. 1988), and mice and bats, for example, can perceive ultrasonics (Griffin and Galambos 1941).

Some mammals, like echolocating bats for instance, use their acoustic system not only for spatial orientation but also for finding prey. The animal emits a high-frequency sound that is reflected – echoed – by an obstacle or prey back to the ear to be analyzed. Echolocation is extremely useful and replaces the bats' poor vision at night (Schnitzler et al. 2003).

Auditory systems of vertebrates have evolved to cope with two different environmental media – water and air. The impedance of tissues of aquatic animals and of water are very similar (Hemilä et al. 2010). Therefore, incoming sound waves can travel directly from the water to the hair cells of the inner ear. Terrestrial vertebrates, on the other hand, face an impedance difference between air and tissue. Because of this impedance difference, 99.9% of the acoustic energy would be reflected and lost at the junction of air and tissue (Purves et al. 2001). As a consequence, the evolution of a tympanic middle ear was necessary to enable hearing in a terrestrial environment. The tympanic middle ear converts sound pressure in air to particle motion in the fluid of the inner ear. The mammalian ear is generally divided into three sections: the outer, middle, and inner ear (Neuweiler and Heldmaier, 2003; see Figure 1).

4.1 The outer ear

The outer ear consists of the pinna, or auricle, and the ear canal (external auditory meatus). The pinna catches surrounding sound waves and bundles them into the ear canal. Some species can move their pinnae to use them as sound antennae, while others (such as humans) do not have this ability. The very different shapes and sizes of pinnae throughout the animal kingdom lead to a peripheral filtering of frequencies and an amplification of certain frequency bands (Zenner 1994).

4.2 The middle ear

The middle ear consists of an air-filled bulla with an airborne sound detector – the tympanic membrane. The tympanic membrane is connected to three bones that in turn are linked to the oval window of the inner ear. Early reptilian ancestors had only one acoustic ossicle (columella) (Crompton and Parker 1978). The two additional auditory ossicles are autapomorphic for mammals and have evolved from bones (articular and quadrate) of the mandibular joint of their reptilian ancestors (Pickles 2008). In mammals, these acoustic ossicles are called the stapes, incus, and malleus.

The acoustic ossicles form a chain that transfers airborne sound energy from the tympanic membrane to the oval window. Additionally, the acoustic ossicles serve as pressure amplifiers. For example, during the process where the sound energy absorbed by the area of the tympanic membrane is transferred to the smaller oval window, the pressure is enhanced and amplified because the same force is applied to a smaller area. Instead of losing 99.9% of the acoustic energy, at least 65% is transmitted from the outer to the inner ear (Purves et al. 2001).

4.3 The inner ear

The inner ear of mammals is a masterpiece when it comes to the ability to analyze frequencies of sound waves (Neuweiler and Heldmaier 2003). The inner ear, or cochlea, is

a spiral structure composed of three fluid-filled chambers that are embedded in an osseous capsule of the head. The peripheral scala vestibuli and scala tympani are filled with perilymph, which is a liquid containing a low concentration of potassium and a high concentration of sodium. In between, the scala media contains a high potassium fluid – the endolymph. This unequal distribution of ions results in the endocochlear potential. The different compartments are connected by tight junctions, creating a permeability barrier and regulating the flux of ions (Madara 1998).

Both scala vestibuli and scala tympani merge at the tip of the cochlea, the so-called helicotrema. Incoming sound waves are transmitted via the three acoustic ossicles to the oval window and the scala vestibuli. Sound waves can only produce a vibration of fluids when the transmitting fluid is versatile. The round window of the scala tympani is a flexible membrane that functions as a balancer of this fluid motion and alone makes the deflection in the sensory organ possible (Pickles 2008).

The scala media contains the actual sensory organ and is separated from the scala tympani by the basilar membrane. The basilar membrane incorporates one row of inner hair cells (IHCs) and three rows of outer hair cells (OHCs), forming the organ of Corti. Bundles of cilia of the OHCs are embedded in the tectorial membrane. At the outside of the scala media lies the stria vascularis, from which potassium is actively transported into the scala media to set the endocochlear potential to approximately +70 mV (Nobili et al. 1998). The Reißner's membrane separates the scala media from the scala vestibuli.

When a sound wave arrives at the oval window, a pressure difference between the scala vestibuli and scala tympani is produced. As a consequence, a traveling wave across the basilar membrane and scala media is triggered and moves along the endolymph to the apex of the cochlea. During this process, the bundles of cilia of the OHCs are deflected, leading to an opening of channels and a depolarization of the OHCs. The OHC response is correlated with the amplitude of the deflection of the basilar membrane. The cilia of the IHCs are deflected by the motion of the endolymph, and the strength of response is correlated with the oscillation speed of the basilar membrane. Depolarization of IHCs triggers the release of neurotransmitters at the ribbon synapses with their spiral ganglion neurons (Bear et al. 2007). Indeed, auditory information conveyed from the environment to the central auditory processing regions of the brain is encoded by the IHCs, whereas OHCs serve as amplifiers of the specific frequency. The width of the basilar membrane

increases and stiffness decreases from the basal to the apical end, resulting in a gradient where the traveling wave elicited by high frequencies reaches its maximal amplitudes at the basal end and low frequencies closer to the apical end of the cochlea (Bekesy 1960; see Figure 1). This resolution of topographic representation of frequencies is called tonotopy and is maintained throughout almost the entire ascending auditory pathway.

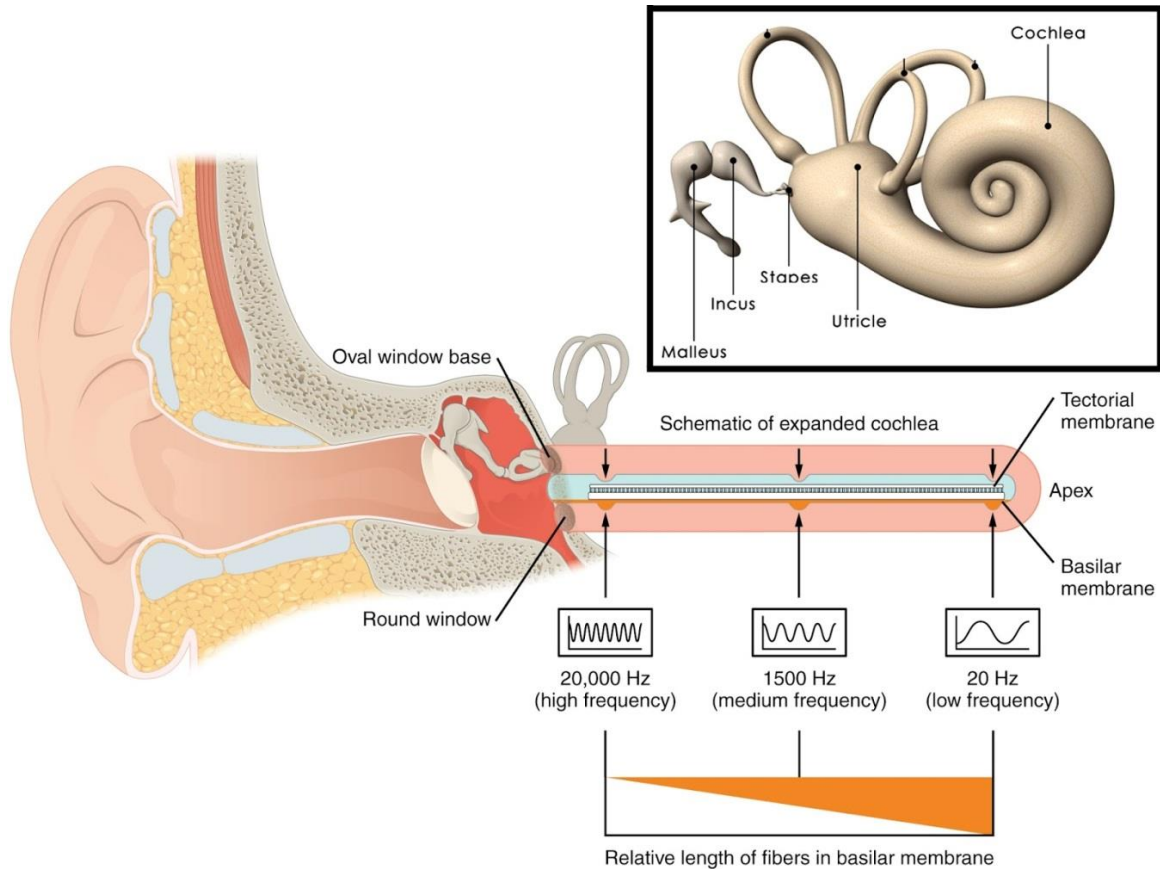


Figure 1: The outer, middle, and inner ear of humans. The inner ear with the cochlea and the three auditory ossicles is enlarged in the inset (top). For a clearly arranged overview, the cochlea with its basilar membrane is artificially expanded (bottom). The basal part of the basilar membrane (proximal to the oval window) is narrow and stiff. It is deflected by high-frequency stimulations. The width of the basilar membrane increases while the stiffness decreases on its way to the apical part where low frequencies are detected. Tonotopic frequency detection starts already in the inner ear. (From Betts et al. 2013)

4.4 The central auditory pathway

Sound information transduced by IHCs activates neurotransmitter release at ribbon synapses, and sound information is transformed into action potentials (APs) in spiral ganglion neurons, which project as the auditory nerve to the cochlear nucleus (CN) (Bear et al. 2007). The CN is subdivided into the ventral cochlear nucleus (VCN) and dorsal cochlear nucleus (DCN). The VCN can be further divided into the anterior and posterior ventral cochlear nucleus (AVCN and PVCN; Cant and Benson 2003). Tonotopic organization from the cochlea is maintained within the AVCN, PVCN, and DCN (Covey and Casseday 1995). These three subdivisions contain many different neuronal types with specific characteristics, such as octopus cells in the PVCN (Covey and Casseday 1986; Friauf and Ostwald 1988; Adams 1997; Schofield and Cant 1997) and spherical and bushy cells in the AVCN (Cant and Benson 2003), which leads to a diverse processing of auditory information. Neurons in the CN ascend to several pathways described below (for overview see Figure 2).

The ability to localize sound is important for the survival of individuals. Humans, for instance, use two different mechanisms for sound localization: determination of interaural time differences (ITDs) and interaural intensity differences (IIDs) (Grothe et al. 2010). Sound sources with frequencies below 3 kHz are analyzed with ITDs in the medial superior olive (MSO). The MSO is a binaural auditory nucleus that is innervated by excitatory projections from the ipsi- and contralateral AVCN (Goldberg and Brown 1969; Cant and Casseday 1986; Smith et al. 1993) and by inhibitory projections from the medial and lateral nuclei of the trapezoid body (Clark 1969; Perkins 1973; Cant and Hyson 1992; Kuwabara and Zook 1992; Grothe and Sanes 1994). The typical MSO neuron is bipolar with a laterally and medially oriented dendrite (Ollo and Schwartz 1979; Smith 1995; Smith et al. 2000; Scott et al. 2005; Rautenberg et al. 2009). The lateral dendrites are innervated by the ipsilateral CN, whereas the medial dendrites receive inputs from the contralateral CN. The MSO neurons work as coincidence detectors, meaning that they only respond when both binaural excitatory signals arrive at the same time. These neurons are sensitive to a specific ITD.

Frequencies above 3 kHz are analyzed by the lateral superior olive (LSO) and medial nucleus of the trapezoid body (MNTB) to localize sound sources. High-frequency sounds

cannot be localized via ITDs, since the phase-lock information of the sound wave is equivocal at high frequencies (Palmer and Russell 1986). Instead, high-frequency sound waves that arrive at the near ear leave an acoustic shadow that is produced by the head of the individual, which will result in an attenuation of the sound intensity at the far ear. Therefore, the brain processes IIDs to analyze high-frequency sounds. The LSO is a binaural auditory brainstem nucleus that receives excitatory inputs from the ipsilateral AVCN (Cant and Casseday 1986) but also inhibitory inputs from the MNTB, which is innervated by axons emerging from the globular bushy cells of the contralateral AVCN. These form the calyx of Held synapses in the MNTB (Moore and Caspary 1983; Kuwabara et al. 1991). Resulting from these projections, the LSO on the side of the sound source receives a net excitation. The inhibition of the LSO by the MNTB will increase when the sound source moves from the ipsilateral ear to the midline. If the sound source is located directly lateral to the ear, inhibition will be minimal (Moore and Caspary 1983).

Binaural pathways are essential for sound localization. Nevertheless, localizing sounds is not the only cue that sound perception involves. The ventral nucleus of the lateral lemniscus (VNLL), a monaural brain stem nucleus of the ascending auditory pathway, may play a critical role in the analysis of temporal sound patterns (Aitkin et al. 1970; Covey and Casseday 1991; Recio-Spinoso and Joris 2014). A more detailed description of the VNLL follows in the next Section 4.5.

The intermediate nucleus of the lateral lemniscus (INLL) receives contralateral inputs from the VCN – like the VNLL – but also receives inputs from the contralateral superior olivary complex (SOC), as the dorsal nucleus of the lateral lemniscus (DNLL) does. In contrast to its similarities with the VNLL and DNLL, the INLL receives projections from the ipsilateral MNTB and minor projections from the LNTB (Glendenning et al. 1981). Therefore, at least in some mammals, the intermediate nucleus of the lateral lemniscus forms a distinct nucleus within in the lateral lemniscus (Glendenning et al. 1981; Schofield and Cant 1997).

The DNLL receives bilateral inputs from the brainstem and is involved in binaural processing of auditory information. It is located dorsally to the INLL and ventrally to the inferior colliculus (IC). It receives its main excitatory inputs from the ipsilateral MSO and contralateral LSO (Adams 1979; Glendenning et al. 1981; Zook and Casseday 1982a; Shneiderman et al. 1988). Additionally, inhibitory inputs are sent from the ipsilateral LSO

4.5 Ventral nucleus of the lateral lemniscus

The ventral nucleus of the lateral lemniscus (VNLL) is a monaural brainstem nucleus of the ascending auditory pathway. Previous research has suggested that it may have a critical role to play in the analysis of temporal sound patterns (Aitkin et al. 1970; Covey and Casseday 1991; Recio-Spinoso and Joris 2014). For instance, speech perception is a temporally dynamic process that requires robust mechanisms to reliably process information from the environment to the auditory cortex (Prather 2013). Neurons in the VNLL receive glutamatergic excitatory inputs from several neuron types of the contralateral VCN and a major glycinergic inhibitory input from the ipsilateral MNTB (Glendenning et al. 1981; Schofield and Cant 1997; Irfan et al. 2005; Kelly et al. 2009; see Figure 2 for overview). Projections from the octopus cell region in the PVCN innervate the VNLL with calyx-like inputs (Covey and Casseday 1986; Friauf and Ostwald 1988; Adams 1997; Schofield and Cant 1997; Felix Li et al. 2017) that mediate information with high temporal fidelity (Berger et al. 2014). Response patterns of octopus cells make them especially useful for extracting features of speech due to their broad frequency tuning (Golding et al. 1995), their phase-locked responses to amplitude-modulated tones (Rhode and Greenberg 1994), and their precise responses to speech containing formant sounds (Rhode 1998). Therefore, octopus cells are well suited to extract and convey information for analyzing speech components (Oertel 2005).

Most VNLL neurons are immunopositive for glycine and/or GABA and send inhibitory projections to the ipsilateral inferior colliculus (IC) (Saint Marie et al. 1997; Riquelme et al. 2001; Zhang and Kelly 2006). Because of the large number of glycinergic and GABAergic neurons in the VNLL, this nucleus represents a prominent inhibitory source for the IC (Saint Marie and Baker 1990; Pollak et al. 2011). Neurons of the VNLL that are innervated by large calyx-like synapses are well suited to a fast onset inhibition in the IC. It is postulated that this robust onset inhibition regulates incoming excitatory inputs (Nayagam et al. 2005). Several theories have been proposed to explain how this onset inhibition influences further signal transmission. One theory maintains that the first spikes in a neuron population are inhibited, and the following spikes become temporally aligned with the responses of other neurons (Paolini et al. 2004). The second theory involves a temporal coincidence of abated inhibition and an excitatory event. That is, only if the rebound after the inhibition and an excitatory input occur at the same time a spike will be

elicited (Chase and Young 2007; Nayagam et al. 2005). Furthermore, a third theory holds that the onset inhibition regulates the responsive behavior of neurons. For instance, neurons that respond to long-lasting tones only fire when the excitatory input still persists after the inhibition has ended (Spencer et al. 2015). Last but not least, spectral splatter that is usually produced at the onset of sound emission is suppressed by onset inhibition to focus on the analysis of the actual temporal information laid within, for example, speech (Spencer et al. 2015).

The VNLL has been extensively studied in echo-locating bats (Covey and Casseday 1986, 1991; Metzner and Radtke-Schuller 1987; Vater et al. 1997). In bats, the VNLL can be subdivided into two regions – a columnar (VNLLc) and a multipolar (VNLLm) region. This subdivision was made due to the regions' physiological, morphological, and synaptical properties (Covey and Casseday 1986, 1991; Huffman and Covey 1995; Vater et al. 1997). Neurons in the VNLL show diverse responses to sounds in terms of temporal response patterns and binaurality (Batra and Fitzpatrick 1997, 2002; Nayagam et al. 2006; Zhang and Kelly 2006; Recio-Spinoso and Joris 2014). Studies on brain slices have revealed various firing patterns in response to depolarizing current injections (Wu 1999; Zhao and Wu 2001; Irfan et al. 2005) that resemble firing patterns of VNLL neurons *in vivo* (Zhang and Kelly 2006), such as sustained, onset burst and onset firing. Furthermore, although different firing patterns were recognized, a preference for onset firing was identified (Rhode et al. 1983; Covey and Casseday 1991; Smith et al. 2005; Zhang and Kelly 2006).

4.6 Large calyx-like synapses in the auditory brainstem

It has been demonstrated that large somatic synapses in the auditory circuitry are suitable for carrying auditory information with high temporal precision (Trussell 1999). In mammals, at least three large auditory synapses have been identified (see Figure 3). First are the endbulbs of Held that terminate on bushy cells in the AVCN and arise from auditory nerve fibers (Liberman 1991; Ryugo and Sento 1991). Second are the calyces of Held – the largest known synapses thus far – which terminate to neurons of the MNTB and ascend from globular bushy cells of the AVCN (Friauf and Ostwald 1988; Smith et al. 1991). Lastly, anatomical studies suggest that some VNLL neurons receive a major excitatory

input sent from the octopus cell area of the contralateral PVCN (Adams 1997; Schofield and Cant 1997; Felix Ii et al. 2017).

Calyx-like synapses are truly distinctive from other synapses because they are large, single axosomatic synapses that reliably mediate a fast transmission of temporal information (Schneggenburger and Forsythe 2006; Baydyuk et al. 2016). Furthermore, calyces like the calyx of Held contain several hundred active zones (Sätzler et al. 2002; Taschenberger et al. 2002) where a synchronous release of glutamate causes large postsynaptic responses that are well suited for preserving temporal information of auditory signals (von Gersdorff and Borst 2002). These nerve terminals, and other synapses of the central nervous system, contain a vesicle fusion machinery that is composed of a SNARE (soluble N-ethylmaleimide-sensitive-factor attachment receptor) complex that is associated with calcium-sensor proteins, such as synaptotagmin I and II (Syt1 and Syt2), to trigger a fast and temporally precise transmitter release into the synaptic cleft (Goda and Stevens 1994; Sabatini and Regehr 1999; Südhof 2013; Schneggenburger and Rosenmund 2015). Postsynaptic responses of neurons innervated with large, calyx-like synapses are, at least in mature animals, mediated almost exclusively by AMPA receptors (Futai et al. 2001). Additionally, large amounts of calcium-binding proteins such as calretinin and parvalbumin are found in these synapses, enhancing the buffering capacity and leading to a shortening of effective calcium currents and, consequently, increasing the temporal resolution to distinguish between different consecutive auditory signals (von Gersdorff and Borst 2002).

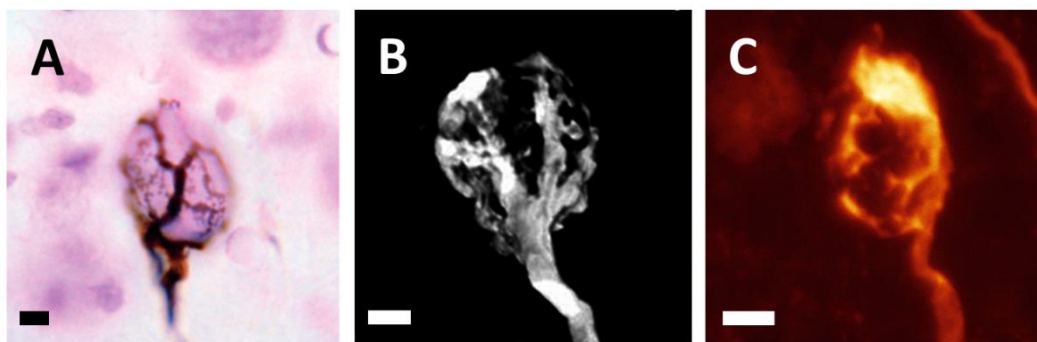


Figure 3: Three large mammalian auditory synapses. **A.** A horseradish peroxidase (HRP) labeled endbulb of Held from an adult cat. (Adapted from Ryugo and Spirou, 2009). **B.** Calyx of Held from an adult mouse filled with biotinylated dextran amine (BDA). (Adapted from Wang & Augustine, 2014) **C.** Calyx-like synapse in the ventrolateral part of the VNLL filled with tetramethylrhodamine-labeled dextran (microRuby). (Franziska Caspari & Ursula Koch, unpublished data)

Scale bar: 5 μm .

4.7 Development of intrinsic neuronal properties in the auditory brainstem

During the development of auditory brainstem nuclei, a maturation of intrinsic passive and active neuronal properties takes place, such as resting potential, input resistance, membrane time constants, and ionic channel distributions. The reduction of overall cell size including soma shrinking and decline of dendritic arborization leads to a decrease in cell capacitance resulting in faster charging of the membrane (Rautenberg et al. 2009; Franzen et al. 2015; Baumann and Koch 2017). Furthermore, some authors have described a decrease in input resistance during the development of auditory brainstem neurons (Magnusson et al. 2005; Scott et al. 2005; Hoffpauir et al. 2010; Rusu and Borst 2011; Walcher et al. 2011; Ammer et al. 2012; Franzen et al. 2015), which also reduces the integration time in these neurons. As a consequence, faster charging speed influences the ability to fire action potentials. Additionally, action potential firing properties of auditory brainstem neurons undergo developmental changes due to a rearrangement of voltage-gated potassium currents (Scott et al. 2005; Franzen et al. 2015). Recent studies on the VNLL of gerbils demonstrate that neurons with calyx-like inputs undergo a developmental change from a sustained to an onset-type firing pattern within the first week after hearing onset (Berger et al. 2014; Franzen et al. 2015). Moreover, MNTB principal neurons also undergo a similar developmental pattern. While at prenatal day E17 almost two thirds of the neurons show a sustained firing, 95% of the neurons exhibit an onset-type firing at postnatal day P6 (Hoffpauir et al. 2010). Taken together, these neuronal modifications lead to a faster generation of action potentials that, in turn, result in a fast and precise transmission of auditory signaling (Wu and Oertel 1987; Kandler and Friauf 1995; Ahuja and Wu 2000; Kuba et al. 2002; Scott et al. 2005; Ammer et al. 2012). It has been demonstrated that auditory-evoked activity is essential for a typical development of intrinsic neuronal properties. Auditory-evoked activity leads to a higher expression of low-voltage-activated potassium channels that then influence the firing behavior of neurons (Leao et al. 2004a). Pharmacological blockage of low-voltage-activated potassium currents leads to an augmented firing of action potentials (Leao et al. 2004a).

4.8 Synaptic development in the auditory brainstem

It is not only the intrinsic neuronal properties of auditory brainstem nuclei that undergo change during development, but also their synaptic inputs, leading to a change in the transmission of auditory signals.

The calyx of Held is one of the most thoroughly investigated synapses in the central nervous system and is therefore well suited for demonstrating the time course of synaptic development (Iwasaki and Takahashi 1998; Taschenberger et al. 2002; von Gersdorff and Borst 2002; Hoffpauir et al. 2006, 2010; Rodriguez-Contreras et al. 2008; Borst and Soria van Hoeve 2012; Xiao et al. 2013). Principal neurons of the MNTB that are innervated by the large glutamatergic calyces of Held already show their mature one (synapse) – to – one (neuron) innervation pattern at P2 (see Figure 4) (Hoffpauir et al. 2006). One pre-calyceal synapse that is found among a few innervating excitatory synapses at P1 develops quickly into a calyx synapse, while the remaining synapses are eliminated (Hoffpauir et al. 2006; Rodriguez-Contreras et al. 2008; Xiao et al. 2013; Kochubey et al. 2016). Before hearing onset, which occurs at around P12 in rodents (Akil et al. 2016), the calyx of Held has a spoon-shaped structure that subsequently is fenestrated to a finger-like, soma-encircling terminal in the first week after hearing onset (Kandler and Friauf 1993; Wimmer et al. 2006; Ford et al. 2009). In the time course of this morphological change, a drastic increase in the number of active zones occurs (Taschenberger et al. 2002), accompanied by a developmental decrease of NMDA receptors (Taschenberger and von Gersdorff 2000; Futai et al. 2001; Joshi and Wang 2002) and a speeding of AMPA receptor-mediated currents (Taschenberger and von Gersdorff 2000; Joshi et al. 2004). It has been proposed that these morphological and biophysical adaptations within the first three postnatal weeks are crucial for a fast and precise transmission of temporal information (Borst and Soria van Hoeve 2012).

Interestingly, calyx formation in the MNTB occurs with neither spontaneous nor auditory nerve activity (Youssoufian et al. 2005), but rather is regulated by intrinsic factors (Hoffpauir et al. 2006, 2010; Erazo-Fischer et al. 2007; Rodriguez-Contreras et al. 2008; Youssoufian et al. 2008). Although synaptic refinement in the MNTB is independent from neuronal activity, the precise tonotopic formation of neurons within the MNTB and further morphological modulations of the calyx shape require spontaneous activity (Leao et al. 2006; Ford et al. 2009). In addition to morphological adjustments of the calyx of Held that

occur during development, adaptations of calcium currents (Yang and Wang 2006) and calcium channel subtypes (Iwasaki and Takahashi 1998) also take place that lead to changes in presynaptic transmitter release and to a shortening of the presynaptic action potential waveform (Taschenberger and von Gersdorff 2000).

The interplay of the different intrinsic active and passive properties together with refinement of synaptic inputs generates the basis for the fast and precise voltage signaling that is required for sound analysis.



Figure 4: Developmental refinement of the calyx of Held in the MNTB. At P1 several excitatory terminals are found in MNTB neurons (left). Growth of one input and elimination of redundant inputs occur at P2 (middle). In postnatal week three, fenestration of the calyx of Held modifies the shape (right). (Adapted and modified from Kochubey et al. 2016)

4.9 Biophysical background of electrophysiological measurements

4.9.1 Passive membrane properties

The ion concentration inside and outside neurons is very different. The inside is rich in potassium and low in sodium, while the ion distribution of the outside is the opposite (Höber 1905; Bernstein 1912; Hodgkin 1951; Egri and Ruben 2012). Due to a selective permeability of ions through ion channels, the resting membrane potential is set to a certain value (Höber 1905; Bernstein 1912; Hodgkin 1951). At rest, the dominant permeability for potassium ions results in a membrane potential of approximately -60 mV, which is a relative inside-to-outside value (Purves 2001). The resting membrane potential can be determined by the Goldman-Hodgkin-Katz equation (formula 1) which takes into consideration the different internal and external concentrations of sodium, potassium, and chloride together with their specific permeability (Bowman and Baglioni 1984).

$$U_m = \frac{RT}{F} \cdot \ln \frac{P_{Na} \cdot [Na^+]_o + P_K \cdot [K^+]_o + P_{Cl} \cdot [Cl^-]_i}{P_{Na} \cdot [Na^+]_i + P_K \cdot [K^+]_i + P_{Cl} \cdot [Cl^-]_o} \quad \text{(formula 1)}$$

U_m	membrane potential
R	universal gas constant (8.314 J/(mol·K))
T	absolute temperature in Kelvin
F	Faraday constant (96485.33 C/mol)
P	specific permeability
Na	sodium
K	potassium
Cl	chloride
o	outside
i	inside

Cell membranes function as capacitors and resistors (Newman 2008). The lipid double layer is a capacitor that can store charge, while the number of embedded ion channels defines the degree of resistance – that is, the fewer channels activated, the higher the resistance (Newman 2008). Changing the membrane voltage requires a charging and discharging of the membrane capacitance (Newman 2008). In general, the size of neurons determines their capacitance: the larger the neuron, the larger the capacitance, and vice versa (Golowasch et al. 2009).

The relationship can be described by Ohm's law

$$R = \frac{U}{I} \rightarrow U = R \cdot I. \quad \text{(formula 2)}$$

R	resistance
U	voltage
I	current

To change the membrane voltage, a redistribution of internal and external ions through an activation of ion channels needs to take place (Lodish et al. 2000). Since an activation of ion channels leads to an increase of conduction, it is also common to speak of conductance (Bezanilla 2008).

$$g = \frac{1}{R} \quad (\text{formula 3})$$

g conductance
R resistance

The more channels that are open in the membrane, the larger the overall conductance is (Tour et al. 1998), described by

$$g_{tot} = g_1 + g_2 + \dots + g_n \quad (\text{formula 4})$$

g_n conductance

Furthermore, input resistance is defined as a degree of open channels at a membrane potential close to the resting potential (R_{in} small: many channels open; R_{in} larger: many channels not activated) (Dabrowski et al. 2013).

Moreover, the time (τ) it takes to change the membrane potential is the product of the membrane capacitance and input resistance (Newman 2008).

$$\tau = C_m \cdot R_{in} \quad (\text{formula 5})$$

τ is called the membrane time constant and affects the speed with which the membrane potential rises or falls in response to synaptic input or current injection (Koch et al. 1996). In addition to a theoretical approach, τ can be estimated experimentally by plotting an exponential fit to a passive voltage response, since it has been demonstrated that small hyperpolarizing voltage responses are most suitable for extracting τ (Spruston and Johnston 1992).

4.9.2 Active membrane properties

Electrical potentials across membranes may be affected by the activation of ion channels (Alberts et al. 2002). Voltage-gated ion channels open (activate) in response to changes in membrane potential and further change the conductance across the membrane due to a selective permeability to certain ions such as sodium and potassium (Alberts et al. 2002). Action potentials, for instance, are initiated by the activation of voltage-gated sodium channels, resulting in a fast inward sodium current (Hodgkin and Katz 1949). The action

potential threshold is reached when the inward sodium current is larger than the outward potassium current (Hodgkin and Huxley 1952). So far, there are nine voltage-gated sodium channels known ($Na_v1.1$ - $Na_v1.9$), all with different activation and inactivation rates and, therefore, properties (Bagal et al. 2015). Finally, the action potential initiation is terminated by an inactivation of sodium channels (Bagal et al. 2015) and/or an activation of potassium channels (Egri and Ruben 2012). As a result, a repolarization of the membrane is achieved (Egri and Ruben 2012). The particular combination of ion channels in the membrane determines the action potential threshold, waveform, and spiking pattern (Platkiewicz and Brette 2010). The large variety of potassium channels in particular adds diversity to neuronal responses (Gittelmann and Tempel 2006; Chi and Nicol 2007; Guan et al. 2007; Kole et al. 2007; Shu et al. 2007; Goldberg et al. 2008). For instance, a large number of slowly inactivating or non-inactivating voltage-gated potassium channels are known: $K_v1.1$, $K_v1.2$, $K_v1.3$, $K_v1.5$, $K_v1.6$, $K_v1.7$, $K_v1.8$, $K_v2.1$, $K_v2.2$, $K_v3.1$, $K_v3.2$, $K_v7.1$, $K_v7.2$, $K_v7.3$, $K_v7.4$, $K_v7.5$, $K_v10.1$ (DeCoursey et al. 1985; Christie et al. 1989; Stühmer et al. 1989; Snyders et al. 1993; Bertoli et al. 1994; Sprunger et al. 1996; Spencer et al. 1997; Kupper 1998; D'Adamo et al. 1999; Klemic et al. 2001; Sankaranarayanan et al. 2005; Jensen et al. 2007; Johnston et al. 2008; Tripathi et al. 2011; Kinoshita et al. 2012). However, a few rapidly inactivating voltage-gated potassium channels have also been identified: $K_v1.4$, $K_v3.3$, $K_v3.4$, $K_v4.1$, $K_v4.2$, $K_v4.3$ (Fernandez et al. 2003; Gebauer et al. 2004; Tomczak et al. 2017). In addition to their inactivation rate, the rate of activation and voltage dependence defines their individual characteristics.

4.9.3 I_h – HCN-channel mediated current

Hyperpolarization-activated cyclic nucleotide-gated (HCN) channels are voltage-gated cation channels that are involved in rhythmic activity in the brain and heart (DiFrancesco 1993; Pape 1996). Four different subtypes are known (HCN1–4), all with different voltage dependences and activation/inactivation kinetics (Ludwig et al. 1998; Santoro et al. 1998; Ishii et al. 1999; Seifert et al. 1999). When a hyperpolarization occurs after the repolarization phase of an action potential (afterhyperpolarization – AHP), HCN-channels, if present, become activated and lead to an inward current of sodium ions, which results in a depolarization (Pape 1996). Therefore, I_h plays a significant role in determining the resting membrane potential (Pape 1996; Robinson and Siegelbaum 2003). It also greatly

influences the integration time of inhibitory inputs by depolarizing the membrane and thereby shortening the inhibitory response (Atherton et al. 2010).

4.9.4 AMPA and NMDA receptors

The large majority of excitatory synaptic transmission in the central nervous system is mediated either by ionotropic AMPA (α -amino-3-hydroxy-5-methyl-4-isoxazolepropionic acid) or NMDA (N-methyl-D-aspartic acid) receptors (Dingledine et al. 1999). While both are glutamatergic, they exhibit different sets of subunits with, therefore, different physiological properties. The AMPA receptors consist of four subunits (GluR1–4) (Collingridge et al. 2009). Subunit GluR2 in particular is responsible for the characterization of AMPA receptor physiological properties (Isaac et al. 2007). Therefore, absence or presence of this subunit is a determining factor. For example, AMPA receptors containing GluR2 are impermeable for calcium and show a linear rectification pattern (linear current-voltage relation), whereas AMPA receptors lacking this subunit are permeable for calcium and display a strong inward-rectification current for positive membrane potentials (Adesnik and Nicoll 2007; Derkach et al. 2007).

The NMDA receptors consist of NR1 and NR2 subunits, of which NR2 determines NMDA receptor properties with its biophysical features such as ion conductance and synaptic plasticity (Bliss and Collingridge 1993; Lau and Zukin 2007). Moreover, NR2 itself consists of two parts, NR2A and NR2B. The former is known for faster kinetics and a higher channel open probability than the latter (Parsons et al. 1998; Lau and Zukin 2007). The NMDA receptors are voltage dependent and are blocked by either extracellular magnesium or zinc during resting potential (Nowak et al. 1984; Peters et al. 1987). A depolarization of the cell leads to a detachment of magnesium or zinc and a channel opening with sodium and calcium moving inward and potassium outward (Dingledine et al. 1999; Liu and Zhang 2000; Cull-Candy et al. 2001; Paoletti and Neyton 2007). The kinetics of NMDA receptors are much slower than those of AMPA receptors (Traynelis et al. 2010), and it has been proposed that NMDA receptor-mediated currents are indispensable for the formation of neuronal networks during development (Collingridge et al. 2013). Since NMDA receptors are blocked at resting potential, AMPA receptors are responsible for basic glutamatergic neurotransmission.

4.9.5 Presynaptic and postsynaptic properties

Synaptic transmission is the essential process for communication between neurons and can be either excitatory, inhibitory, or a mix of both (Niciu et al. 2012). Excitatory neurotransmission is usually triggered by glutamate, whereas inhibitory postsynaptic responses are generally mediated by neurotransmitters GABA (γ -aminobutyric acid) and glycine (Purves 2001). Glutamate is removed from the synaptic cleft and transported into the cytosol against its concentration gradient by the excitatory amino acid transporters (EAATs), of which five have been identified so far (O'Shea 2002).

The neurotransmitter GABA is synthesized from cytosolic glutamate via the glutamate decarboxylase (GAD), and glycine is transported from the extracellular medium via glycine transporters (GlyT1-2) (Guastella et al. 1992; Liu et al. 1993; Bak et al. 2006). In excitatory synapses, on the one hand, cytosolic glutamate penetrates the vesicular membrane through vesicular glutamate transporters (VGluT1-3) (Takamori 2006), whereas GABA and glycine are transported into vesicles via vesicular inhibitory amino acid transporters (VIAATs) (McIntire et al. 1997; Sagné et al. 1997; Gasnier 2004). Action potentials that are initiated in the axon initial segment lead to voltage changes of the presynaptic membrane in the terminal that, in turn, cause an opening of voltage-gated calcium channels and a subsequent calcium influx into the cell (Llinás et al. 1982). The SNARE complexes that contain calcium detector proteins such as synaptotagmin I and II are located in the vicinity of these calcium channels and mediate a calcium-dependent exocytosis of neurotransmitter into the synaptic cleft (Schneppenburger and Neher 2005; Südhof and Rothman 2009; Pang and Südhof 2010). This in turn has effects on postsynaptic receptors (see Figure 5). Glutamate receptors can be divided into ionotropic and metabotropic receptors (Niciu et al. 2012). While ionotropic receptors are ion channels for calcium and sodium that evoke an immediate postsynaptic response, metabotropic receptors are G-protein coupled receptors that cause interactions with second messengers (Niciu et al. 2012). Fast glutamatergic synaptic transmission is mediated by ionotropic glutamate receptors, of which three groups are known in the brain: AMPA, NMDA, and kainate receptors (Dingledine et al. 1999). Binding of glutamate to the receptors generates postsynaptic responses. An AMPA-mediated current generates a fast rise and decay of current through the membrane, while an NMDA receptor-mediated current provides a prolonged period of depolarization (Traynelis et al. 2010).

The GABA_A and glycinergic receptors are ligand-gated ion channels that permit the influx of chloride and hyperpolarize the membrane potential in neurons of mature animals (Lüscher and Keller 2004), while GABA_B receptors are G-protein coupled and function as second messengers (Legendre 2001). Ionotropic GABA_A and glycine receptor-mediated currents decrease the excitability of membranes by moving the potential further away from the threshold that is required to fire action potentials (Jacob et al. 2008).

The reversal potential of an ion type in relation to the threshold potential determines whether an input is excitatory or inhibitory (Purves 2001). Generally speaking, an excitatory effect occurs if ions have a more positive reversal potential than the threshold potential, and an inhibitory effect if the reversal potential is more negative (Purves 2001).

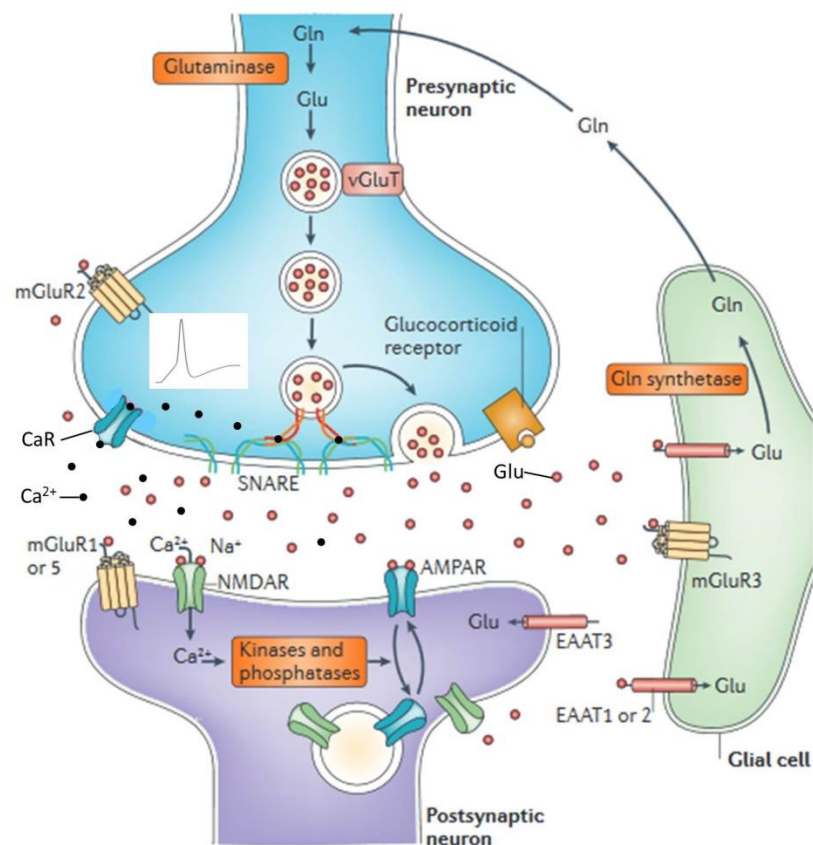


Figure 5. Glutamatergic synaptic transmission in the central nervous system. Glutamate is synthesized from glutamine and filled into vesicles via vesicular glutamate transporters (vGluT). Action potentials transduced in the axon initial segment depolarize the presynaptic membrane and activate voltage-gated calcium channels that mediate calcium influx. Calcium interacts with the SNARE complex that triggers vesicle fusion with the presynaptic membrane. Glutamate is released into the synaptic cleft and binds on postsynaptic AMPA or NMDA receptors. An activation of AMPA and NMDA receptors depolarizes the postsynaptic membrane and processes auditory information, for example. (Adapted and modified from Popoli et al. 2011)

Gln: glutamine; Glu: glutamate; vGluT: vesicular glutamate transporter; mGluR: metabotropic glutamate transporter; CaR: calcium-receptor; Ca²⁺: calcium ion; NMDAR: NMDA receptor; AMPAR: AMPA receptor; Na⁺: sodium ion; EAAT: excitatory amino acid transporter

The postsynaptic neuron may receive both excitatory and inhibitory inputs. The resulting inhibitory and excitatory voltage changes are summed, and the net response of both defines an excitatory or inhibitory postsynaptic effect (Carvalho and Buonomano 2009). The shape of the postsynaptic response is influenced by pre- and postsynaptic factors (Regehr 2012) and can be estimated with train stimulations during short-term plasticity experiments.

Presynaptic factors that influence postsynaptic responses are (1) calcium current modulation, (2) depletion of the readily releasable pool (RRP), and (3) replenishment of the RRP. As mentioned above, calcium plays a major role in neurotransmitter release and release probability (Burnashev and Rozov 2005; Neher and Sakaba 2008; de Jong and Verhage 2009). The amount of transmitter released is largely dependent on the cytosolic calcium concentration, since it triggers vesicle fusion with the presynaptic membrane (Jahn et al. 2003; Schneggenburger and Neher 2005; Südhof and Rothman 2009). The internal calcium concentration can be regulated by calcium-binding proteins in the presynaptic terminal (Roberts 1993; Neher 1998; Matveev et al. 2004). The affinity of calcium-binding proteins for binding calcium determines the release probability of vesicles containing neurotransmitter through the removal of effective calcium from the presynapse (Roberts, 1993). The amount of residual calcium in the cytosol influences a postsynaptic depression or facilitation. A high concentration of residual calcium causes a higher probability of neurotransmitter release, potentially resulting in a postsynaptic facilitation, whereas a low calcium concentration decreases the release probability, leading to a postsynaptic depression (Regehr, 2012). In summary, the closing of calcium channels and the buffering affinities of calcium-binding proteins determine the duration of transmitter release from the presynaptic terminal (Fogelson and Zucker 1985; Simon and Llinás 1985).

Depletion of the RRP is another factor determining the responsive abilities of postsynaptic receptors. During repetitive fiber stimulation, a depletion of vesicles occurs (Purves et al. 2001). There are usually hundreds of vesicles available within each active zone (Legendre 2001). Vesicles that are immediately available after presynaptic stimulation and are located in close vicinity of voltage-gated calcium channels belong to the RRP (Legendre 2001). Furthermore, it has been proposed that postsynaptic depression after repetitive stimulations is caused by a depletion of RRP vesicles, since the replenishment of these vesicles requires seconds (Hori and Takahashi 2012). The rate of vesicle pool replenishment depends on the time of neurotransmitter uptake from the synaptic cleft, vesicle endocytosis, and vesicle filling (Gandhi and Stevens 2003).

Postsynaptic responses are influenced not only by presynaptic but also by postsynaptic factors (Regehr, 2012). Postsynaptic factors include (1) receptor kinetics, (2) receptor saturation, and (3) receptor desensitization. The following paragraph explains the influence of postsynaptic factors on glutamatergic synapses. Receptor kinetics of AMPA and NMDA receptors differ due to different binding and gating properties (Jahr and Lester 1992), since a colocalization of both AMPA and NMDA exposes them to the same concentration of glutamate (Clements 1996). The AMPA receptor-mediated currents rise within microseconds and decay within a few micro- to milliseconds, whereas NMDA receptors display slow kinetics (Colquhoun et al. 1992; Hestrin 1992; Silver et al. 1992). Furthermore, saturation of postsynaptic receptors with glutamate may constrain the postsynaptic response, especially when a large amount of neurotransmitter is released into the synaptic cleft (Wadiche and Jahr 2001; Foster et al. 2002). As a result, the postsynaptic response may reflect an underestimation of the presynaptic release (Regehr, 2012). Last but not least, receptor desensitization resulting in an unavailability of receptor activation by glutamate may occur after repetitive stimulations with this neurotransmitter. This desensitization leads in turn to a decrease of the postsynaptic response and an overestimation of postsynaptic depression (Trussell et al. 1993; Chen et al. 2002; Xu-Friedman and Regehr 2004). Though AMPA receptor desensitization can be prevented pharmacologically (Francotte et al. 2006), during measurements of short-term plasticity presynaptic mechanisms may be influenced by desensitization and saturation of postsynaptic glutamatergic receptors (Regehr, 2012).

Postsynaptic depression as a response to repeated stimulations, on the one hand, is thought to play a role in sensory adaptation by responding to a novel stimulation with an increased postsynaptic amplitude (Chung et al. 2002). Furthermore, depression can be applied to enable cells to respond to relative changes and not absolute changes of stimuli (Regehr, 2012). Postsynaptic facilitation, on the other hand, increases the postsynaptic response to repeated stimuli resulting in a functional strengthening of stimuli that are important for memory forming (Goldman-Rakic 1995). As result, the expression of, for example, AMPA receptors is enhanced, and the postsynaptic receptor density increases (Willard and Koochekpour 2013).

4.10 Deafness

Hearing loss is a common sensory loss in humans and leads to deafness if the degree of loss is so severe that a subject is unable to perceive sounds even with amplification (Raviv et al., 2010; Elzouki, A.Y, 2012). The causes of hearing loss are diverse, including both hereditary causes and environmental factors. Environmental factors that can cause hearing loss are exposure to loud noises over a significant amount of time, trauma, and infections (Yorgason et al. 2006). As a result, by age 70, about 60% of people have suffered hearing loss of at least 25 dB (Gratton and Vázquez 2003). However, only 30% of acquired hearing loss is caused by an environmental influence, while 70% has a genetic origin (Raviv et al. 2010). Today, more than 100 genes have been identified that are involved in hereditary hearing loss (Nishio et al. 2015).

4.11 Deaf mouse models and the impact of deafness on central auditory structures

Deaf mouse models for deafness are created to imitate different origins of hearing loss in humans and help to understand underlying mechanisms and the effects on auditory processing in the central nervous system. There are different approaches to creating new mouse models. Usually, deafness can be induced by spontaneous mutations, mutagens, or specific targeting of genes (Brown et al. 2008). The following paragraphs introduce some deaf mouse models that are relevant for this study.

4.11.1 Deafwaddler

Deafwaddler (*dfw*) is originally a spontaneous mutation that leads to deafness and a waddling walk in mice (Penheiter et al. 2001), and in 1998 it was first discovered that a mutation of the gene encoding the **p**lasma **m**embrane **c**alcium **A**T Pase 2 (PMCA) occurred (Street et al. 1998). In mice this gene is located on chromosome 6 (Street et al. 1995) and is homologous to the human gene 3p25-26 (Penheiter et al. 2001). The deafwaddler mutant results from a substitution of a nucleotide (glycine to serine) at a highly conserved amino-acid position (Penheiter et al. 2001). The protein PMCA2 is expressed in stereocilia of

auditory and vestibular hair cells and in neurons of the spiral ganglion and is very important for a proper inner ear development (Penheiter et al. 2001). Although deafwaddler mice are deaf and have poor balance, PMCA2-knock-out (KO) mice display a more severe phenotype (Kozel et al. 1998). It is known that PMCA2 contributes to the removal of calcium from cells (Tucker and Fettiplace 1995) and from stereocilia (Lumpkin and Hudspeth 1998; Yamoah et al. 1998).

Neurons of the MNTB in *dfw* mice show an increase in miniature excitatory postsynaptic current (mEPSC) amplitude, suggesting larger presynaptic transmitter release (Weatherstone et al. 2017). Furthermore, MNTB neurons are tonotopically organized, and neurons responding to high-frequency sounds are located closer to the midline (Sonntag et al. 2009). Interestingly, cell size in the MNTB also differs from medial to lateral (Weatherstone et al. 2017). Neuronal cell capacitances of hearing mice display a gradual decrease from low to high frequencies (Weatherstone et al. 2017). In a recent study, Weatherstone et al. (2017) have suggested that hearing loss caused by a lack of calcium removal has large effects on the proper development of MNTB neurons. Furthermore, a loss of auditory-evoked activity also influences potassium channel expression in MNTB neurons (Leão et al. 2010).

4.11.2 DFN

Currently, there are 159 identified genomic loci that are involved in deafness. These loci are presented on the website www.genenames.org, where they are named after their location on the chromosome, whether it is recessive or dominant, and its consecutive number (DFN: deafness; A: autosomal dominant; B: autosomal recessive, X: X-chromosome linked, Y: Y-chromosome linked, “#”: number of discovery). The following paragraphs describe some of these loci, since they help to understand the mechanisms described in this thesis.

4.11.2.1 dn/dn

Another deaf mouse model with a different origin of deafness is the *dn/dn* deaf mouse, with the deafness-related name DFNA36. These mice are congenitally deaf with neuroepithelial degeneration of the cochlea, while no other physical defects are known (Bock et al. 1982;

Keats and Berlin 1999). The *dn/dn* model is a natural mutation of the transmembrane cochlear-expressed gene 1 (*tmc1*; Kurima et al. 2002), located on the human chromosome 9q21.13. Expression of this protein is found exclusively in the cochlea. Furthermore, a mutation of *tmc1* leads to a loss of auditory nerve activity from early on (Leao et al. 2004a; Youssoufian et al. 2008). However, it has been demonstrated that spontaneous auditory nerve activity during the early postnatal days is crucial for the development of some mammalian brainstem nuclei (Pasic and Rubel 1989; Rubel and Fritzsche 2002). Previous studies have found enhanced excitatory postsynaptic currents in the cochlea nucleus (Oleskevich and Walmsley 2002) and altered inhibitory postsynaptic currents in the MNTB (Leao et al. 2004b). Moreover, cell excitability of MNTB neurons is also enhanced in these mice, indicated by a reduced current threshold and an elicitation of an augmented spike number (Leao et al. 2004a). The *dn/dn* mice display a reduced expression of low-voltage-activated potassium channels (K_v1 ; Leao et al. 2004a), leading to the conclusion that both synaptic and intrinsic conductances are under activity-dependent control.

4.11.2.2 DFNB9

While these previously mentioned forms of genetic hearing disorders result from impairment of inner hair cell development, degeneration of those inner hair cells, or defects in proper cochlea compartmentalization, deafness can also result from impaired signal transmission from the cochlea to the brain (Dror and Avraham 2010).

Otoferlin has been found to play a crucial role for vesicle exocytosis at ribbon synapses, since it is thought to be an important calcium sensor and mediator for vesicle fusion (Roux et al. 2006). Mutations of otoferlin are found in humans on chromosome 2p22-23, while the mice homologue is located on chromosome 5. The human hearing disorder with a mutation in otoferlin is autosomal recessive and is catalogued under DFNB9 (Yasunaga et al. 1999). The auditory system is extremely fast and dependent on a precise temporal signal transmission from the inner hair cell ribbon synapse to ascending auditory nuclei. Analysis of sound information includes pitch detection, sound localization, and speech perception (Schnupp et al. 2011). Inner hair cell stimulation leads to exocytosis of transmitter at the ribbon synapse within micro- to milliseconds (Glowatzki and Fuchs 2002; Goutman 2012; Li et al. 2014). Active zones of synapses in the basolateral region of inner hair cells are organized in a ribbon shape, hence their name, ribbon synapse. Furthermore, approximately 10 to 30 active zones contain a large pool of immediately available vesicles for maintaining

a fast and precise transmission of auditory signaling (von Gersdorff and Matthews 1997; Lenzi et al. 1999; Moser and Beutner 2000). Usually, synapses of the central nervous system contain certain proteins, namely synaptogmin I and II (Syt1 and Syt2), that are required for vesicle fusion with the presynaptic membrane and function as calcium sensors (Südhof 2013). In inner hair cells, however, these proteins Syt1 and Syt2 are absent (Safieddine and Wenthold 1999; Beurg et al. 2010). Instead, synapses of inner hair cells contain otoferlin as a calcium sensor and trigger for vesicle fusion with the presynaptic membrane (Roux et al., 2006; see Figure 6). Otoferlin is a calcium-binding membrane protein of the ferlin family and consists of six C2 domains (C2A-C2F) and two Fer domains (Yasunaga et al. 1999; Roux et al. 2006; Lek et al. 2010). Otoferlin mutants (OTOF^{-/-}) showed no synaptic exocytosis in response to calcium influx, in spite of typical calcium currents and no apparent morphological changes (Roux et al. 2006). Due to a lack of transmitter release, otoferlin mutants are deaf (Roux et al. 2006).

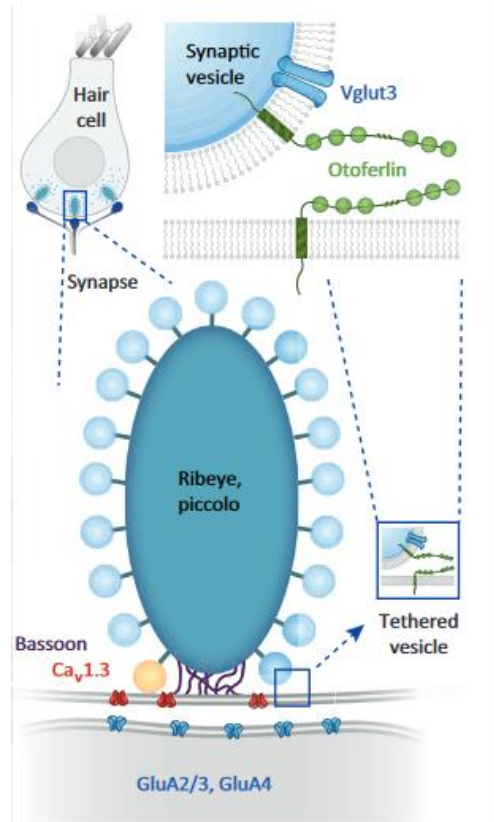


Figure 6: Inner hair cell of the cochlea and its functional composition of the ribbon synapse. Otoferlin functions as a calcium sensor and trigger for vesicle fusion with the presynaptic membrane. (From Pangrsic et al. 2012)

Moreover, loss of afferent activity can result in many alterations in the circuitry, such as changes in potassium currents, loss of tonotopicity as a consequence of changes in potassium currents, and alterations in expressions of calcium-binding proteins (Caicedo et al. 1997).

4.12 Hypothesis

Based on earlier research on the calyx development in the MNTB of deaf mice, we suspect a developmental synaptic maturation in the VNLL of mice that is independent of auditory-evoked activity. Furthermore, deafness has been found to affect potassium channel expression and we therefore assume that neuronal intrinsic properties such as the firing behavior are greatly influenced by the lack of sensory experience.

4.13 Aim of this study

Currently, the intrinsic and synaptic properties of VNLL neurons and their spatial distribution within the VNLL have not been systematically studied in animals when neuronal properties are considered to be mature (Khurana et al. 2012). To identify whether different neuron types are systematically distributed within the VNLL, as has been found for echo-locating bats (Vater and Feng 1990; Huffman and Covey 1995), in Part 1 of this thesis I, together with my colleagues, characterized the intrinsic and synaptic properties of VNLL neurons in acute brain slices of young adult mice relative to their location within the VNLL.

In Part 2 of this thesis, I focused on the ventral part of the VNLL and studied the development of the calyx-like synapse that has been described in other studies (Adams 1997; Schofield and Cant 1997; Berger et al. 2014) and in the first part of this thesis. To identify when during development neurons of the ventral part of the VNLL develop their specific synaptic properties, I performed experiments on acute brain slices of P10, P13, and P22 mice.

The refinement of synaptic inputs and the development of neurons with only an onset firing pattern occurs after hearing onset, as indicated by the experiments performed in Part 2 of this thesis. Therefore, I was interested in evaluating intrinsic or environmental influences that lead to the development of these specific neuronal characteristics in the ventral part of the VNLL. In order to identify whether or not these developmental changes are activity evoked, I used a deafness mouse model, where the protein otoferlin is dysfunctional $OTOF^{(-/-)}$ -KO), resulting in the loss of transmitter release in the IHCs of the cochlea (Roux

et al. 2006) and, consequently, deafness. Littermates with a functioning protein (OTOF^(+/+)-wild type (WT)) were used as controls. Prior to these experiments, I studied the developmental changes in WT animals between P10 and P22 in order to identify changes in this strain and relate my results to the subsequent WT-KO comparisons.

4.14 Scientific relevance

Functional understanding of sound localization has been intensively studied in the past decades and is well understood. Nevertheless, the processing and analysis of speech at the level of the auditory brainstem is still quite unclear. In these studies, we aim to help unravel the neuronal mechanisms involved in speech detection. Furthermore, we hope to reveal whether auditory-evoked activity is necessary for proper neuronal development in the VNLL and to examine how these result affect research in human hearing loss.

5 Material and methods

5.1 Animals

All experiments and animal breeding followed EU ethical guidelines and were carried out in accordance with protocols approved by the German federal authorities (Landesamt für Gesundheit und Soziales, State of Berlin).

Mice used for experiments were bred either in the animal facility located at the Institute of Biology, AG Neurophysiology (AG Prof. Ursula Koch), Freie Universität Berlin or at the FEM (Forschungseinrichtungen für experimentelle Medizin) associated with the Charité Berlin.

Animals were kept on a 12h:12h light:dark cycle and had ad libitum access to standard laboratory food pellets and drinking water. The temperature was held steady at approximately 22°C, and humidity in the room was maintained at 50%. In order to keep the animals content, cage enrichments such as shelters and toys were provided.

5.2 Breeding

5.2.1 C57Bl/6

Type C57Bl/6 mice were obtained from the FEM Berlin and further bred in the in-house mouse breeding facility. Most electrophysiological experiments of Parts 1 and 2 were performed on brain slices of C57Bl/6J mice at the ages of postnatal days 10–11 (P10–11), P13–14 and P22–23. Additionally, immunostainings were performed in mice of these ages and 20–25-week-old animals. Littermates of both sexes were used for experiments.

5.2.1 VGAT

One series of electrophysiological experiments of Part 1 of this thesis was performed at P22–23 on VGAT-ChR2-YFP⁺ [B6.Cg-Tg(Slc32a1-COP4*H134R/EYFP)8Gfng/J; The Jackson Laboratory] mice to determine inhibitory regions within the lateral lemniscus, as channelrhodopsin-associated yellow fluorescent protein (YFP) is only expressed in

vesicular GABA transporter (VGAT)-expressing neurons, hence GABAergic or glycinergic neurons (Zhao et al. 2011). Animals were bred in the in-house animal facility. At P2-3 expression of the mhChR2::EYFP construct was visually determined by directing a blue light beam (460-495 nm) with a specialized lamp (FS/ULS-02B2, BLS-Ltd, Hungary) to the mice. A yellow/green shimmer through the skull confirmed the expression of EYFP in the brain. The YFP⁺ littermates were tattooed for subsequent identification. Littermates of both sexes were used for experiments.

5.2.3 OTOF

Heterozygous (OTOF^(+/-)) and homozygous KO (OTOF^(-/-)) were obtained from Nicola Stenzke's lab in Göttingen. Animals were kept and cross-bred in the in-house animal breeding facility in order to perform *in vitro* electrophysiological and immunohistochemical experiments on homozygous KO and wild type (OTOF^(+/+)) mice. Results of this experimental work are presented in Part 3 of this thesis.

Animals were created by Ellen Reisinger et al. (2011). These mice have a C57Bl/6 background and were genetically modified. A targeting construct that consisted of a loxP-flanked neomycin cassette was inserted in the genome and replaced exons 14 and 15 of a 9.2 kb genomic DNA fragment of the otoferlin gene. The otoferlin gene of mice consists of 50 exons that contain the coding DNA. A thymidine kinase (TK) cassette for negative selection was added after the 5.3 kb long arm. This targeting construct was electroporated into 129ola embryonic stem cells. A subsequent positive selection was followed by the neomycin resistant cassette. A selective antibiotic G418 was added to the cell culture, and only cells with an inserted neomycin resistance survived. An additional negative selection was carried out by the activity of the inserted thymidin kinase from the herpes simplex virus 1. Thymidin kinase is also coded on the targeting construct but outside of loxP-flanked homologue sequence. Therefore, it is not included in the genome after homologue recombination, so an application of ganciclovir kills all cells with the thymidine kinase. This procedure ensures that cells are only picked where the gene was correctly modified (Reisinger et al. 2011).

Heterozygous (OTOF^(+/-)) mice were bred to obtain litters containing both homozygous KO (OTOF^(-/-)) and WT (OTOF^(+/+)) mice. A tail cut of all littermates was taken between P3 and P5 and used for genotyping. Littermates were tattooed and documented. For further

experiments, young mice (P10–11 and P22–23) were chosen blindly to exclude bias by the experimenter. A repeated genotyping of the chosen mouse confirmed the genotype retrospectively.

5.3 Genotyping

Prior to experiments, genotyping of otoferlin mice was performed to identify all three genotypes born in this litter, but only homozygous KO and WT animals were used for experiments.

Tail cuts of all littermates were kept separately overnight in polyethylene glycol at room temperature for extracting DNA from the tissue. A master mix for the polymerase chain reaction (PCR) procedure was prepared, containing following chemicals: 10x Taq buffer B, 2.5 mM MgCl₂, 0.15 mM 4dNTP, 0.375 μM primer ofotof sense 1 (wt), 0.375 μM primer ofotof sense 2 (ko), 0.375 μM primer ofotof antisense, 5 U/μl Taq polymerase water (all chemicals from Bio&Sell, Feucht, Germany). The protocol for the PCR program and master mix recipe were kindly provided to us by Nicola Strenzke.

An agarose gel was prepared, containing following chemicals: 1x TBE buffer (8.9515 mM TRIS base, 8.954 mM boric acid, 2.533 mM EDTA [all chemicals from Carl Roth, Karlsruhe, Germany]), 2% agarose (Bio&Sell, Feucht, Germany), and 1% Ethidium bromide (Carl Roth, Karlsruhe, Germany). The DNA containing probes together with 6x loading dye (Fermentas, Thermo Fisher Scientific, Waltham, MA, USA) were loaded onto the gel and run for approximately 40 minutes at 120 V. Electrophoresis was stopped when bands were clearly separated (see Figure 7).

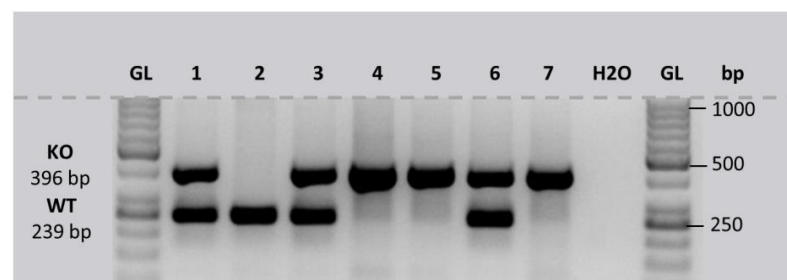


Figure 7: Representative genotyping result. DNA products were amplified with WT primers (239 bp) and KO primers (396 bp). Heterozygous mice showed both DNA bands (239 and 396 bp).

GL: gene ladder; H2O: water, no DNA; bp: base pairs

5.4 Solutions

The following solutions were used for electrophysiological experiments.

The **slicing solution** contained (in mM): 2.5 KCl, 26 NaHCO₃, 1.25 NaH₂PO₄*H₂O, 6 MgCl₂, 0.5 CaCl₂, 25 glucose, and 200 sucrose.

The **recording solution** – artificial cerebrospinal fluid (ACSF) contained (in mM): 125 NaCl, 2.5 KCl, 1.25 NaH₂PO₄*H₂O, 2.6 NaHCO₃, 6 MgCl₂, 0.5 CaCl₂, and 25 glucose.

The **ACSF solution for I_h** isolation was prepared according to Baumann et al. 2013 and contained (in mM): 1 3,4-diaminopyridine, 10 TEA-Cl, 0.2 BaCl₂, 0.001 TTX, 0.05 NiCl₂, 0.1 CdCl₂, 0.01 DNQX, 0.025 DL-AP5, and 0.001 strychnine. NaCl concentration was reduced to maintain isoosmolarity.

The **potassium gluconate solution** for current clamp recordings and I_h measurements contained (in mM): 125 K-gluconate, 5 KCl, 10 HEPES, 1 EGTA, 2 Na₂ATP, 2 MgATP, 0.3 Na₂GTP, and 10 Na-phosphocreatinine. The pH was set to 7.25.

The **CsCl solution** for recordings of synaptic currents contained (in mM): 41 CsCl, 99 Cs-methylsulfonate, 10 HEPES, 10 Cs-EGTA, 2 Na₂ATP, 2 MgATP, 0.3 Na₂GTP, 1 CaCl₂, 5 TEA-Cl, and 5 QX 314. The pH was set to 7.25.

To block AMPA and NMDA receptor-mediated currents, DNQX and DL-AP5 were added to the ACSF. Strychnine and SR95531 were added to the bath to block glycine and GABA_A receptor-mediated currents.

All agents were purchased from Sigma-Aldrich (Seelze, Germany) and Biotrend (Köln, Germany).

5.4 Brain Slice preparation

Prior to the brain removal, slicing and recording solutions were prepared. The slicing solution was also put on ice water and bubbled with carbogen (95% O₂ and 5% CO₂).

Animals were anesthetized with isoflurane (AbbVie, Ludwigshafen, Germany) and quickly decapitated. Brains were gently removed, glued to the platform of the slicing chamber and

put into the vibratome (VT1200S, Leica, Germany). Ice-cold and carbogenated slicing solution was added to the chamber to cover the brain. 180 μm thick slices were cut at a slow pace of 0.02 mm/s. Slices were collected and transferred to an incubation chamber with ACSF at 32°C. They were kept at 32°C for approximately 20 minutes and were cooled down to room temperature until they were used for recordings.

5.5 Patch-clamp electrophysiology and data acquisition

Whole-cell patch-clamp recordings were made from visually identified VNLL neurons using a Multiclamp 700 A amplifier (Axon Instruments, CA, USA) and a Digidata1440A (Molecular Devices, CA, USA). Patch pipettes were pulled from borosilicate glass capillaries (BioMedical Instruments, Germany, 0.86 mm inner diameter and 1.5 mm outer diameter) on a DMZ Universal Puller (Zeitz Instruments, Germany) and filled with either potassium gluconate solution (for current clamp and I_h measurements) or cesium chloride solution (for voltage-clamp measurements; see above). All experiments were performed at 32°C. Patch pipettes had resistances of 2–4 M Ω .

To study the intrinsic membrane properties with respect to their location within the VNLL, the VNLL was subdivided into three regions – dorsal, middle, and ventral – based on the nomenclature proposed for gerbils by Benson and Cant, 2008. For Part 1 of this thesis we recorded from dorsal and ventral regions, whereas for Parts 2 and 3 we made recordings only of neurons in the ventrolateral part of the VNLL. The ventral VNLL was considered as the ventral end of the fiber bundle of the lateral lemniscus, and the dorsal VNLL was determined with respect to the dorsal nucleus of the lateral lemniscus (DNLL). Neuronal locations were determined in the acute slice preparation by anatomical landmarks and delineated in a sketch of the VNLL. In some experiments, Alexa 555 was added to the internal solution in order to later verify the visually determined location of a neuron within the VNLL (data not shown).

5.6 Data acquisition

Bridge balance was adjusted for current-clamp recordings. During voltage-clamp recordings, series resistance ($<10\text{ M}\Omega$) was compensated to a residual resistance of 2–2.5 $\text{M}\Omega$ and was not allowed to change more than 20% during the recording. For measuring passive and active membrane properties, 1000 ms long hyperpolarizing and depolarizing current steps from -300 pA to 1000 pA were injected.

Channelrhodopsin was activated with a 5–10 ms light pulse of an arc lamp which yields similar depolarization amplitudes of VGAT-positive neurons as a 26.3 mW/mm^2 blue LED (Zhao et al. 2011).

The HCN currents were activated by applying depolarizing and hyperpolarizing voltage steps from -40.5 to 120.5 mV. Tail currents were measured at the holding potential of -100.5 mV that followed each voltage step. Current densities were obtained by estimating cell surface size from the capacitance of the amplifier.

Synaptic currents were evoked by stimulating the ascending fibers approximately 50 μm ventral to the recorded neuron with a glass electrode filled with 2 M NaCl. Stimuli consisted of brief biphasic pulses (200 ms, intensities 3–80 V) triggered by an analog stimulus isolation unit (BSI-950, Dagan Corporation, USA). The threshold for synaptic responses was usually between 5 and 20 V. For determination of AMPA and NMDA receptor-mediated currents, a minimal stimulation paradigm was applied. The AMPA receptor-mediated currents were measured at a holding potential of -60 mV, while for the NMDA component, 10 μM DNQX were added to the bath, and a holding potential of +40 mV was provided. For the analysis of the input number, the stimulation intensity was gradually increased in increments of 2 to 10 V. Inhibitory (glycinergic and GABAergic) or excitatory (AMPA and NMDA) postsynaptic currents were isolated by applying 1 μM strychnine and 10 mM SR95531 or 10 mM DNQX and 25 mM DL-AP5 to the bath, respectively.

The mEPSCs were measured in a gap-free paradigm for at least three minutes, while inhibitory currents and voltage-gated sodium channels were pharmacologically blocked with 1 μM strychnine, 10 mM SR95531 and 1 μM TTX, respectively. Cells were voltage-clamped to -70 mV to increase the driving force and to obtain a better signal-to-noise ratio.

Short-term plasticity was determined using trains of stimuli at different frequencies (1, 10, 50, 100, 200, and 300 Hz; 15 pulse; 10 repetitions). For Part 1 a minimal stimulation paradigm was applied, whereas in Part 3 a maximal stimulation paradigm was used in order to subsequently determine the RRP and its properties.

For all electrophysiological measurements, stimulus generation and recordings were acquired using pCLAMP (Axon Instruments, USA). Currents and voltage signals were low-pass filtered at 10 kHz with a Bessel filter, sampled at a rate of 20-100 kHz, and analyzed using Clampfit 10.0 (Axon Instruments, USA) and customized macros in IGOR Pro (Wavemetrics, USA).

5.7 Data analysis

5.7.1 Membrane properties

A junction potential of -10.5 mV was subtracted for recordings using a K-Gluconate solution. The resting membrane potential was calculated as the mean value of the first 80 ms before hyperpolarizing or depolarizing steps were applied. Membrane time constant and input resistances were evaluated from the voltage response to a current injection of -100 pA. Membrane time constants were calculated by fitting single-exponential functions to the voltage traces. Input resistances were measured at peak and at steady state shortly before the hyperpolarizing step ended, according to Ohm's law. Amplitude values at peak and steady state were used to calculate the I_h component as follows:

$$I_h = \frac{voltage_{peak} - voltage_{steady\ state}}{voltage_{steady\ state}} \cdot 100.$$

For analyzing the active membrane properties, the action potential or the train of action potentials elicited by the lowest current injection was used to measure current threshold, voltage threshold, action potential half-width, and amplitude. The current threshold equals the injected current step that elicited the first action potential or train of action potential. Furthermore, the precise voltage threshold was determined as the maximal value of the third derivative located at the point where the action potential starts to rise suddenly (Lu et al. 2012). Half-width was measured at the half-maximal amplitude of the action potential,

while the action potential amplitude was measured as net voltage between resting potential and the peak of the action potential.

5.7.2 I_h measurements

The I_h amplitude of I_h currents was calculated 1 ms before the offset of the voltage step. Half-maximal activation of I_h was computed from tail currents. Tail current amplitudes were measured 20 ms after the termination of the hyperpolarizing voltage steps. These amplitudes were normalized to the maximal amplitude of each neuron. Values were fitted to a Boltzmann function to obtain the half-maximal voltage $V_{1/2}$.

5.7.3 Postsynaptic currents after single stimulations

During synaptic stimulation experiments, the number of input fibers was determined by visually identifying groups of similar excitatory postsynaptic current (EPSC) and inhibitory postsynaptic current (IPSC) amplitudes while stimulation intensities were gradually increased from 3 to 80 V. Each group presumably reflects the activation of an individual input fiber (Kim and Kandler 2003; Walcher et al. 2011). A 10–90% rise time and tau decay (fitting of a single-exponential function) of synaptic currents were assessed from responses evoked by minimal stimulation. The minimal stimulation strength is defined as stimulation strength where a stepwise increase of 2 V results in the first measurable postsynaptic current (PSC).

5.7.4 Miniature EPSCs

For each cell, an individual template to identify all real miniature events was created using Clampfit 10.0. The miniature EPSCs were counted, and the frequency was determined by this value and the duration of the measurement. Furthermore, mEPSCs were averaged, and amplitudes, charges, and time constants were calculated. Charges were calculated as an integral of the event using Clampfit 10.0. Time constants were determined as described for postsynaptic currents (see Section 5.7.3).

5.7.5 Short-term plasticity

To estimate short-term plastic changes of excitatory and inhibitory inputs to repetitive stimulations (1–300 Hz, 15 pulses, 10 repetitions), PSC amplitudes of the trains were normalized to the first amplitude. For calculating net amplitudes at high frequencies, a decay function was fitted to the preceding current pulse and set as a new baseline. The amplitude of the respective pulse was measured as a subtraction of the maximum and the new baseline. From these normalized depression curves, steady-state depression was obtained by the mean of the last three PSC amplitudes.

To analyze presynaptic properties such as the RRP, release at the maximal response, and the ratio of these two, an Elmquist-Quastel plot (EQ plot; see Figure 8) was calculated. There, the individual release is plotted as a function of the cumulated release throughout the train stimulation. The individual release was calculated as the amplitude of the respective EPSC divided by the average mEPSC amplitude of the particular age and/or genotype. The cumulated release was determined by a stepwise cumulation. A linear regression was inserted in the plot to the first three data points of cumulated release and was extrapolated to the x-intercept. This value theoretically resembles the RRP and was used for further calculations. The release at the maximal response is the number of vesicles released at the EPSC with the largest amplitude among the train stimulation. The ratio was determined by dividing the release at the maximal response by the RRP.

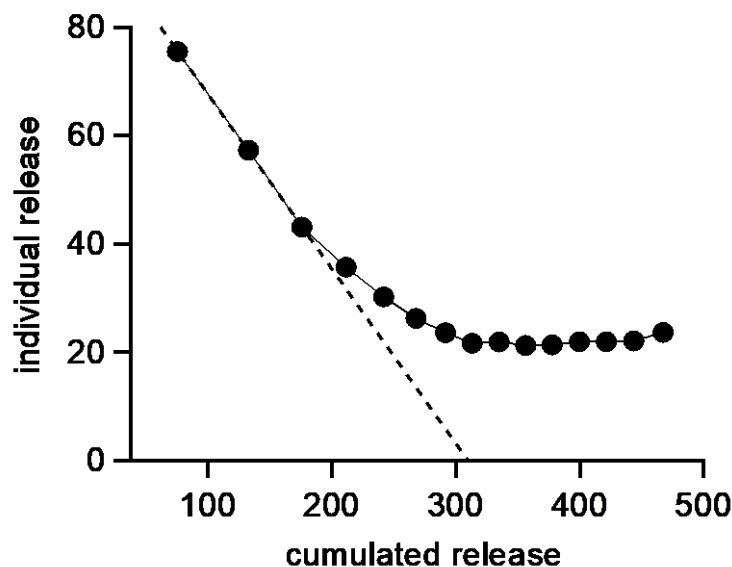


Figure 8: Elmquist-Quastel plot of a representative WT animal. The individual release is plotted as a function of the cumulated release. A linear regression is calculated for the first three individual releases and extrapolated to the x-intercept. This value represents the theoretical readily releasable pool.

5.8 Statistics

Results are given as mean \pm standard error of the mean (SEM). Data were first analyzed for homogeneity of variance and normality, and according to the result statistical significance was determined using unpaired student's t-test, a single-factor ANOVA followed by a Scheffé's *post hoc* test, or a two-factor ANOVA followed by a Dunn's *post hoc* test for data that qualified for parametric distributions. Non-parametric distributions were statistically analyzed using either a Mann-Whitney test or a Kruskal-Wallis test followed by a Games-Howell or Tukey's *post hoc* test. Statistical thresholds were * $P < 0.05$, ** $P < 0.01$, and *** $P < 0.001$. Programs used for statistical analysis were Microsoft Excel (Microsoft, Redmond, WA, USA), RealStatistics as add-in for Microsoft Excel, GraphPad Prism 6 (GraphPad Software, San Diego, USA), and IgorPro (Wavemetrics, Portland, OR, USA).

5.9 Immunohistochemistry

Eighteen animals (12 C57Bl/6 and 6 otoferlin WT and KO) were anesthetized by an intraperitoneal injection of Fentanyl (Janssen-Cilag), Medetomidin (Ratiopharm) and Metformin (Pfizer). They were perfused transcardially with 0.1 M phosphate buffer (PB; 7.4) for 3 minutes followed by paraformaldehyde (Carl Roth, Karlsruhe, Germany; PFA; 4% in 0.1 M pB; pH 7.4) for 15 minutes. Immediately after perfusion, brains were removed and post-fixed overnight in 4% PFA at 4°C. Brains were thoroughly washed at room temperature with 0.1 M phosphate buffer saline (PBS; pH 7.4). Coronal brain sections of 50 μ m were obtained using a vibratome (VT1200, Leica, Germany). Sections containing the VNLL were collected. Unspecific binding was blocked by incubating the sections in solution containing 10% normal donkey serum (NDS; GeneTex, USA), 0.2% Triton-X-100 (Carl Roth, Karlsruhe, Germany), and 0.1 M PBS for an hour at room temperature. Slices were subsequently incubated overnight in the primary antibody solution containing mouse anti-HCN1 (NeuroMab; dilution 1:1000), and/or goat anti-calretinin (Millipore; dilution 1:4000), and/or rabbit anti-VGluT1 (SynapticSystems; dilution 1:500), and/or chicken anti-MAP2 (Neuromics; dilution 1:1000), 3% NDS, and 0.2 Triton-X-100 in 0.1 M PBS. Slices were thoroughly washed in PBS for half an hour and incubated in the

secondary antibody solution containing Alexa 488 donkey anti-mouse (Life Technologies; dilution 1:250), and/or Cy3 donkey anti-goat (Dianova; dilution 1:300), and/or DyLight405 donkey anti-rabbit (Dianova; dilution 1:300), and/or Alexa 647 donkey anti-chicken (Dianova; dilution 1:300), 3% NDS, and 0.2% Triton-X-100 in 0.2 M PBS. An overview of all antibodies used is provided in Table 1. Negative controls were obtained by omitting the primary antibody. Sections were washed several times in 0.1 M PBS, mounted, and covered with homemade anti-fading mounting media (Indig et al. 1997).

Table 1 | List of primary and secondary antibodies used in the experiments.

Primary antibodies			
Antibody against	Host	Dilution	Company
HCN1	Mouse	1:1000	Neuromab
Calretinin	Goat	1:4000	Millipore
VGluT1	Rabbit	1:500	SynapticSystems
MAP2	Chicken	1:1000	Neuromics
Secondary antibodies			
Host: Donkey			
Antibody against	Fluorophore	Fluorophore	Company
Mouse	Alexa488	1:250	Life Technologies
Goat	Cy3	1:300	Dianova
Rabbit	DyLight405	1:300	Dianova
Chicken	Alexa647	1:300	Dianova

5.10 Confocal microscopy

All sections were analyzed with a Leica SP8 confocal laser scanning microscope (TSC SP8, Leica Microsystems). The microscope was equipped with a 5x HCX PL FLUOTAR objective (NA 0.15), a 20x HC PL APO Imm Corr objective (0.75 NA) and a 63x HCX PL APO immersion oil objective (1.4 NA). The pinhole was set to 1 Airy unit for each channel. Illumination and detection pathways were separated for each fluorophore, and individual color channels were sequentially acquired to avoid bleed-through artifacts. The acquisition settings were adjusted to cover the entire dynamic range of detectors and remained unchanged during the course of the imaging process. Four laser lines were used for visualization. DyLight 405, Alexa 488, Cy3 and Alexa 647 were excited by an UV laser line, an Ar-Ion-Laser line of 488 nm, the single DPSS 561 nm laser line, and HeNe single laser line of 633 nm, respectively. Z-stacks of confocal images were obtained, and maximal projections of 4 to 6 single optical sections were used for high magnification figures. Stacks of confocal images were analyzed and processed using ImageJ (NIH, USA).

6 Results

Statement of involvement

The results are divided into three individual projects. Not all data were obtained by me, Franziska Caspari. Therefore, a statement of involvement of which experiments I performed is given here.

Part 1: Characterization of the VNLL

I performed all electrophysiological experiments in the dVNLL and some in the vVNLL. The remaining electrophysiological data were obtained by Dr. Veronika Baumann, and immunostainings were done by Dr. Elisabet Garcia-Pino. I performed the analysis of all data that I obtained.

Part 2: Development of the calyx-like synapse in the VNLL

I performed all experiments and analyses in this part.

Part 3: The impact of deafness on intrinsic and neuronal development in the VNLL

I performed all experiments and analyses in this part.

6.1 Part 1 – Characterization of the VNLL

We are interested in investigating the VNLL because it may play an important role in the analysis of acoustic temporal features found in speech (Aitkin et al. 1970; Covey and Casseday 1991; Recio-Spinoso and Joris 2014). In the first part of this thesis, we characterize the VNLL along its ventrodorsal axis, since this has not been systematically achieved in previous studies. We aim to identify similarities and differences in intrinsic and synaptic properties of the VNLL. Furthermore, the margins of the VNLL – especially of the dorsal VNLL – are still unclear, and we wish to define them through an electrophysiological approach.

6.1.1 Intrinsic properties differ between neurons of the dorsal and the ventral parts of the VNLL

Neuron types are largely determined by their biophysical membrane properties, which are dependent on the composition of ion channels in the membranes. To find out whether there is a systematic distribution of neuronal cell types across the VNLL, we analyzed intrinsic membrane properties with respect to their location within the VNLL in a brain slice preparation of young adult mice (P22–23).

The VNLL is an elongated structure with ventral and dorsal areas that are enriched with neurons (Figure 9A). In ventral VNLL (vVNLL) neurons, depolarizing current injections elicited an onset-type firing pattern in 34 out of 37 samples (Figure 9B). In the remaining three neurons, depolarization induced an onset-burst firing pattern (data not shown). In all vVNLL neurons, a negative current injection led to a large hyperpolarization followed by a slowly depolarizing voltage sag. In the dorsal part of the VNLL (dVNLL), positive current injections induced either an onset-type firing pattern (n=19) or a sustained firing pattern (n=9; Figure 9C). In onset-type firing neurons, negative current injections induced a small hyperpolarization which repolarized rapidly. In sustained-firing neurons, the hyperpolarization was more pronounced with a prominent voltage sag. Onset-type firing neurons of the vVNLL and dVNLL significantly differed in their resting membrane potential, their membrane time constant, and their input resistance (Figure 9D–F; Table 2). Onset-type firing neurons of the dVNLL were fastest and exhibited the smallest peak input

resistance, suggesting different subpopulations of onset-type firing neurons in the vVNLL and dVNLL.

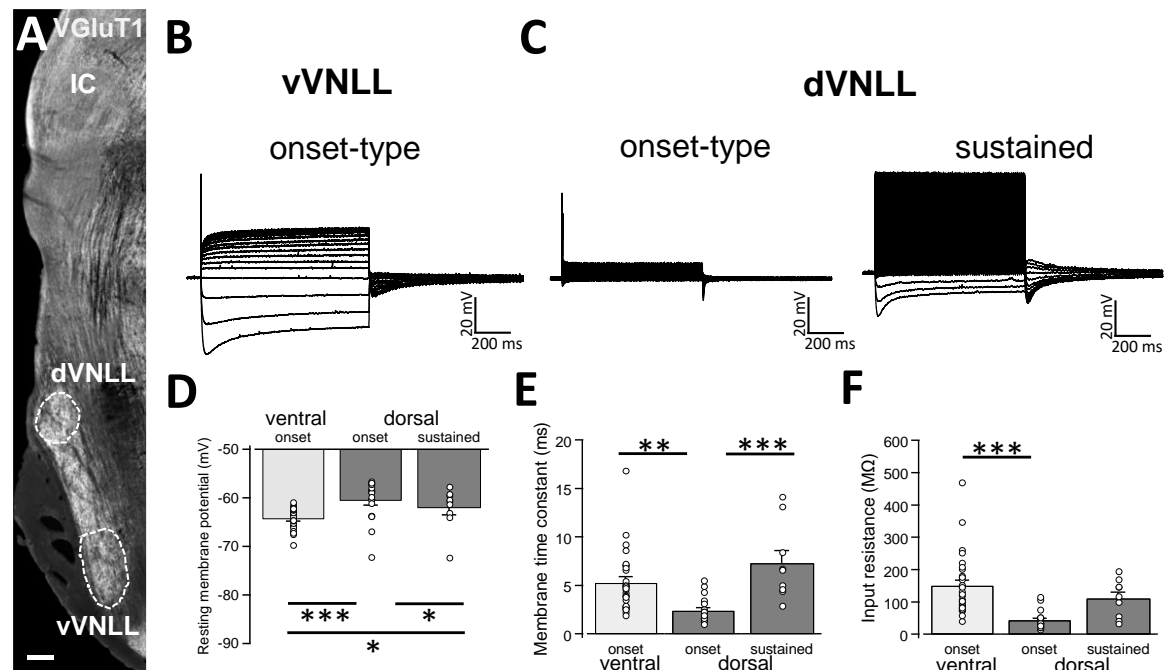


Figure 9: Intrinsic properties differ between vVNLL and dVNLL neurons. **A.** Low-power image with VGlut1-labeling illustrates the relative location of the VNLL within the auditory brainstem. The dorsal and ventral parts of the VNLL (dVNLL and vVNLL, respectively) are marked with a dashed line to show the respective recording sites. Scale bar: 200 μ m. **B.** Representative voltage responses to hyperpolarizing and depolarizing current injections recorded from vVNLL neurons. Depolarizing current injections elicited an onset-type firing pattern in vVNLL neurons. **C.** Depolarizing current injections elicited different types of firing patterns in dVNLL neurons: onset-type (left) and sustained (right) firing pattern. **D.** Resting potential is significantly different between all neuronal subtypes. Ventral onset: $n=34$; dorsal onset: $n=19$; dorsal sustained: $n=9$. **E.** Membrane time constant is significantly different between onset-firing neurons and between dorsal neurons. A single-exponential function is fitted to the first few milliseconds of the voltage response to a current injection of -100 pA; tau is extracted. **F.** Input resistance is significantly different between onset firing ventral and dorsal neurons.

All data sets were tested for normality and homogeneity of variance, and according to the result, statistical significance was determined by a non-parametric Kruskal-Wallis test followed by either a Tukey's or Games-Howell *post hoc* test.

Significant differences are labeled with * ($P<0.05$), ** ($P<0.01$), and *** ($P<0.001$).

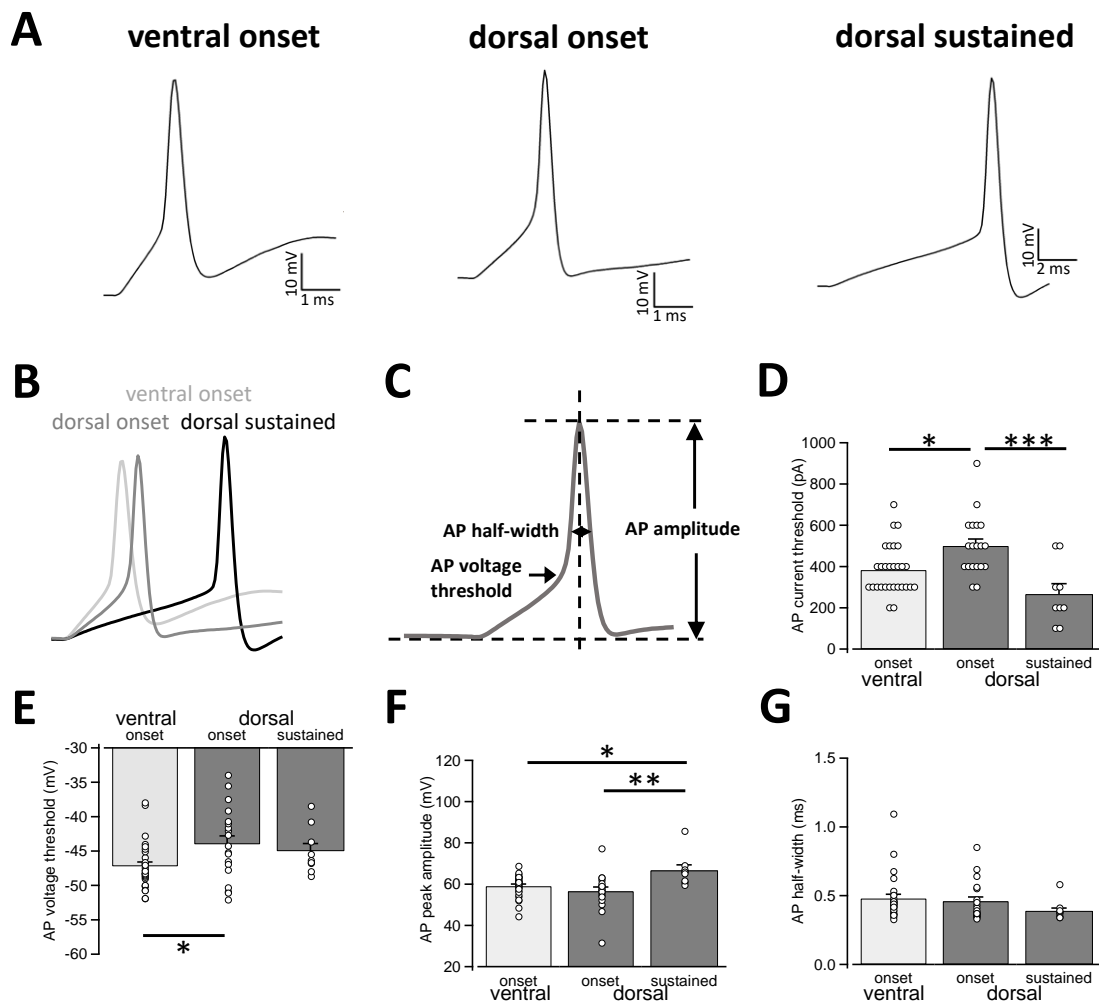


Figure 10: Heterogenous firing properties differ between neurons of the dVNLL and vVNLL. **A.** Representative expanded voltage traces recorded from a vVNLL neuron (left) and from dVNLL neurons (middle: onset; right: sustained) during the first suprathreshold depolarizing current injection. **B.** Overlap of all first suprathreshold action potentials shown in **A**. **C.** Schematic diagram illustrating the analysis of the active membrane properties. The first action potential (AP) elicited by the lowest current injection was used for analysis. **D.** Current threshold eliciting the first action potential for vVNLL and dVNLL neurons. Significant differences are given for onset-firing neurons between ventral and dorsal parts and between onset- and sustained-firing neurons of the dorsal part. **E.** Voltage threshold is significantly different between onset-firing neurons of vVNLL and dVNLL neurons. **F.** AP amplitude is significantly different in sustained-firing neurons compared to onset-firing subtypes of both the vVNLL and dVNLL. **G.** AP half-width of the first elicited AP for vVNLL and dVNLL neurons.

vVNLL onset-type neurons: $n=34$; dVNLL onset-type neurons: $n=19$; and dVNLL sustained: $n=9$.

All data sets were tested for normality and homogeneity of variance, and according to the result, statistical significance was determined by a non-parametric Kruskal-Wallis test followed by either a Tukey's or Games-Howell *post hoc* test.

Significant differences are labeled with * ($P < 0.05$), ** ($P < 0.01$), or *** ($P < 0.001$).

We next analyzed active membrane properties of the different VNLL cell types at the first suprathreshold response (Figure 10A). Onset-firing neurons of the ventral and the dorsal regions differed significantly in current and voltage threshold, whereas sustained-firing neurons of the dorsal part displayed differences from onset-type firing neurons of both regions regarding AP amplitude (Figure 10D-F; Table 2). Sustained-firing neurons of the dVNLL had the lowest current threshold and largest AP amplitudes, while onset-type firing cells of the same region had the highest current threshold of all neurons measured (Figure 10D-F; Table 2). The AP half-width did not differ between vVNLL and dVNLL neurons (Figure 10G; Table 2).

We conclude that the dVNLL consists of two different subpopulations of neurons with distinct intrinsic membrane properties. The population of vVNLL neurons, however, seems to be fairly uniform in its intrinsic properties.

Table 2 | Summary of membrane properties of dVNLL and vVNLL neurons

Values are mean \pm SEM. The level of significance between ventral and dorsal was determined using Scheffé's *post hoc* test following a single-factor ANOVA test (* $P < 0.05$, ** $P < 0.01$, *** $P < 0.001$).

a: significant differences between dVNLL onset-type and dVNLL sustained-firing neurons

b: significant differences between dVNLL sustained-firing and vVNLL neurons

c: significant differences between vVNLL and dVNLL onset-type firing neurons

n.s.: not significant

	Ventral	Dorsal		P
	onset (n=34)	onset (n=19)	sustained (n=9)	
Passive membrane properties				
resting potential (mV)	-64.5 \pm 0.4	-60.6 \pm 0.9	-62.1 \pm 1.4	* .*.*** a, b, c
input resistance (M Ω)	151.7 \pm 43.8	43.8 \pm 6.3	111.4 \pm 19.4	*** c
membrane time constant (ms)	5.36 \pm 0.51	2.41 \pm 0.29	7.31 \pm 1.30	*** .** a, c
Active membrane properties				
current threshold (pA)	376.5 \pm 19.4	500.0 \pm 33.3	266.7 \pm 50.0	*** . * a, c
voltage threshold (mV)	-36.7 \pm 0.6	-33.5 \pm 1.2	-34.5 \pm 1.1	* c
AP amplitude (mV)	58.7 \pm 0.9	56.6 \pm 2.0	66.7 \pm 2.6	** . * a, b
AP half-width (ms)	0.47 \pm 0.03	0.46 \pm 0.03	0.39 \pm 0.02	n.s

6.1.2 VNLL neurons have large hyperpolarization-activated currents (I_h) compared to ventral VNLL neurons

Differences in the resting membrane potential and the dorsal voltage sag induced by hyperpolarization in dorsal and ventral VNLL neurons indicate a differential distribution of HCN channels between the two parts. Our electrophysiological measurements of I_h in different parts of the VNLL revealed only small I_h amplitudes in the vVNLL (Figure 11A, left), whereas I_h amplitudes were large in dVNLL neurons (Figure 11A, right). Consequently, I_h density was significantly larger in dVNLL neurons compared with vVNLL neurons (at -110.5 mV vVNLL: -24.0 ± 3.4 pA/pF, $n=13$; dVNLL: -84.3 ± 12.9 pA/pF, $n=12$; student's unpaired t-test, $P=0.0006$; Figure 11B, C). Half-maximal activation voltage for HCN channels in the dVNLL was -88.3 ± 3.0 mV ($n=10$, Figure 11D), while tail currents evoked in vVNLL neurons were too small to be reliably analyzed. Consistently, immunostainings against the HCN1 subunit revealed that this subunit is strongly expressed in the dVNLL, whereas neurons in the vVNLL are mostly HCN1 negative (Figure 11E1–3), indicating that HCN1 channels are the predominant isoform in dVNLL neurons.

Neurons in the vVNLL all have onset-type firing patterns, little I_h , and relatively large input resistance during hyperpolarization. By contrast, all dVNLL neurons have large I_h currents and small input resistance, which results in short membrane time constants during hyperpolarization.

6.1.3 Lateral vVNLL neurons have extremely large excitatory postsynaptic currents

We were further interested in discovering to what extent the excitatory and inhibitory input properties differ between the two regions. Inputs were stimulated in the fiber bundle about 50 μm ventral to the recorded neuron, and EPSCs were isolated pharmacologically. Stimulation intensity was systematically increased to estimate the number of input fibers (=step number; see Chapter 5 “Material and methods”). During these experiments, we noticed that the vVNLL can be subdivided into two neuronal populations based on the estimated number and peak amplitude of excitatory inputs the neurons received. A large population of vVNLL neurons located in a cluster lateral to the fiber bundle all exhibited

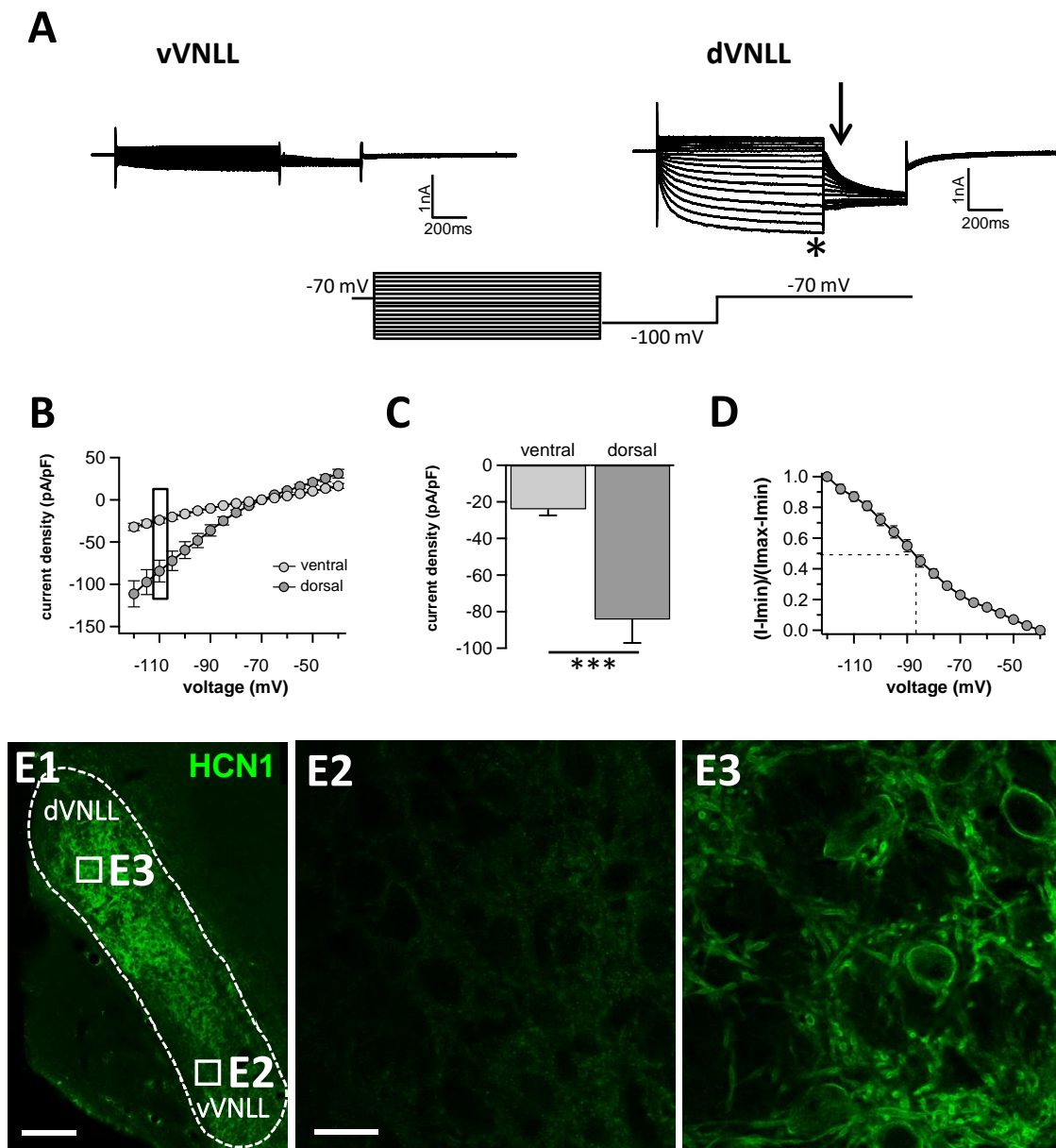


Figure 11: Dorsal VNLL neurons have larger hyperpolarization-activated currents (I_h) and stronger HCN1 immunoreactivity. **A.** Representative current traces recorded from vVNLL (left) and dVNLL (right) neurons to voltage steps ranging from -40 to -120 mV in 5 mV step increments. Each voltage step lasted for 1 s and was followed by a voltage step to -100 mV for 0.5 s to elicit the tail current to determine the voltage dependence of I_h activation. Holding potential was set to -70 mV. **B.** Current density-voltage relationship for dVNLL and vVNLL neurons. Current amplitudes were measured at steady-state (indicated by the asterisk in A). Rectangular labeling exemplified in C. **C.** Current density at -110 mV for vVNLL and dVNLL neurons is significantly different. vVNLL: $n=12$; dVNLL: $n=13$. **D.** The voltage-dependence of I_h -activation was determined from the tail current 20 ms after the end of the voltage steps (indicated by the arrow in A). Values were fitted with a Boltzmann function. Half-maximal activation voltage for dVNLL neurons was at around -88 mV ($n=10$). Half-maximal voltage of vVNLL neurons is not shown because almost no current is present. Data are obtained from eight C57/Bl6J mice. **E.** Confocal images of HCN1 immunostaining in the VNLL. **E1.** Overview illustrating a gradient of HCN1 staining in the VNLL. **E2.** High magnification of a region within the vVNLL reveals that HCN1 staining is almost absent. **E3.** High magnification of a region within the dVNLL shows strong HCN1 staining confined to the membrane. Same scale as in E2. Scale bar: E1 (200 μm); E2 (20 μm). (Continued on page 62)

Figure 11 continued:

All data sets were tested for normality and homogeneity of variance, and according to the result, statistical significance was determined by an unpaired student's t-test.

Significant differences are labeled with *** ($P < 0.001$).

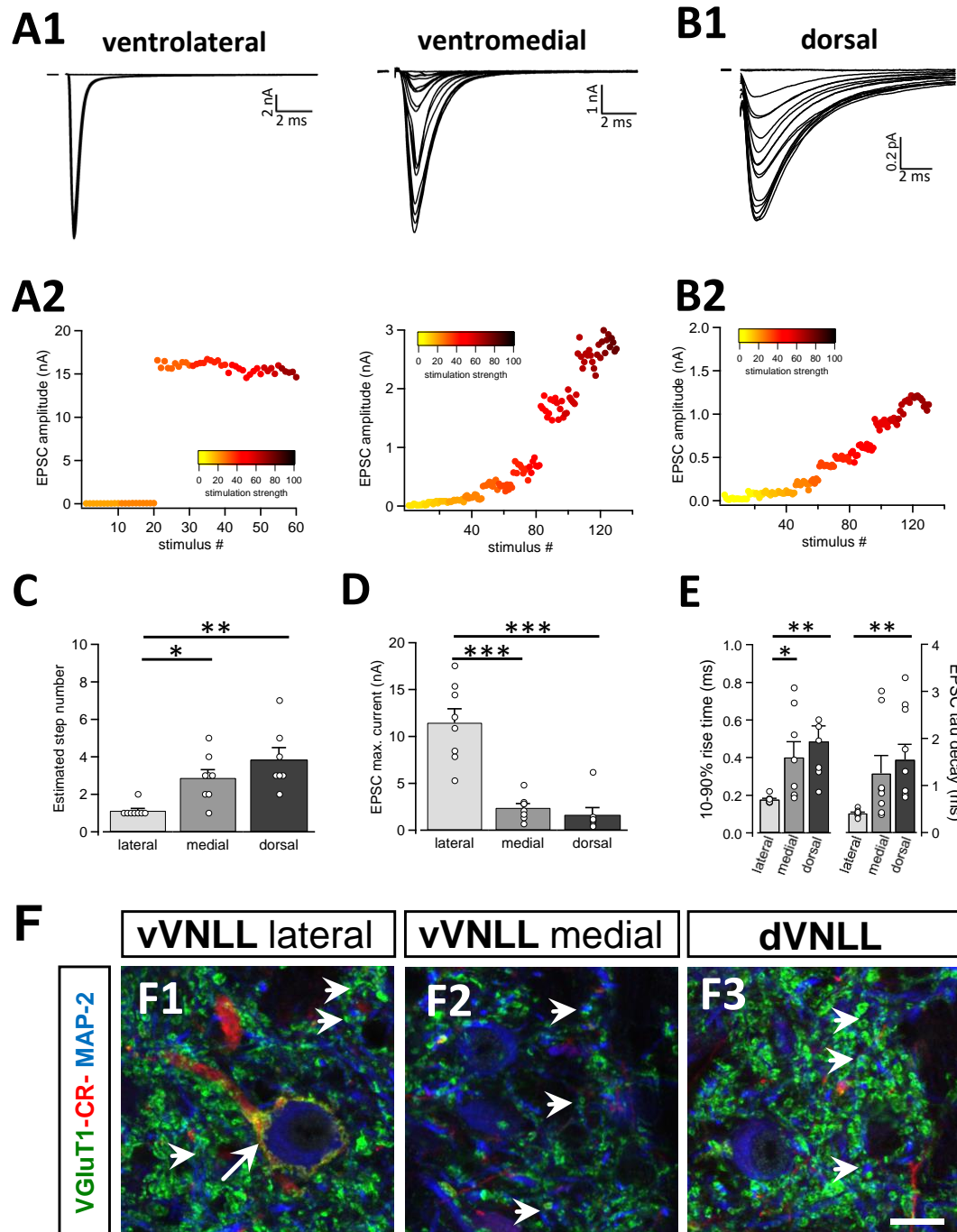


Figure 12: Excitatory postsynaptic currents are larger and the excitatory inputs are stronger in vVNLL neurons. A1. Representative EPSC traces of ventrolateral (left) and ventromedial (right) VNLL neurons. Responses were evoked by increasing stimulation strength. One strong input was found in most ventrolateral neurons, whereas medial neurons (Continued on page 63)

← **Figure 12 continued:** showed multiple inputs. All traces represent the average of at least three consecutive recordings to the same stimulus strength. **A2.** EPSC amplitude as a function of stimulus number recorded from ventrolateral and ventromedial vVNLL neurons shown in A1. **B1.** Representative EPSC traces of dVNLL neurons. Responses were evoked with increasing stimulation strength. This neuron shows seven distinct current steps. Note the considerably smaller maximal amplitude compared with ventrolateral VNLL neurons. All traces represent the average of at least three consecutive recordings to the same stimulus strength. **B2.** EPSC amplitude as a function of stimulus number recorded from the dVNLL neuron shown in B1. **C.** Number of EPSC steps evoked by increasing stimulation strength in vVNLL and dVNLL neurons. Ventrolateral VNLL neurons generally receive one, maximally two excitatory inputs, whereas ventromedial and dVNLL neurons receive one to seven inputs. vVNLL: lateral n=8, medial n=8; dVNLL n=7. **D.** Maximal EPSC amplitude is significantly larger in ventrolateral vVNLL neurons. **E.** Rise time (left) and tau decay time (right) were measured in vVNLL and dVNLL neurons applying a minimal stimulation paradigm. Ventrolateral neurons are significantly faster than dVNLL neurons. **F.** Confocal images depicting VGluT1, calretinin (CR), and MAP-2 immunofluorescence in the lateral vVNLL (F1), the medial vVNLL (F2), and the dVNLL(F3). Note a VGluT1 and calretinin-positive ring found only around lateral vVNLL neurons (F1: long arrow), whereas punctate VGluT1-staining in the neuropil is widely distributed along the VNLL (F1–F3). Scale bar: 10 μm .

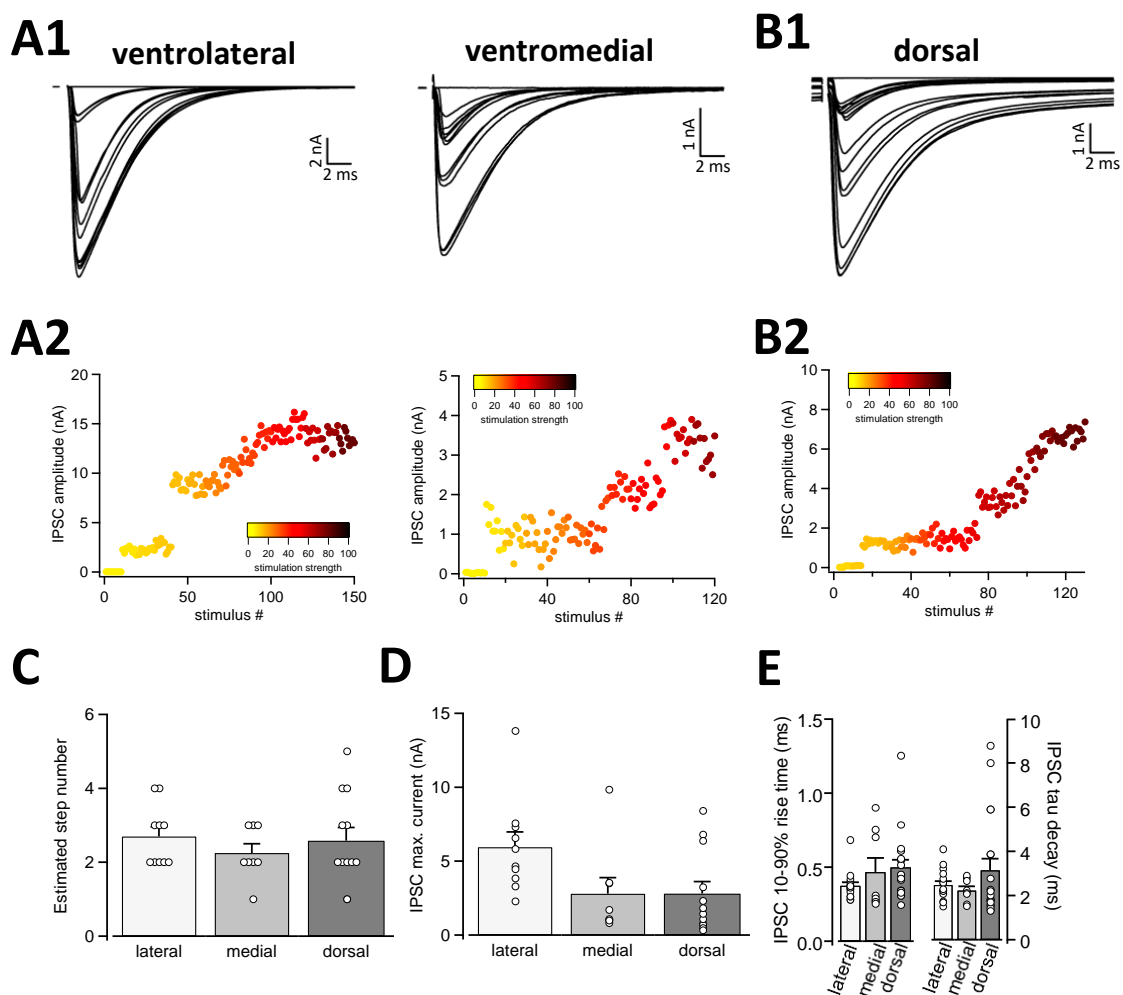
All data sets were tested for normality and homogeneity of variance, and according to the result, statistical significance was determined by a single-factor ANOVA test followed by a Scheffé's *post hoc* test. Significant differences are labeled with * ($P < 0.05$), ** ($P < 0.01$), or *** ($P < 0.001$).

an all-or-none EPSC response with extremely large amplitudes irrespective of stimulation strength (Figure 12A1–A2; left). This was different in the ventromedial part of the VNLL, where neurons are scattered within the fiber bundle. There, the EPSC amplitude gradually increased with rising stimulation strength, which indicates a convergence of several input fibers (Figure 12A1–A2; right). Step number and maximally evoked EPSC amplitude differed significantly between ventrolateral and ventromedial VNLL neurons (Figure 12C, D; Table 3). Excitatory input properties of neurons in the dVNLL very much resembled those found in the medial neurons of the vVNLL (Figure 12B1–B2; Table 3). Moreover, 10–90% rise time and tau decay time of EPSCs were much faster in ventrolateral than in ventromedial and dorsal neurons (Figure 12E; Table 3). We reanalyzed membrane properties according to their mediolateral location in the vVNLL. Nevertheless, membrane properties were very similar in medial and lateral VNLL neurons, despite the profound differences in excitatory input characteristics (resting membrane potential: ventrolateral -64.4 ± 0.4 mV, n=29; ventromedial -65.2 ± 0.8 mV, n=5; input resistance: ventrolateral -150.0 ± 17.3 M Ω ; ventromedial $-158.8 \pm$ M Ω ; membrane time constant: ventrolateral 5.30 ± 0.58 ms; ventromedial 5.71 ± 1.11 ms; data not shown). These physiological findings were corroborated by a differential distribution of VGluT1 and calretinin-positive presynaptic structures in different parts of the VNLL. Whereas in the ventrolateral VNLL

a distinct perisomatic VGluT1-positive ring, colocalized with calretinin, was detected around the somata (Figure 12F1), in both the ventromedial VNLL and the dorsal VNLL. VGluT1-staining appeared scattered in the neuropil, presumably representing dendritic inputs (Figure 12F2–F3). This implies that neurons in the ventrolateral VNLL receive one large excitatory synapse with calyx-like properties similar to MNTB neurons. In contrast, medioventral and dorsal VNLL neurons integrate several excitatory inputs with smaller amplitudes that terminate predominantly on the dendrites.

6.1.4 Inhibitory postsynaptic currents are similar in all vVNLL neurons

We were also interested in whether inhibitory input characteristics differ between the various subregions of the VNLL (Figure 13A1, A2, B1, and B2). In all three regions of the VNLL, the number of inhibitory inputs was very similar (Figure 13C; Table 3). In accordance with the excitatory input strength, maximal inhibitory input amplitude was larger in ventrolateral neurons compared with other VNLL areas (Figure 13D; Table 3),



← **Figure 13: Inhibitory inputs are similar in vVNLL and dVNLL neurons.** **A1.** Representative IPSC traces of ventrolateral (left) and ventromedial (right) VNLL neurons. Responses were evoked by increasing stimulation strength. Multiple inputs were found in both ventrolateral and ventromedial neurons. All traces represent the average of at least three consecutive recordings to the same stimulus strength. **A2.** IPSC amplitude as a function of stimulus number recorded from the ventrolateral and ventromedial vVNLL neurons shown in A1. **B1.** Representative IPSC traces of dVNLL neurons. Responses were evoked by increasing stimulation strength. This neuron shows four distinct current steps. All traces represent the average of at least three consecutive recordings to the same stimulus strength. **B2.** IPSC amplitude as a function of stimulus number recorded from the dVNLL neuron shown in B1. Multiple current steps can be seen. **C.** Number of IPSC steps evoked by increasing stimulation strength in vVNLL and dVNLL neurons. VNLL neurons receive two to three inputs. vVNLL: lateral n=10, medial n=8; dVNLL n=12. **D.** Maximal IPSC amplitude is similar in all VNLL regions. **E.** Rise time (left) and tau decay time (left) were measured in vVNLL and dVNLL neurons, applying a minimal stimulation paradigm. vVNLL: lateral: n=16; medial: n=10; dVNLL: n=14.

but values did not reach the level of significance. The temporal characteristics of inhibitory inputs were very similar in all parts of the VNLL (Figure 13E; Table 3).

Taken together, we determine that VNLL neurons exhibit similar inhibitory synaptic responses, suggesting a common origin of these inputs.

6.1.5 Synaptic short-term plasticity of excitatory and inhibitory inputs is similar in vVNLL and dVNLL neurons

We further characterized short-term plasticity (STP) of excitatory and inhibitory synapses in vVNLL and dVNLL neurons (15 stimuli at 1, 50, 100, 200, and 300 Hz). All excitatory and inhibitory inputs to VNLL neurons showed pronounced synaptic short-term depression that depended on the stimulation frequency (Figure 14A–B and D–E). In order to compare synaptic short-term depression of vVNLL and dVNLL neurons, the steady-state depression as a function of stimulus frequency is illustrated in Figure 14C and F. For both EPSCs and IPSCs, steady-state depression did not differ between vVNLL and dVNLL neurons for almost any stimulus frequency. Only for stimulation frequencies of 100 Hz steady-state depression of EPSCs was significantly smaller for vVNLL compared to dVNLL neurons (vVNLL: $50 \pm 7\%$; dVNLL: $68 \pm 5\%$, * $P < 0.05$, unpaired student's t-test). This is a further indication that excitatory inputs differ between the ventrolateral region and the other regions of the VNLL, whereas inhibitory input properties are very similar amongst neurons in the entire VNLL.

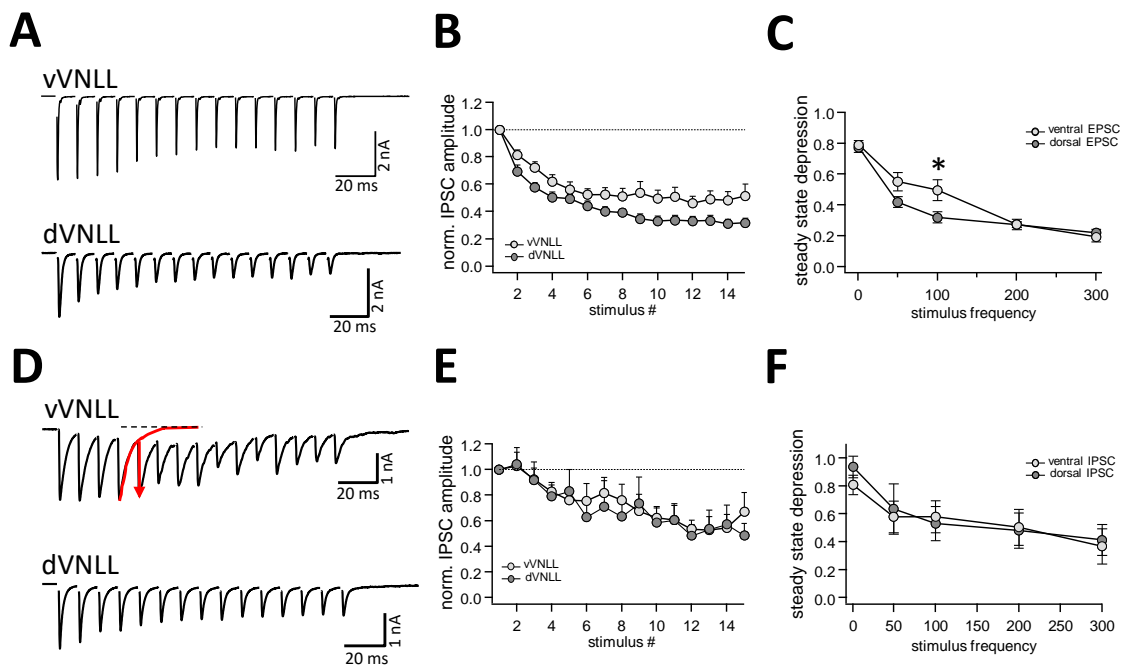


Figure 14: Synaptic short-term plasticity of excitatory and inhibitory inputs is similar in vVNLL and dVNLL neurons.

A. Representative EPSC traces in response to 15 stimulations at 100 Hz, illustrating short-term plasticity in ventrolateral (top) and dorsal (bottom) VNLL neurons. Net amplitudes at high frequencies were calculated by fitting a decay function (red trace in D) to the preceding current pulse, which was used to set a new baseline. The amplitude of the respective pulse was measured as a subtraction of the maximum and the new baseline (illustrated as red arrow in D). Same procedure was used for excitatory and inhibitory trains. **B.** Normalized EPSC amplitudes for 100 Hz stimulus in ventrolateral and dorsal VNLL neurons. **C.** Steady-state depression of EPSCs in ventrolateral and dorsal VNLL neurons. Steady-state depression is significantly different between vVNLL and dVNLL neurons for 100 Hz. **D.** Representative IPSC traces in response to 15 stimulations at 100 Hz, illustrating short-term plasticity in ventrolateral (top) and dorsal (bottom) VNLL neurons. **E.** Normalized IPSC amplitudes for 100 Hz stimulus in ventrolateral and dorsal VNLL neurons. **F.** Steady-state depression of IPSCs in ventrolateral and dorsal VNLL neurons.

EPSCs: vVNLL: $n=9$, dVNLL: $n=9$; IPSCs: vVNLL: $n=11$, dVNLL: $n=12$.

All data sets were tested for normality and homogeneity of variance, and according to the result, statistical significance was determined by an unpaired student's t-test. Significance is labeled with * ($P<0.05$).

Table 3 | Summary of synaptic properties of dVNLL and vVNLL neurons of C57Bl/6J mice

Values are mean \pm SEM. The level of significance between ventral and dorsal was determined using Scheffé's *post hoc* test following a single-factor ANOVA test or Games Howell *post hoc* test following Kruskal-Wallis for non-parametric distributions (* $P < 0.05$, ** $P < 0.01$, *** $P < 0.001$).

a: significant differences between lateral and medial neurons of the VNLL

b: significant differences between dVNLL and lateral vVNLL neurons

n.s.: not significant

	Ventral		Dorsal	P
	Lateral	Medial		
Excitatory postsynaptic currents				
Estimated fiber #	1.13 \pm 0.13 (8)	3.00 \pm 0.46 (8)	3.85 \pm 0.63 (7)	* _a ; ** _b
Maximal current (nA)	11.47 \pm 1.48 (8)	2.39 \pm 0.45 (8)	1.66 \pm 0.76 (7)	*** _a ; *** _b
10–90% rise time (ms)	0.18 \pm 0.01 (9)	0.40 \pm 0.08 (8)	0.44 \pm 0.04 (14)	* _a ; ** _b
Tau decay (ms)	0.31 \pm 0.01 (9)	1.24 \pm 0.37 (8)	1.63 \pm 0.24 (14)	** _b
Inhibitory postsynaptic currents				
Estimated fiber #	2.70 \pm 0.26 (10)	2.38 \pm 0.26 (8)	2.58 \pm 0.36 (12)	n.s.
Maximal current (nA)	5.95 \pm 1.03 (10)	2.80 \pm 1.08 (8)	2.80 \pm 0.81 (12)	n.s.
10–90% rise time (ms)	0.37 \pm 0.02 (16)	0.49 \pm 0.07 (10)	0.48 \pm 0.07 (14)	n.s.
Tau decay (ms)	2.47 \pm 0.17 (16)	1.88 \pm 0.11 (10)	3.06 \pm 0.68 (14)	n.s.

6.1.6 Neurons in the dorsal and ventral VNLL are all inhibitory

To test whether the neurons we recorded from were inhibitory and therefore part of the VNLL, we recorded from neurons of VGAT-ChR2-YFP⁺ mice. We tested the transmitter phenotype of neurons in both the vVNLL and dVNLL by applying short pulses of white light onto the slice while recording the membrane potential. All VNLL neurons, in both the dorsal and ventral parts, showed a pronounced depolarization in response to the light stimulus (Figure 15A, B, and D). The amplitude of the depolarization varied depending on the input resistance of the neuron (vVNLL: 3.8 ± 0.8 mV, n=6; dVNLL: onset-type 2.2 ± 0.4 mV, n=9, sustained 8.8 ± 2.3 mV, n=6; INLL: -1.4 ± 0.4 mV, n=8; Figure 15D). A population of small neurons in between our region of interest (dVNLL) and the DNLL did not depolarize during light application (Figure 15C and D). We therefore consider this

population to be glutamatergic and, according to Ito et al. (2011), to be INLL neurons, whereas our sample of neurons exhibits an inhibitory neurotransmitter type and thus is located within the VNLL.

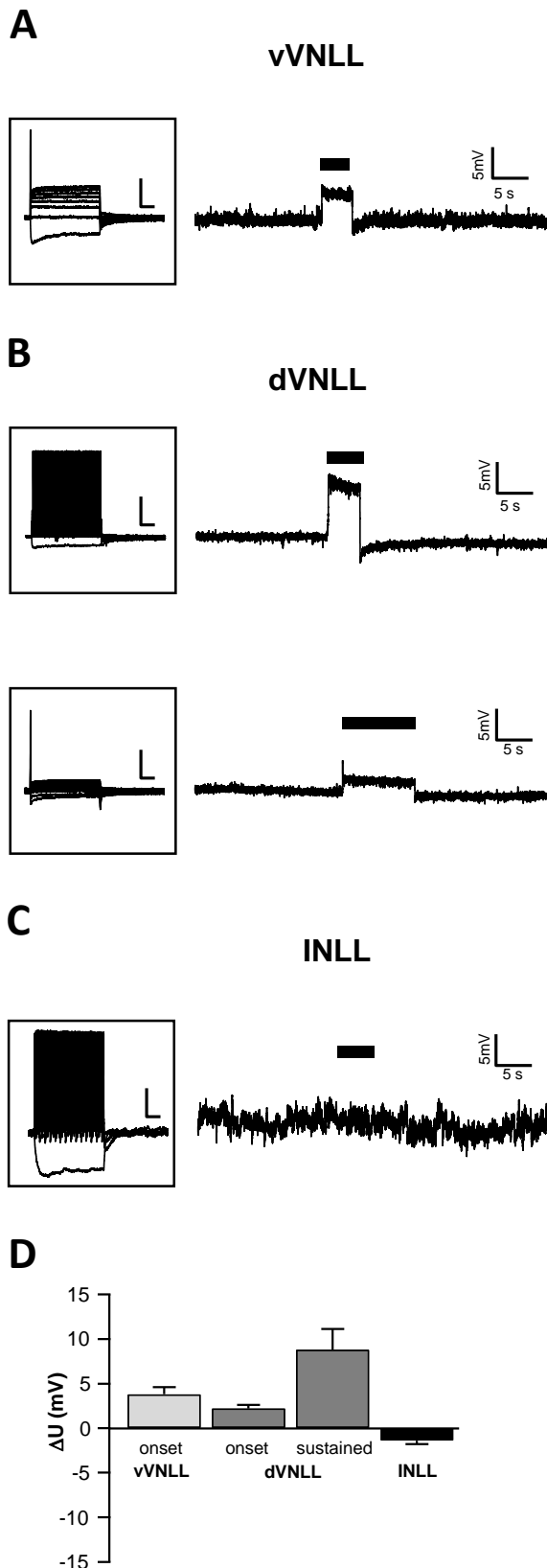


Figure 15: Both vVNLL and dVNLL neurons are inhibitory.

A. Representative voltage trace of a vVNLL neuron to light stimulation (indicated by the black bar). The neuron depolarizes in response to the light pulse. The inset depicts the corresponding firing pattern of the neuron. **B.** Representative voltage traces of an onset-type and a sustained-firing dVNLL neuron to light stimulation (indicated by the black bar). Both neurons depolarize in response to the light pulse. The insets illustrate the corresponding firing patterns of the respective dVNLL neuron. **C.** Representative voltage trace of an INLL neuron to light stimulation (indicated by the black bar). The inset depicts a representative IV curve for INLL neurons. **D.** Voltage deflection in response to light stimulation in VNLL and INLL neurons (vVNLL: $n=6$, dVNLL: sustained $n=6$, onset-type $n=9$; INLL: $n=8$). Scale bar insets: 200ms, 20mV.

6.2 Part 2 – Development of the calyx-like synapse in the VNLL

In Part 1 of this thesis, we found that the VNLL consists of three distinct regions differing in their firing patterns and synaptic inputs. The ventrolateral part in particular, from now on referred to as vVNLL, showed some very unique features such as neurons that fire exclusively in an onset-type manner and, moreover, have an interesting excitatory synaptic innervation. Neurons located in this ventrolateral cluster receive large calyx-like inputs that are comparable to MNTB innervation patterns (Borst et al. 1995; von Gersdorff and Borst 2002). Although previous studies demonstrated that VNLL neurons receive these large inputs ascending from the octopus cell region in the PVCN (Adams 1997; Schofield and Cant 1997; Felix Li et al. 2017), it was novel that, at least in mice, these neurons are organized in a cluster located in the ventrolateral part and that the dorsal VNLL and medioventral VNLL neurons showed especially distinct neuronal properties. Part 2 of this thesis focuses on the development of the calyx-like synapse in the vVNLL. We were interested in investigating when these neuronal particularities advance during development.

6.2.1 NMDA-current components of vVNLL neurons undergo a significant reduction during development

We were interested how AMPA and NMDA receptors are involved in neurotransmission during development and how the different current components change during the formation of mature synaptic properties.

The AMPA receptor-mediated currents were measured by pharmacological blockage of inhibitory current components (GABAergic and glycinergic currents) with SR95531 and strychnine in the ACSF. Neurons were voltage-clamped to -60 mV to avoid the opening of NMDA-receptors. A glass electrode was placed approximately 50 μm ventral to the recording site to electrically stimulate vVNLL neurons. In order to measure NMDA receptor-mediated currents, AMPA receptors were also pharmacologically blocked by DNQX, and the neuron was clamped to +40 mV.

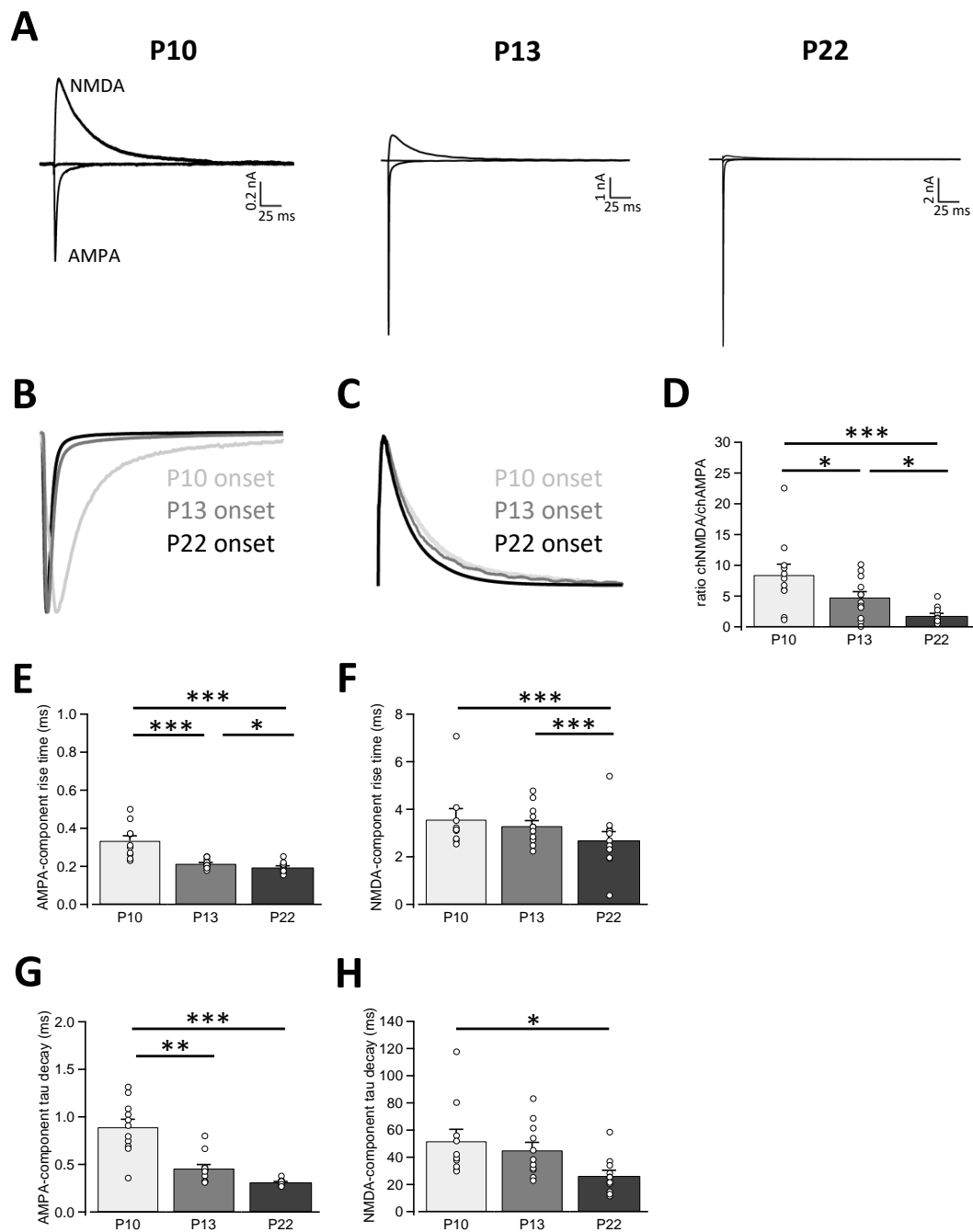


Figure 16: AMPA and NMDA components of vNLL neurons in Bl6 mice at P10, P13, and P22 undergo significant changes in size and time constants during development. **A.** AMPA and NMDA receptor-mediated currents of a representative P10 (left), P13 (middle), and P22 (right) animal. **B.** Normalized AMPA components of neurons shown in **A.** **C.** Normalized NMDA component of neurons shown in **A.** **D.** Charge ratios of NMDAR/AMPA-mediated currents of all measured neurons (P10: n=11, P13: n=12, P22: n=11). Significant differences are found between all age groups. **E.** AMPA-component rise time of all measured neurons. Rise times are significantly different between all age groups. **F.** NMDA-component rise time of all measured neurons. **G.** AMPA-component tau decay in all measured neurons. Tau decay times of P10 animals are significantly slower than in both older age groups. **H.** NMDA-component tau decay in all measured neurons. Tau decay times of P10 animals are significantly slower than in P23.

All data sets were tested for normality and homogeneity of variance, and according to the result, statistical significance was determined by a non-parametric Kruskal-Wallis test followed by either a Tukey's or Games-Howell *post hoc* test. Significant differences are labeled with * ($P < 0.05$), ** ($P < 0.01$), or *** ($P < 0.001$).

Figure 16A displays representative current traces of AMPA and NMDA receptor-mediated currents of P10, P13, and P22 animals. The P10 animals exhibited a much larger NMDA component, while their AMPA component was smaller than in P13 and P22 animals. The NMDA component was dramatically reduced less than two weeks after hearing onset. The normalized AMPA (Figure 16B) and NMDA (Figure 16C) receptor-mediated current traces of all age groups illustrate the different receptor kinetics analyzed in Figure 16E–H. Furthermore, we wished to compare the charge that is transmitted by these two current components, since NMDA receptors exhibited slow receptor kinetics, whereas AMPA receptors had much faster kinetics (Figure 16E–H; Table 4), and the charge resembled a clearer view on the actual current flux through the receptors. Therefore, we calculated the charge transmitted by NMDA and AMPA receptors and related them by determining the ratio of both charges. The results are depicted in Figure 16D (see also Table 4). Here, all age groups were significantly different from one another. A gradual decrease of the NMDA component is clear. In addition, rise times of the AMPA receptor-mediated current component decreased significantly after hearing onset and remained similar afterwards (Figure 16E), while the NMDA receptor rise times sped up only later in development (Figure 16F; Table 4). Furthermore, tau decays of AMPA receptors developed faster kinetics at P22 compared with both younger age groups (Figure 16G; Table 4). Tau decays of the NMDA component, however, decreased gradually during development, creating a significant difference only between P10 and P22 animals (Figure 16H; Table 4).

Altogether, a drastic change of AMPA and NMDA components takes place during development. Not only does the size of the NMDA receptor-mediated current decrease significantly while the AMPA receptor-mediated component increases, but receptor kinetics also undergo developmental reduction and become significantly faster.

Table 4 | Summary of AMPAR- and NMDAR-mediated currents of vVNLL neurons of P10, P13, and P22 Bl6 mice

Values are mean \pm SEM. The level of significance between groups was calculated with a Kruskal-Wallis test followed by Games-Howell or Tukey's *post hoc* tests (* $P < 0.05$, ** $P < 0.01$, *** $P < 0.001$).

a: significant differences between P10 and P13 animals

b: significant differences between P10 and P22 animals

c: significant differences between P13 and P22 animals

n.s.: not significant

	P10 n=11	P13 n=12	P22 n=11	P
Ratio chNMDA/chAMPA	8.43 \pm 1.75	4.77 \pm 0.94	1.79 \pm 0.41	* _a ; *** _b ; * _c
AMPA				
Rise time (ms)	0.33 \pm 0.03	0.21 \pm 0.01	0.19 \pm 0.01	*** _a ; *** _b ; * _c
Tau decay (ms)	0.89 \pm 0.08	0.46 \pm 0.04	0.31 \pm 0.01	** _a ; *** _b
NMDA				
Rise time (ms)	3.57 \pm 0.46	3.29 \pm 0.23	2.69 \pm 0.34	n.s.
Tau decay (ms)	51.8 \pm 8.8	45.1 \pm 5.9	26.3 \pm 4.1	* _b

6.2.2 Calyx-like excitatory inputs develop in the vVNLL around hearing onset in mice

We were further interested in how the development of excitatory postsynaptic currents in Bl6 animals progresses and whether synapse refinement is comparable to the early emergence found in calyx of Held synapses in the MNTB (Hoffpauir et al. 2006; Nakamura and Cramer 2011). The calyx of Held is already formed at P2, and only the shape is differentiated after that. To measure the strength of synaptic inputs and calculate receptor rise and decay times, we stimulated in the fiber bundle about 50 μ m ventral to the recorded neuron, and EPSCs were isolated pharmacologically. To estimate the number of fiber inputs, the stimulation intensity was gradually increased. We assume that each stepwise increase of EPSC amplitude as a response to a stimulation increment reflects the activation of additional synaptic inputs. Figure 17A1 illustrates a P10 example. In this example, three distinct EPSC current steps to a gradual increase of stimulation strength were found. This indicates the existence of three excitatory synaptic inputs to this specific vVNLL neuron.

Neurons of the vVNLL of P10 animals were innervated by one to seven fibers (Figure 17A1–A2 and E; Table 5). More than 80% of the recorded neurons exhibited more than one input (Figure 17E; Table 5). In neurons of P13 animals, however, a maximum of presumably two excitatory inputs was found (Figure 17B1–B2 and E; Table 5). The innervation pattern of neurons of P22 animals was similar compared with animals at P13, suggesting that synapse refinement takes place shortly after hearing onset (Figure 17C1–C2 and E; Table 5). Normalized EPSCs of the representative neurons of P10, P13, and P22 animals illustrated in Figure 17A, B, and C are displayed in Figure 17D. The differences in time constants between the age groups are especially clear. Significantly fewer neurons had two excitatory inputs in P13 and P22 animals compared with P10 animals (Figure 17E; Table 5). In addition, the maximally evoked postsynaptic current was significantly smaller in P10 animals (Figure 17F; Table 5). Furthermore, reduction of 10–90% rise times and tau decay times of EPSCs occurred still after P13, although the refinement of synaptic inputs was already completed, resulting in a significant difference between all age groups (Figure 17G; Table 5).

We conclude that during the development of the vVNLL, only neurons with one or maximally two excitatory synaptic inputs remain, and the duration of the postsynaptic response is significantly shortened due to an acceleration of postsynaptic AMPA receptors.

Table 5 | Summary of excitatory postsynaptic currents (EPSCs) of vVNLL neurons of P10, P13, and P22 B16 mice

Values are mean \pm SEM. The level of significance between groups was calculated with a Kruskal-Wallis test followed by Games-Howell or Tukey's *post hoc* tests (* $P < 0.05$, ** $P < 0.01$, *** $P < 0.001$).

a: significant differences between P10 and P13 animals

b: significant differences between P10 and P22 animals

c: significant differences between P13 and P22 animals

	P10 n=21	P13 n=14	P22 n=16	P
Estimated fiber #	3.38 \pm 0.41	1.07 \pm 0.07	1.19 \pm 0.10	*** _a ; *** _b
Maximal current (nA)	4.66 \pm 0.84	7.28 \pm 0.66	9.65 \pm 1.20	* _a ; *** _b
Average step size (nA)	2.37 \pm 0.71	6.81 \pm 0.68	8.20 \pm 1.04	** _a ; *** _b
10–90% rise time (ms)	0.42 \pm 0.04	0.21 \pm 0.01	0.18 \pm 0.00	** _a ; ** _b ; ** _c
Tau decay (ms)	0.93 \pm 0.13	0.43 \pm 0.03	0.30 \pm 0.01	** _a ; *** _b ; ** _c

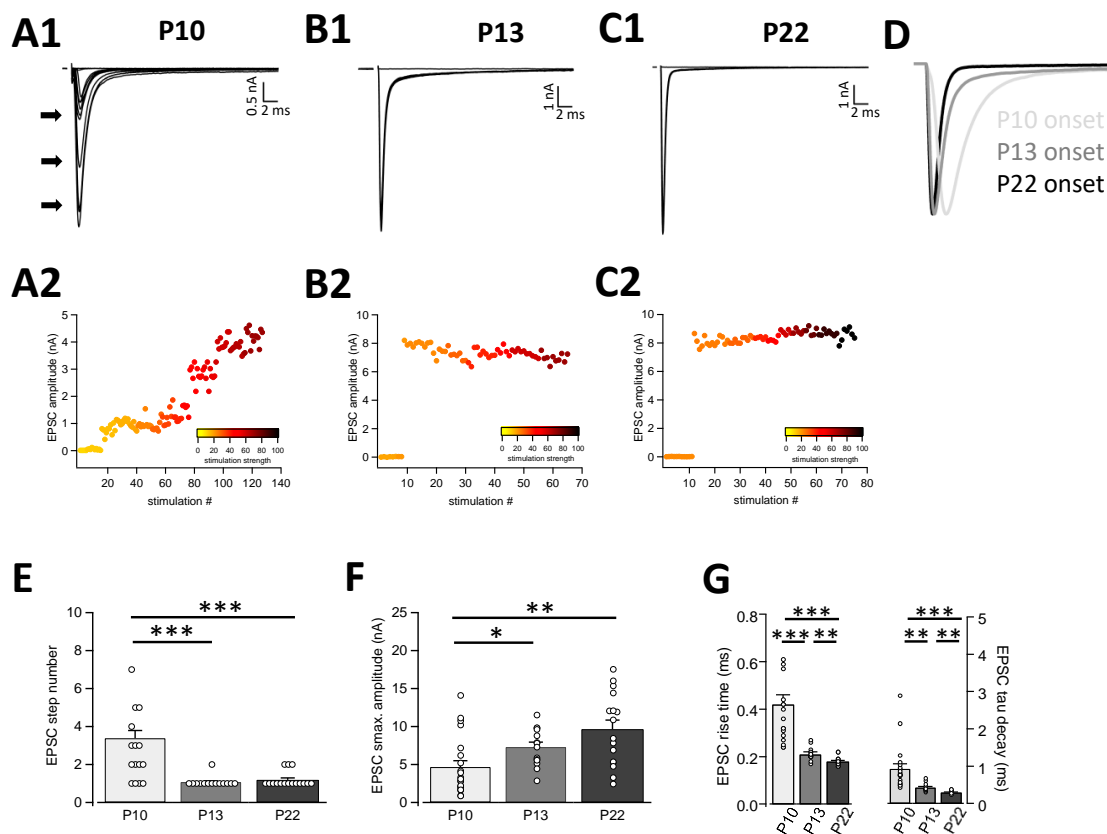


Figure 17: Excitatory postsynaptic currents (EPSC) of vVNLL neurons in BL6 mice at P10, P13, and P22 reduce the number of synaptic inputs while increasing synaptic strength in combination with faster time constants during development. **A1.** Average evoked current responses to increasing stimulation strengths of a representative P10 vVNLL neuron. All traces represent the average of at least five consecutive recordings to the same stimulation strength. Three distinct current steps are visible (arrows). **A2.** EPSC amplitude as a function of stimulus number recorded from a P10 vVNLL neuron shown in A1. The respective stimulation strength is color coded. **B1.** Average evoked current responses to increasing stimulation strengths of a representative P13 vVNLL neuron. All traces represent the average of at least five consecutive recordings to the same stimulation strength. One distinct current step is visible. **B2.** EPSC amplitude as a function of stimulus number recorded from a P13 vVNLL neuron shown in B1. The respective stimulation strength is color coded. **C1.** Average evoked current responses to increasing stimulation strengths of a representative P22 vVNLL neuron. All traces represent the average of at least five consecutive recordings to the same stimulation strength. One distinct current step is visible. **C2.** EPSC amplitude as a function of stimulus number recorded from a P22 vVNLL neuron shown in C1. The respective stimulation strength is color coded. **D.** Normalized maximal EPSC traces from P10 (light gray), P13 (dark gray), and P22 (black) as shown in A, B, and C. **E.** Estimated number of EPSC steps evoked by an increasing stimulation strength in vVNLL neurons of P10, P13, and P22 animals is significantly larger in P10 animals compared with both older age groups. P10: n=21, P13: n=14, P22: n=16. **F.** EPSC maximal amplitude of all recorded vVNLL neurons. Amplitudes in P10 animals are significantly smaller than in either older age group. **G.** EPSC 10–90% rise time (left) and tau decay time (right) of all recorded vVNLL neurons. Rise and decay times were significantly different between all age groups. For calculating tau decay, a single exponential function was fitted to the decay of the current response.

All data sets were tested for normality and homogeneity of variance, and according to the result, statistical significance was determined by a non-parametric Kruskal-Wallis test followed by a Games-Howell *post hoc* test. Significant differences are labeled with * ($P < 0.05$), ** ($P < 0.01$), or *** ($P < 0.001$).

6.3 Part 3 – The impact of deafness on the intrinsic and neuronal development in the VNLL

The first two parts of this thesis examined the characterization of the VNLL and the specific development of the ventrolateral part of the VNLL (vVNLL). In this part, we were interested in whether biophysical and synaptic changes depend on auditory-evoked activity. Therefore, we used a deaf mouse model. Otoferlin is a protein found in inner hair cells of the cochlea that is necessary for detecting calcium and vesicle fusion with the presynaptic membrane (Roux et al. 2006). A lack of otoferlin results in deafness due to an absent transmitter release in the ribbon synapse. Homozygous otoferlin KO (OTOF^{-/-}) are born deaf, whereas their homozygous otoferlin WT (OTOF^{+/+}) siblings hear normally. Our actual interest lay in the mature neuronal and synaptic properties of these mice, but in order to identify developmental delays or immature conditions in KO mice, we first performed experiments on P10 WT and compared the results with those from P22 WT and KO mice.

6.3.1 Spiking patterns of vVNLL neurons change to an exclusive onset-type firing late during development

In Part 1 of this thesis, we demonstrated that vVNLL neurons of P22 animals display an onset firing pattern. Since we were then interested in how these biophysical neuronal properties are designed before hearing onset in the otoferlin mouse strain, we analyzed intrinsic membrane properties in WT animals before hearing onset (P10) and after hearing onset (P22). Injection of depolarizing currents resulted in either onset firing (n=20) or sustained firing patterns (n=7) in P10 animals, whereas P22 neurons elicited only onset-firing action potentials (Figure 18A).

For further analysis, P10 vVNLL neurons were pooled. Resting membrane potentials differed significantly between P10 and P22 animals (Figure 18B; see also Table 6). Input resistances were measured at peak and steady state for hyperpolarizing current injections of -100 pA (Figure 18C; Table 6). Values for peak and steady-state input resistances remained similar during development. Additionally, both values were used to extract the I_h component (voltage change mediated by hyperpolarization-activated cyclic nucleotide-gated channels; see Chapter 5 “Material and methods”) of the respective neuron (Figure

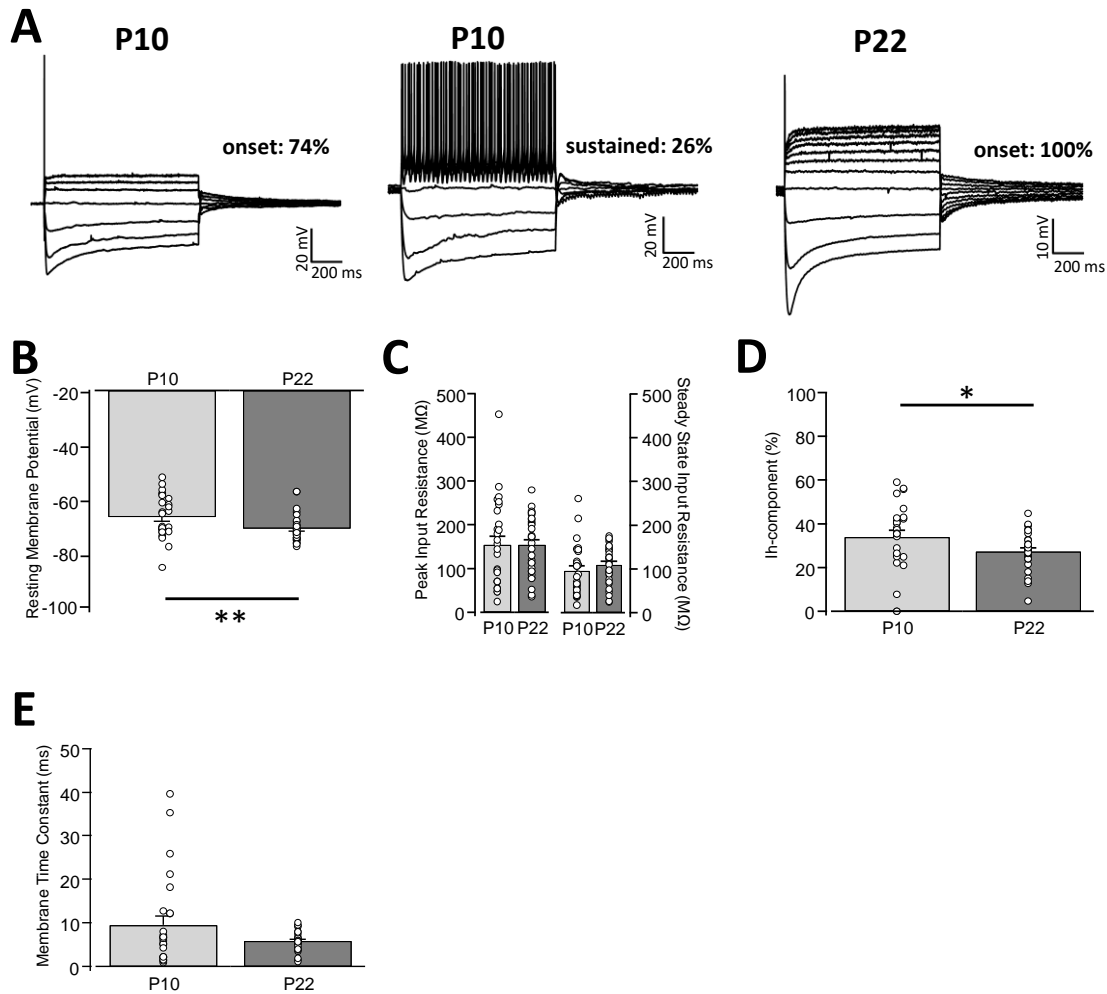


Figure 18: vNLL neurons in P10 and P22 OTOF^(+/+) (WT) animals have different sets of firing patterns and passive intrinsic membrane properties. **A.** Representative voltage responses to hyperpolarizing and depolarizing current injections recorded in P10 (left and middle) and P22 (right) animals. Depolarizing current injections elicited either onset-type (n=20) or sustained (n=7) firing patterns in P10 and only onset (n=30) firing patterns in P22 animals. **B.** Resting membrane potential is significantly different between P10 and P22 WT animals. Values of sustained firing neurons found in P10 animals are shifted to the right for discrimination (also applied in C, D, and E). **C.** Peak input resistance (left) and steady-state input resistance (right) are measured at the peak and at steady state, respectively, of the voltage response to a current injection of -100 pA. No significant differences. **D.** I_h-component is significantly larger in P10 animals. **E.** Membrane time constant shows no significant difference. A single-exponential function is fitted to the first few milliseconds of the voltage response to a current injection of -100 pA; tau is extracted.

All data sets were tested for normality and homogeneity of variance, and according to the result, statistical significance was determined by a non-parametric Kruskal-Wallis test followed by either a Tukey's or Games-Howell *post hoc* test. Significant differences are labeled with * (P < 0.05) or ** (P < 0.01).

18D; Table 6). This I_h component was significantly larger in P10 animals, possibly explaining the more depolarized resting membrane potential in these mice. Membrane time constants were similar in both age groups, although time constants of sustained firing neurons were generally slower (Figure 18F, points shifted to the right; Table 6).

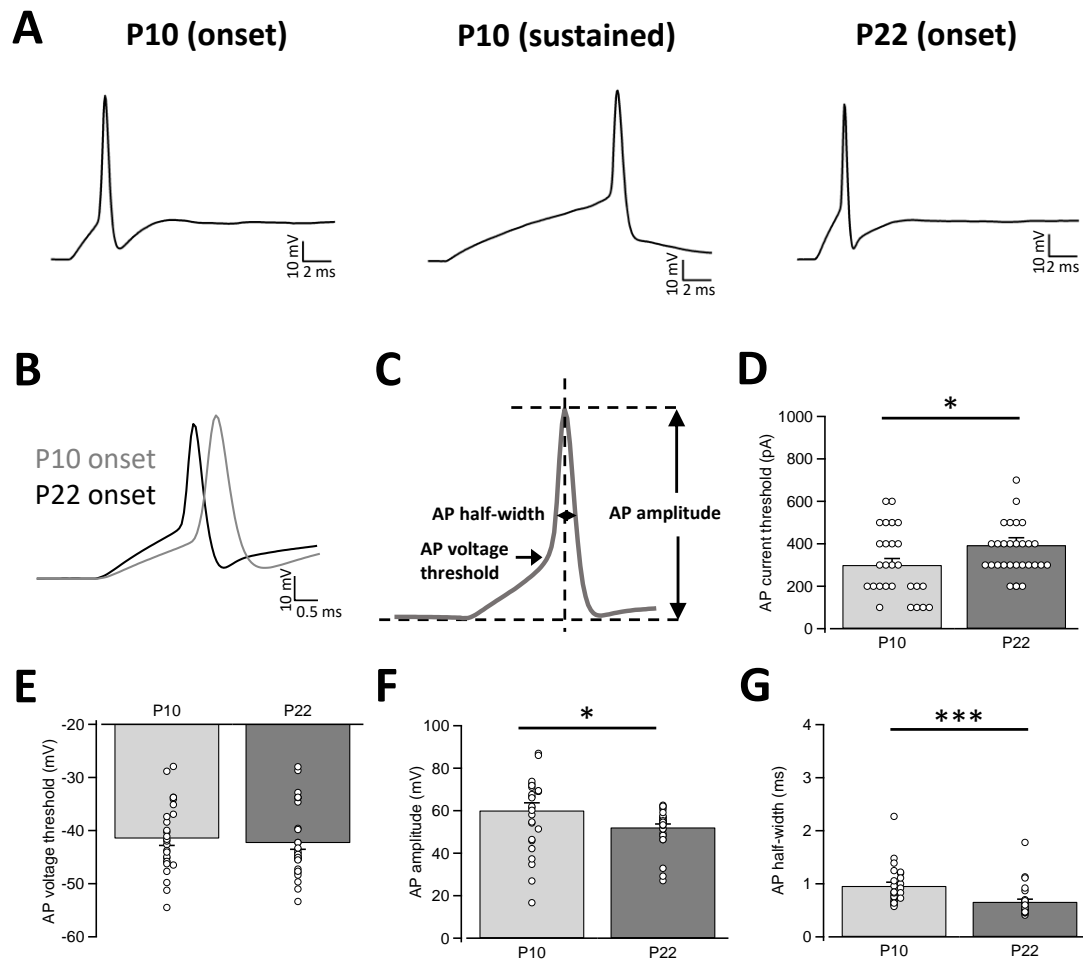


Figure 19: Active firing properties differ between P10 and P22 WT animals in their action potential, current threshold, amplitude, and half-width. **A.** Representative first-suprathreshold voltage traces of onset and sustained-firing neurons of P10 (left and middle) and P22 (right) animals. **B.** Overlap of onset-firing neurons of P10 and P22 animals shown in **A**. The sustained-firing example is excluded due to a late first AP. **C.** Schematic diagram illustrating the analysis of the active membrane properties. The first action potential (AP) elicited by the lowest positive current injection is used for analysis. **D.** AP current threshold eliciting the first action potential or train of action potentials, respectively. Values of sustained-firing neurons found in P10 animals are shifted to the right for discrimination (also applied in **E**, **F**, and **G**). **E.** AP voltage threshold. **F.** AP amplitude. **G.** AP half-width.

All data sets were tested for normality and homogeneity of variance, and according to the result, statistical significance was determined by a non-parametric Kruskal-Wallis test followed by either a Tukey's or Games-Howell *post hoc* test. Significant differences are labeled with * ($P < 0.05$) or *** ($P < 0.001$).

In the next step of the analysis, active intrinsic membrane properties were calculated at the first-suprathreshold voltage response trace (Figure 19A and B). The depolarizing current necessary to elicit an action potential was significantly smaller in P10 animals (current threshold; Figure 19C; Table 6). Sustained-firing neurons had the smallest current thresholds. Furthermore, voltage thresholds were similar (Figure 19D; Table 6), whereas action potential amplitudes were significantly larger in P10 animals (Figure 19E; Table 6). Moreover, action potential half-widths were significantly longer in animals at hearing onset (Figure 19F; Table 6).

We conclude that the vVNLL of P10 animals consists of two subpopulations with different firing patterns. During development, however, intrinsic membrane properties change, and only onset-firing neurons exist in P22 animals.

Table 6 | Summary of membrane properties of vVNLL neurons of P10 and P22 OTOF^(+/+) (WT) and P22 OTOF^(-/-) (KO) mice

Values are mean \pm SEM. The level of significance between groups was calculated with a Kruskal-Wallis test followed by Games-Howell or Tukey's *post hoc* tests (* $P < 0.05$, ** $P < 0.01$, *** $P < 0.001$).

a: significant differences between P10 and P22 WT animals

b: significant differences between P10 WT and P22 KO animals

c: significant differences between P22 WT and P22 KO animals

n.s.: no significant difference

	P10 OTOF ^(+/+) n=27	P22 OTOF ^(+/+) n=30	P22 OTOF ^(-/-) n=27	P
Passive membrane properties				
Resting potential (mV)	-62.7 \pm 1.5	-67.0 \pm 0.9	-63.8 \pm 1.8	** _a ; ** _c
Peak input resistance (M Ω)	154.3 \pm 19.0	153.7 \pm 12.3	154.6 \pm 17.1	n.s.
Steady-state input resistance (M Ω)	96.1 \pm 11.3	109.8 \pm 8.1	107.8 \pm 11.8	n.s.
I _h -component at -100 pA (%)	34.0 \pm 3.0	27.3 \pm 1.6	26.6 \pm 2.8	* _a ; * _b
Membrane time constant (ms)	9.62 \pm 1.96	5.83 \pm 0.41	6.45 \pm 1.02	n.s.
Active membrane properties				
Current threshold (pA)	300 \pm 31	393 \pm 35	270 \pm 27	* _a ; ** _c
Voltage threshold (mV)	-41.5 \pm 1.3	-42.4 \pm 1.2	-38.1 \pm 1.4	** _b ; ** _c
AP amplitude (mV)	60.1 \pm 3.6	52.1 \pm 1.6	54.4 \pm 2.8	* _a ; * _b
AP half-width (ms)	0.96 \pm 0.07	0.66 \pm 0.05	0.73 \pm 0.07	*** _a ; *** _b

6.3.2 Otofelin WT mice undergo the same developmental reduction of excitatory synaptic inputs as found in C57Bl/6 animals

In Part 2 of this thesis, we determined that the number of excitatory synaptic inputs is reduced during later development. Interestingly, the formation of the calyx of Held occurs much earlier, at P2 (Hoffpauir et al. 2006; Nakamura and Cramer 2011). The aim of Part 3 of this thesis is to investigate the influence of congenital deafness on the development of biophysical and synaptic formation. Since WT animals served as controls, we repeated this set of experiments in otoferlin WT animals. To measure the strength of synaptic inputs and calculate receptor rise and decay times, we stimulated in the fiber bundle about 50 μm ventral to the recorded neuron, and EPSCs were isolated pharmacologically. To estimate the number of fiber inputs, the stimulation intensity was gradually increased. We assume that each stepwise increase of EPSC amplitude as a response to a stimulation increment reflects the activation of additional synaptic inputs. Figure 20A1 illustrates a P10 example. In this example, two distinct EPSC current steps to a gradual increase of stimulation strength were found. This indicates the existence of two excitatory synaptic inputs to this specific vVNLL neuron. Neurons of the vVNLL of P10 animals were innervated by one to five fibers (Figure 20A1–A2 and D; Table 7). More than 50% of the recorded neurons exhibited an all-or-none response with large amplitudes independent of the stimulation strength (Figure 20E; Table 7). In neurons of P22 animals, however, a maximum of presumably two excitatory inputs was found (Figure 20B1–B2 and D; Table 7). Significantly fewer neurons with more than one input were found in P22 than in P10 animals (Figure 20D; Table 7), though the maximally evoked postsynaptic current was similar (Figure 20E; Table 7). Moreover, 10–90% rise times and tau decay times of EPSCs were significantly larger in P10 than in P22 animals (Figure 20F and G; Table 7).

We conclude that during the development of the vVNLL in mice of different strains, only a subpopulation of neurons with one or two excitatory synaptic inputs remains, and most inputs in vVNLL neurons of mature mice receive one large excitatory synapse with calyx-like properties.

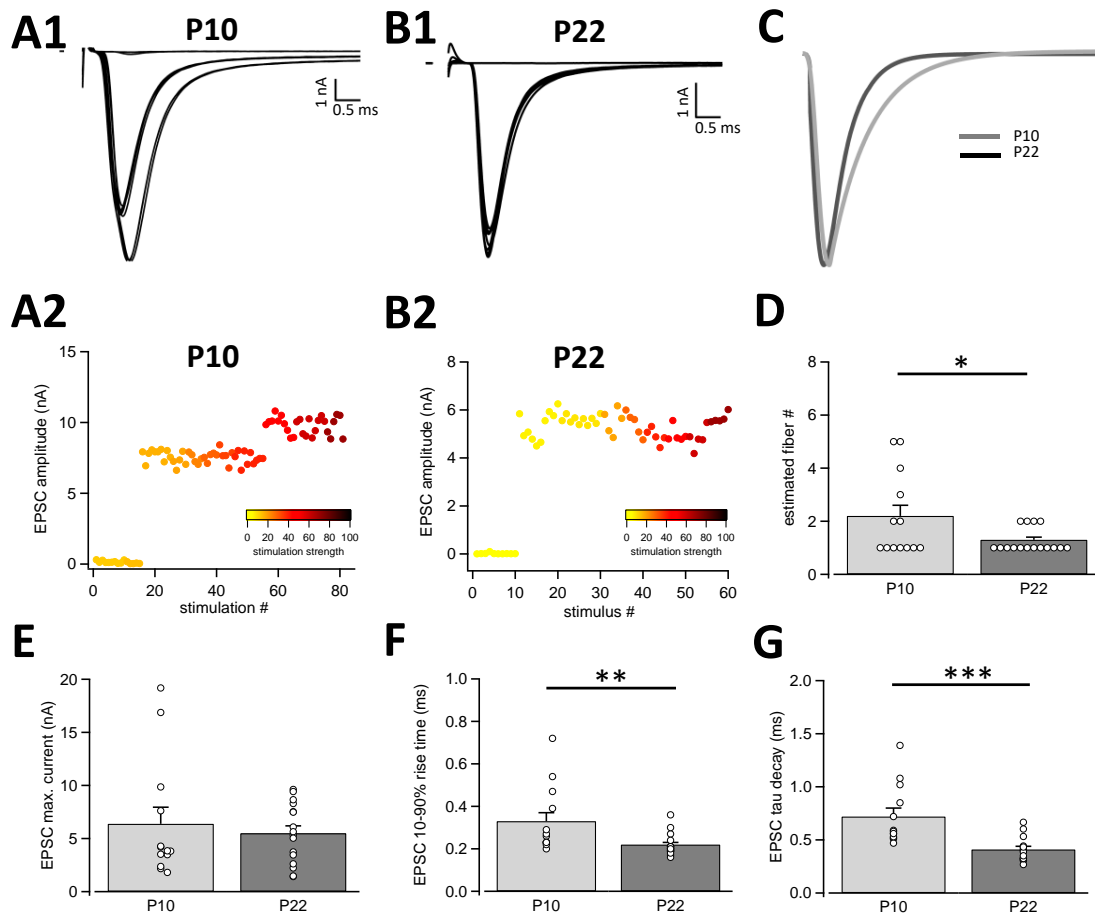


Figure 20: Excitatory postsynaptic currents (EPSC) of vNLL neurons rise and decay faster in P22 OTOF^(+/+) (WT) than in P10 animals. **A1.** Average evoked current responses to increasing stimulation strengths of a representative P10 vNLL neuron. All traces represent the average of at least five consecutive recordings to the same stimulation strength. Two distinct current steps are visible. **A2.** EPSC amplitude as a function of stimulus number recorded from a P10 vNLL neuron shown in A1. The respective stimulation strength is color coded. **B1.** Average evoked current responses to increasing stimulation strengths of a representative P22 vNLL neuron. All traces represent the average of at least five consecutive recordings to the same stimulation strength. One distinct current step is visible. **B2.** EPSC amplitude as a function of stimulus number recorded from a P22 vNLL neuron shown in B1. The respective stimulation strength is color coded. **C.** Normalized maximal EPSC traces from P10 (gray) and P22 (black) as shown in A and B. **D.** Estimated number of EPSC steps evoked by an increasing stimulation strength in vNLL neurons of P10 and P22 animals shows a significant difference; P10: n=13; P22: n=16. **E.** Maximal EPSC amplitude shows no significant difference. Values referring to an estimated fiber number of three, four, and five are shifted slightly to the right to demonstrate their correlation with F and G. **F.** 10–90% rise time is measured by applying a minimal stimulation paradigm. P22 vNLL neurons rise significantly faster than P10 vNLL neurons. **G.** Tau decay is measured by applying a minimal stimulation paradigm. A single-exponential function is fitted to the decay of the current response; tau is extracted. P22 vNLL neurons decay significantly faster than P10 vNLL neurons.

All data sets were tested for normality and homogeneity of variance, and according to the result, statistical significance was determined by a non-parametric Kruskal-Wallis test followed by a Games-Howell *post hoc* test. Significant differences are labeled with * ($P < 0.05$), ** ($P < 0.01$), or *** ($P < 0.001$).

Table 7 | Summary of excitatory postsynaptic currents (EPSCs) of vNLL neurons of P10 and P22 OTOF^(+/+) (WT) and P22 OTOF^(-/-) (KO) mice

Values are mean \pm SEM. The level of significance between groups was calculated with a Kruskal-Wallis test followed by Games-Howell or Tukey's *post hoc* tests (* $P < 0.05$, ** $P < 0.01$, *** $P < 0.001$).

a: significant differences between P10 and P22 WT animals

b: significant differences between P10 WT and P22 KO animals

c: significant differences between P22 WT and P22 KO animals

n.s.: not significant

	P10 OTOF ^(+/+) n=13	P22 OTOF ^(+/+) n=16	P22 OTOF ^(-/-) n=16	P
Estimated fiber #	2.15 \pm 0.44	1.25 \pm 0.11	1.94 \pm 0.30	* _a ; * _c
Maximal current (nA)	6.39 \pm 1.56	5.50 \pm 0.70	3.45 \pm 0.43	* _c
Average step size (nA)	4.75 \pm 1.63	4.20 \pm 0.66	2.29 \pm 0.50	** _c
10–90% rise time (ms)	0.33 \pm 0.04	0.22 \pm 0.01	0.33 \pm 0.04	** _a ; * _c
Tau decay (ms)	0.72 \pm 0.08	0.41 \pm 0.03	0.70 \pm 0.15	*** _a

6.3.3 mEPSC become significantly briefer during development

The shape of the postsynaptic response is influenced by pre- and postsynaptic factors (Regehr 2012) and can be estimated with train stimulations during short-term plasticity experiments. For the analysis of short-term plasticity experiments, data on presynaptic vesicle properties are necessary. In the next steps of our analysis, we aimed to dissect the characteristics of the spontaneous vesicle release and subsequently use these data for the examination of the RRP.

While inhibitory receptors and voltage-gated sodium channels were pharmacologically blocked, mEPSCs were recorded for at least three minutes. Representative mEPSC recordings of P10 and P22 animals are illustrated in Figure 21A and B (top). Recordings of P10 animals generally showed more noise, whereas stable measurements were obtained from neurons at P22. The enlargements in Figure 21 (A and B, bottom) give an impression of typical mEPSCs found in these animals. The mEPSC amplitudes and frequencies were similar in both age groups (Figure 21D and F; Table 8). A normalization of averaged mEPSCs found in examples of Figure 21A and B demonstrates their different time constants and the resulting differences in charge (Figure 21C). The mEPSC charge of P10

animals, however, was significantly larger than that of P22 animals (Figure 21E; Table 8) caused by significant differences in mEPSC rise and tau decay times (Figure 21F and G; Table 8).

We conclude that postsynaptic glutamate receptors develop faster kinetics that influence the shape of mEPSCs while release frequencies remain similar, suggesting stable presynaptic but altered postsynaptic conditions during development.

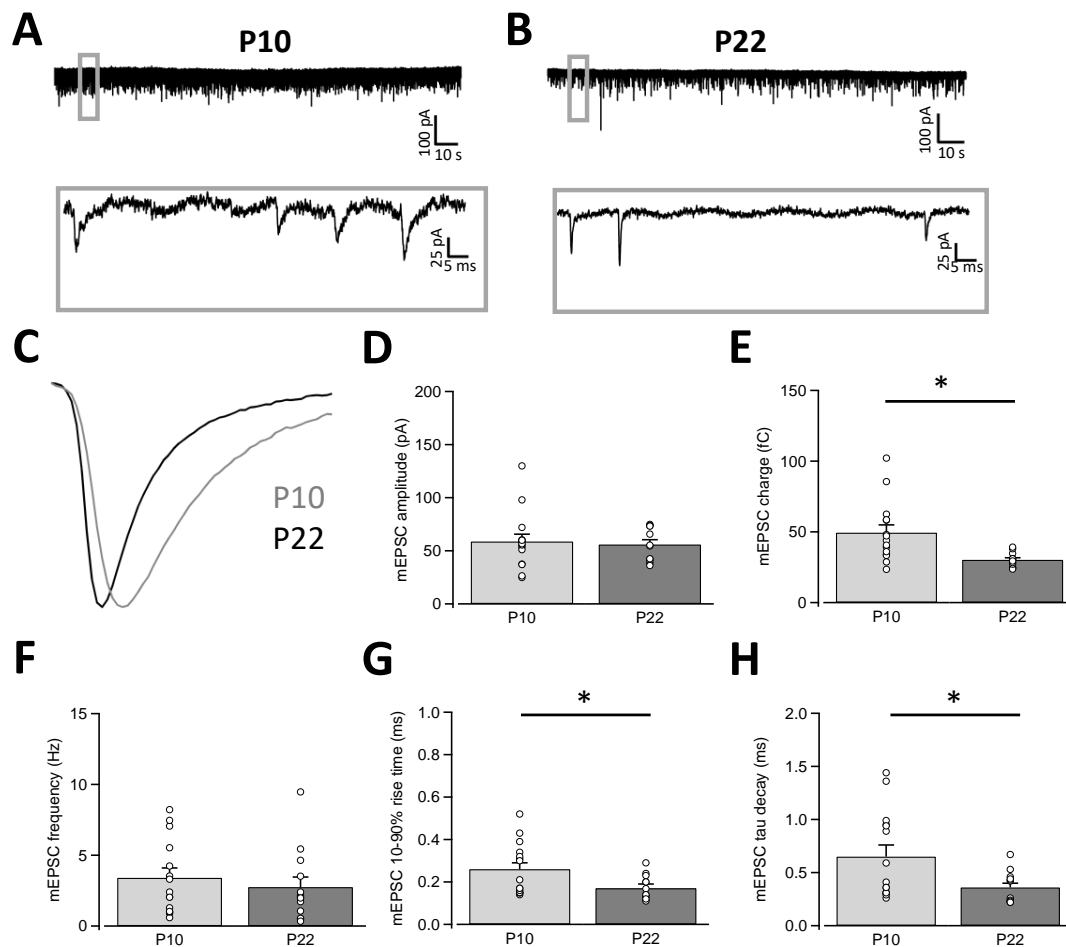


Figure 21: Miniature excitatory postsynaptic currents (mEPSC) of vNLL neurons rise and decay faster in P22 than in P10 OTOF^(+/+) (WT) animals. **A.** Recording of a representative mEPSC of a P10 vNLL neuron (top). Enlargement of four single mEPSCs (bottom). **B.** Recording of a representative mEPSC of a P22 vNLL neuron (top). Enlargement of three single mEPSCs (bottom). **C.** Normalized average mEPSC examples shown in A and B. **D.** Average mEPSC amplitudes of each neuron (P10: n=15; P22: n=13) are depicted as single circles. **E.** mEPSC charges are significantly larger in P10 vNLL neurons. **F.** mEPSC frequency. **G.** mEPSC 10–90% rise time of P22 vNLL neurons rise significantly faster than in P10 vNLL neurons. **H.** mEPSC tau decay is measured by fitting a single-exponential function to the decay of the current response; tau is extracted. P22 vNLL neurons decay significantly faster than P10 vNLL neurons.

All data sets were tested for normality and homogeneity of variance, and according to the result, statistical significance was determined by a non-parametric Kruskal-Wallis test followed by either a Games-Howell or Tukey's *post hoc* test. Significant difference is labeled with * ($P < 0.05$).

Table 8 | Summary of miniature excitatory postsynaptic currents (mEPSCs) of vVNLN neurons of P10 and P22 OTOF^(+/+) (WT) and P22 OTOF^(-/-) (KO) mice

Values are mean \pm SEM. The level of significance between groups was calculated with a Kruskal-Wallis test followed by Games-Howell or Tukey's *post hoc* tests (* $P < 0.05$, ** $P < 0.01$, *** $P < 0.001$).

a: significant differences between P10 and P22 WT animals

b: significant differences between P10 WT and P22 KO animals

c: significant differences between P22 WT and P22 KO animals

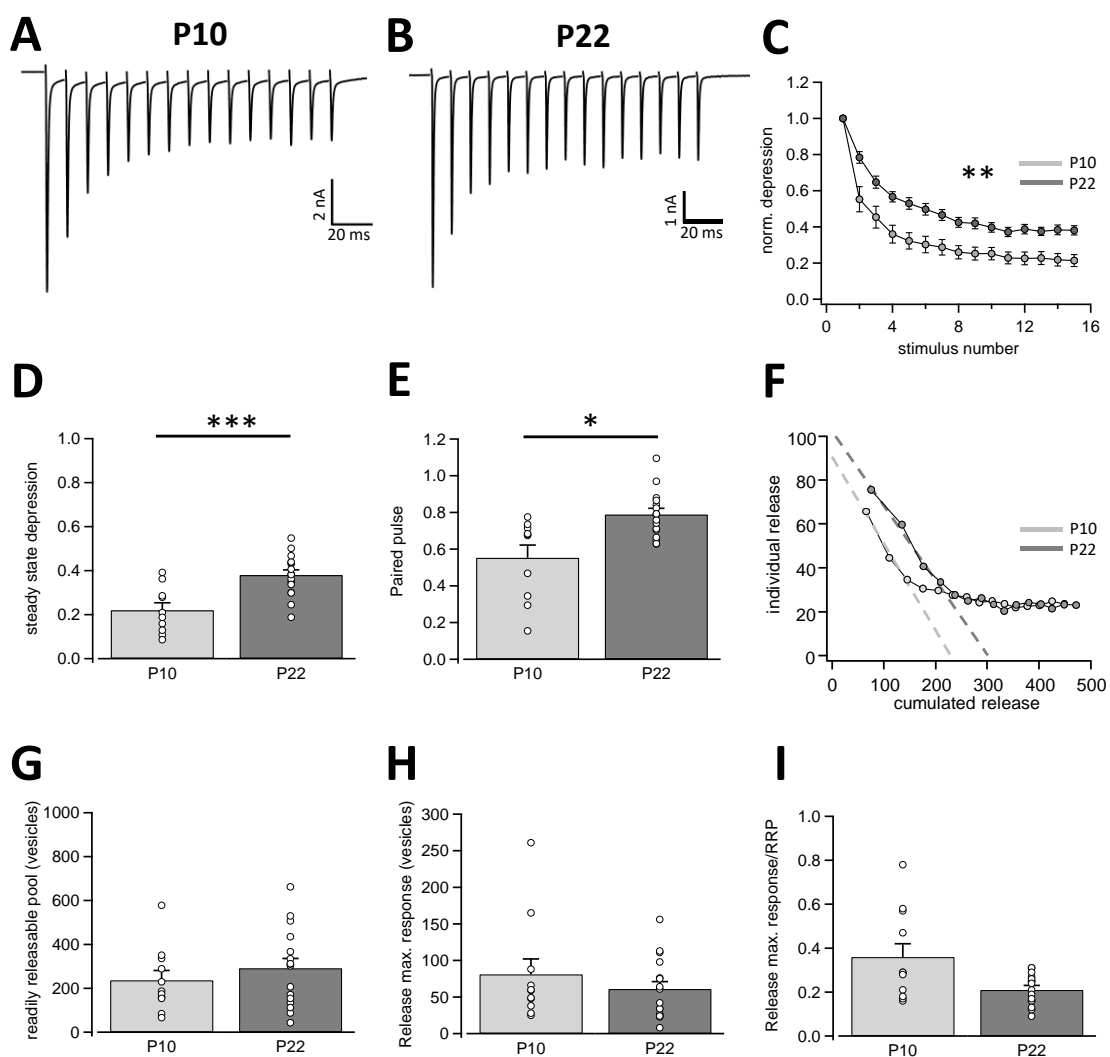
n.s.: no significant difference

	P10 OTOF ^(+/+) n=15	P22 OTOF ^(+/+) n=13	P22 OTOF ^(-/-) n=14	P
Amplitude (pA)	58.7 \pm 6.9	55.9 \pm 4.5	59.0 \pm 6.1	n.s.
Charge (fC)	49.4 \pm 5.5	30.2 \pm 1.5	34.1 \pm 2.1	** _a ; * _b
Frequency (Hz)	3.38 \pm 0.67	2.94 \pm 0.74	6.00 \pm 1.42	* _c
10–90% rise time (ms)	0.26 \pm 0.03	0.17 \pm 0.02	0.22 \pm 0.03	* _a
Tau decay (ms)	0.65 \pm 0.11	0.36 \pm 0.04	0.58 \pm 0.06	* _a ; * _c

6.3.4 Degree of short-term depression is reduced during development

We were also interested in other possible presynaptic developmental changes in otoferlin mice, such as depletion and replenishment of the RRP and its effects on the postsynaptic response strength to stimulation trains. Therefore, we investigated the short-term plasticity (STP) of excitatory inputs in P10 and P22 animals (15 stimuli at 100 Hz). All recorded neurons of both age groups showed a substantial degree of short-term depression (Figure 22A–E). The overall depression from stimulus 2 to stimulus 15 was significantly larger in P10 animals, ranging from 80% in P10 to a 60% depression rate in P22 animals (Figure 22C; Table 9). Steady-state depression also was analyzed (Figure 22D; Table 9) by calculating the average of the last three amplitudes and dividing it by the EPSC amplitude of the first stimulus. Here, the difference between P10 and P22 animals was even more substantial (Figure 22D; Table 9). Additionally, almost all recorded neurons showed a paired-pulse depression in their first two EPSC amplitudes. Only one neuron in a P22 animal exhibited paired-pulse facilitation (Figure 22E; Table 9). Nonetheless, the degree of depression was significantly larger in P10 animals already at the second stimulus (Figure

22E; Table 9). Next, we were interested in whether these changes are reflected in the size of the RRP and its depletion (Figure 22F–I; Table 9). For calculations of the size of the RRP, we used the train stimulation data to calculate an Elmquist-Quastel plot, where the individual release (the amplitude of the respective stimulus divided by the amplitude of the average mEPSC obtained from Figure 21D) is plotted against the cumulated release of the train stimulation data (Figure 22F). It is worth noting that a cumulation of transmitted EPSC charges would have been more accurate in measurements with similar EPSC shapes, but since they significantly narrow during development, a reliable calculation of the RRP and its derived properties would have been impossible. Additionally, desensitization during repeated stimulation is a relevant factor (Neher 2015). Furthermore, it has been suggested by Neher (2015) that during train stimulations, a mixture of RRP and newly replenished vesicles are discharged and, during steady state, discharges of vesicles do not necessarily resemble the only newly replenished vesicles. Therefore, we used the first three amplitudes



← **Figure 22: Synaptic short-term plasticity of excitatory inputs of vVNLL of P10 OTOF ^{+/+} (WT) animals exhibits a higher degree of depression and a smaller paired pulse, but a larger readily releasable pool than P22 WT animals.** **A.** Representative EPSC traces in response to 15 stimulations at 100 Hz illustrating short-term plasticity in vVNLL neurons of P10 animals. **B.** Representative EPSC traces in response to 15 stimulations at 100 Hz illustrating short-term plasticity in vVNLL neurons of P22 animals. **C.** Normalized EPSC depression curve for all recorded vVNLL neurons in P10 and P22 animals (P10: n=10; P22: n=16). An overall significant difference from the second stimulus on was found during development. **D.** Steady-state depression is determined as the average of the last three amplitudes of the 100 Hz EPSC train divided by the first amplitude. **E.** Paired pulse is calculated as the second amplitude divided by first amplitude of the 100 Hz EPSC train. **F.** Elmquist-Quastel plot (EQ plot) - exemplary EQ plot to calculate the RRP from train stimulation data. Individual release of each current amplitude to each stimulus is calculated with the mEPSC amplitude from Figure 21D. Cumulated release is calculated as cumulation of individual releases up to that specific stimulus. A linear regression is applied to the first three cumulative steps and extrapolated to the x-intercept. The x-intercept theoretically matches the RRP. **G.** RRP of all recorded vVNLL neurons in P10 and P22 animals. **H.** Release of the maximal response is determined by a maximal stimulation paradigm and calculated as the amplitude of the largest current response to a 100 Hz stimulation pulse divided by the amplitude of the average mEPSC (shown in Figure. 3.18D). **I.** Ratio of the readily releasable pool (RRP)/release of maximal response (RMR) is calculated from G and H.

All data sets were tested for normality and homogeneity of variance, and according to the result, statistical significance was determined by either a two-factor ANOVA followed by Dunn's *post hoc* test, a single-factor ANOVA followed by a Scheffé's *post hoc* test, or a non-parametric Kruskal-Wallis test followed by a Games-Howell *post hoc* test. Significant differences are labeled with * ($P < 0.05$), ** ($P < 0.01$), or *** ($P < 0.001$).

of the train stimulations to avoid errors. A linear regression is applied to the first three amplitudes and extrapolated to the x-intercept, which theoretically resembles the RRP (Figure 22F, dashed line). From these calculations, we concluded that the RRP was similar among P10 and P22 animals (Figure 22G; Table 9). Furthermore, the release of the maximal response and the ratio of the release at the maximal response and the RRP also remained alike during development (Figure 22H, I; Table 9).

Taken together, our data suggest that both pre- and postsynaptic adjustments occur during development. Presynaptic differences are found in the reduction of the number of synaptic inputs, while vesicle properties remain similar. Postsynaptic modifications include a reduction of time constants and, thus, briefer mEPSCs that indicate a maturation to a faster and more precise processing of synaptic inputs. Reductions in the postsynaptic response strength caused by desensitization cannot be ruled out.

Table 9 | Summary of short-term plasticity of excitatory postsynaptic currents (EPSCs) of vVNLL neurons of P10 and P22 OTOF^(+/+) (WT) and P22 OTOF^(-/-) (KO) mice

Values are means \pm SEM. The level of significance between groups was calculated using either a two-way ANOVA followed by a Dunn's *post hoc* test, a one-way ANOVA followed by a Scheffé's *post hoc* test, or a non-parametrical Kruskal-Wallis test followed by a *post hoc* Tukey's or Games-Howell test (* $P < 0.05$, ** $P < 0.01$, *** $P < 0.001$).

a: significant differences between P10 and P22 WT animals

b: significant differences between P10 WT and P22 KO animals

c: significant differences between P22 WT and P22 KO animals

n.s.: no significant difference

	P10 OTOF ^(+/+) n=11	P22 OTOF ^(+/+) n=16	P22 OTOF ^(-/-) n=14	P
Overall depression course				** a; *b
Steady-state depression	0.22 \pm 0.03	0.38 \pm 0.02	0.32 \pm 0.04	*** a; *b
Paired pulse	0.55 \pm 0.07	0.79 \pm 0.03	0.69 \pm 0.04	* a
Readily releasable pool RRP (ves)	237 \pm 44	292 \pm 44	218 \pm 26	n.s.
Release max. response RMR (ves)	81 \pm 21	61 \pm 10	61 \pm 11	n.s.
Ratio RMR/RRP	0.36 \pm 0.06	0.21 \pm 0.02	0.26 \pm 0.03	n.s.

6.3.5 VGluT1 is a consistent vesicular glutamate transporter in synapses innervating vVNLL neurons

These electrophysiological findings were analyzed under an immunohistochemical view in terms of their VGluT1 and calretinin distribution (Figure 23). Presynaptic factors that greatly determine the postsynaptic response are calcium currents and the presynaptic calcium concentration. Calretinin, on the one hand, is a calcium-binding protein that is found in some presynaptic terminals and is important in reducing the internal calcium concentration and, therefore, terminating vesicle release (Schwaller et al. 2002). On the other hand, VGluT1 is a vesicular glutamate transporter protein found in excitatory synapses of the VNLL (Caspari et al. 2015), where it is associated with membranes of synaptic vesicles carrying glutamate. Glutamate is the neurotransmitter for AMPA and NMDA receptors mediating EPSCs in the VNLL. Calretinin is located in the cytosol and may display the extent of the presynaptic compartment, and a colocalization with VGluT1 enables an unambiguous classification of excitatory synapses. In the vVNLL of P10

animals, a distinct perisomatic VGluT1-positive staining was found (Figure 23A). On the other hand, the expression of calretinin was not as evolved during these early stages of development (Figure 23B). Brain slices of P22 animals containing the vVNLL showed a similar distribution pattern of perisomatic VGluT1-positive rings around numerous neurons (Figure 23D). During development, shortly after hearing onset (data not shown) and several days after hearing onset, calretinin is found in presynaptic terminals and preterminal axons of neurons of the auditory brainstem (Figure 23E; Felmy and Schneggenburger, 2004; Hruskova et al., 2012). Altogether, these data suggest the presence of large and strong excitatory inputs in P22 animals (Figure 23F), while the extent of the synaptic cytosol of P10 animals, by contrast, remains unclear (Figure 23C).

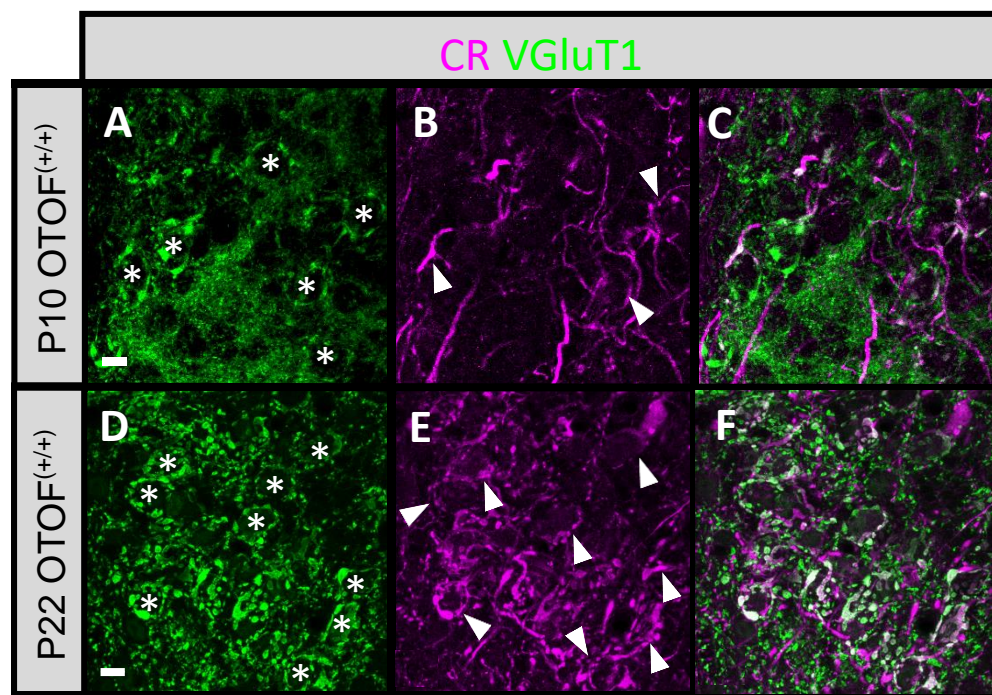


Figure 23: Immunolabelings to visualize excitatory inputs to vVNLL neurons in P10 and P22 OTOF^(+/+) (WT) animals with antibodies against VGluT1 and Calretinin (CR). **A.** A VGluT1-positive perisomatic staining of six neurons (asterisks) of a maximal projection of the vVNLL of a P10 animal. N=2. **B.** Calretinin labeling of a maximal projection of the vVNLL of the P10 animal shown in A. Arrowheads point to CR-positive staining of synaptic inputs to three neurons shown in A. **C.** Merged image of A and B. Colocalization of VGluT1 and CR appears white. **D.** A VGluT1-positive perisomatic staining of nine neurons (asterisks) of a maximal projection of the vVNLL of a P22 animal. N=2. **E.** Calretinin labeling of a maximal projection of the vVNLL of the P22 animal shown in A. Arrowheads point to CR-positive staining of synaptic inputs to eight neurons shown in A. **F.** Merged image of D and E. Colocalization of VGluT1 and CR appears white. Eight out of nine neurons with a perisomatic VGluT1 labeling have CR in their synaptic inputs. Scale bar: 10 μ m.

We conclude that it remains uncertain whether these ring-like structures emerge from one or several excitatory inputs. Our electrophysiological data together with these perisomatic rings of VGluT1 indicate, at least in P22 animals, large and possibly calyx-like synaptic inputs in many vVNLL neurons. Furthermore, a developmental modification of calcium-binding proteins to calretinin can be observed.

6.3.6 Does congenital deafness affect the proper development of vVNLL neurons?

One type of deafness in humans is DNFB9, an autosomal recessive form of deafness caused by a lack of otoferlin, a vesicle-associated protein in the ribbon synapse of inner hair cells in the cochlea (Roux et al. 2006). Deafness as a result of a malfunction in signal transmission in the inner hair cells while the auditory nerve remains intact raises the question of whether central auditory synapses and intrinsic neuronal properties develop normally in congenitally deaf animals in the absence of experience-dependent activity. To investigate this question, mice with a lack of otoferlin (KO) and WT mice were bred in our animal facility. Experiments were performed on siblings of both genotypes.

6.3.7 Deafness impairs the typical development of spiking patterns and intrinsic neuronal properties

To discover whether the vVNLL of hearing and deaf mice develop the same biophysical properties, we analyzed passive and active intrinsic membrane properties in P22 WT and KO animals. Injection of depolarizing currents resulted in either onset firing (n=19) or sustained firing patterns (n=8) in KO animals whereas P22 WT neurons elicited only onset-firing action potentials (Figure 24A).

For further analysis, KO vVNLL neurons were pooled regardless of the firing pattern. Resting membrane potentials differed significantly between WT and KO animals (Figure 24B) but were similar in P10 WT and P22 KO mice (see Table 6 for results and statistics). Furthermore, neither input resistances nor I_h components were different in WT and KO animals (Figure 24C and D; Table 6). Additionally, membrane time constants were also similar in both genotypes (Figure 24F; Table 6), although time constants of sustained-firing neurons were generally slower. Despite time constants being statistically similar in both

age groups and genotypes, the mean value of KO animals lay in between P10 and P22 WT animals, suggesting a transitional state.

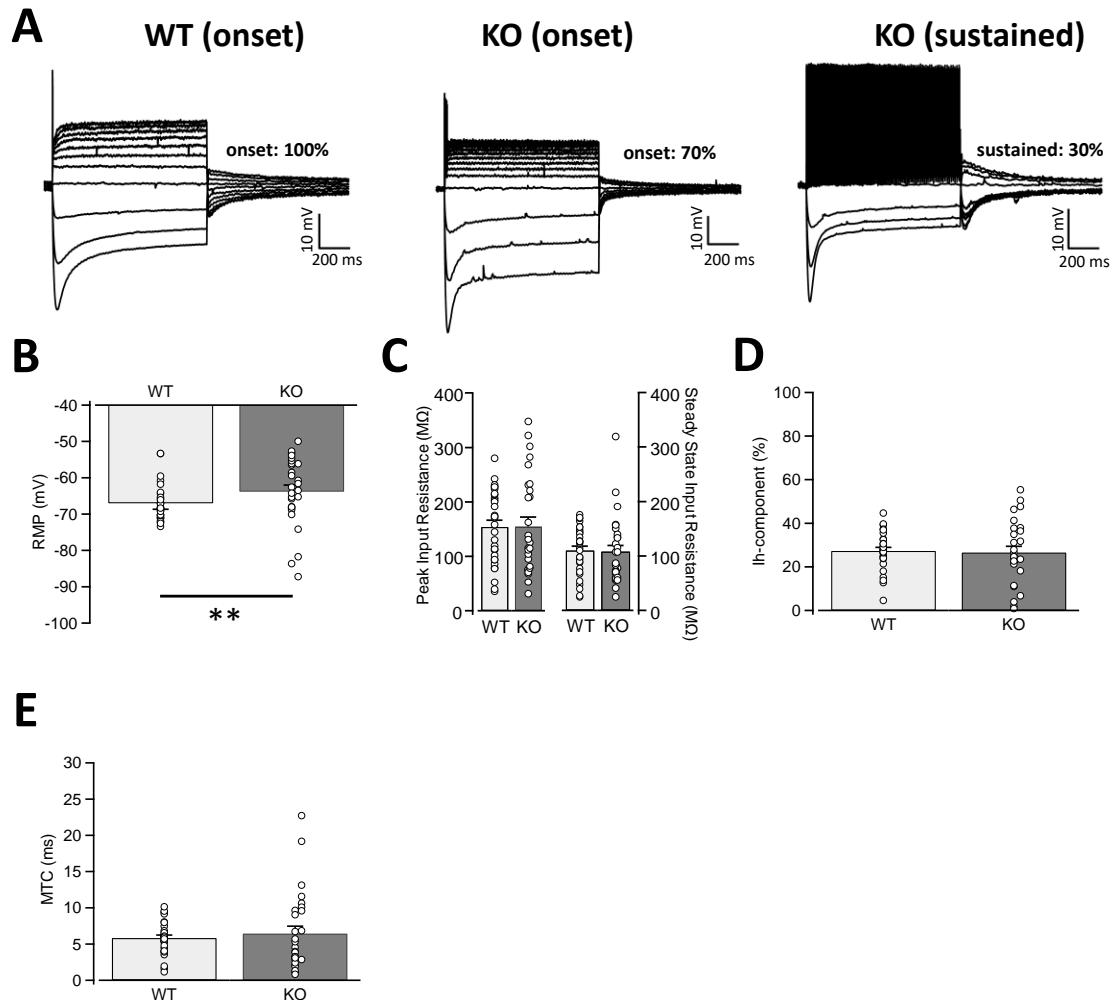
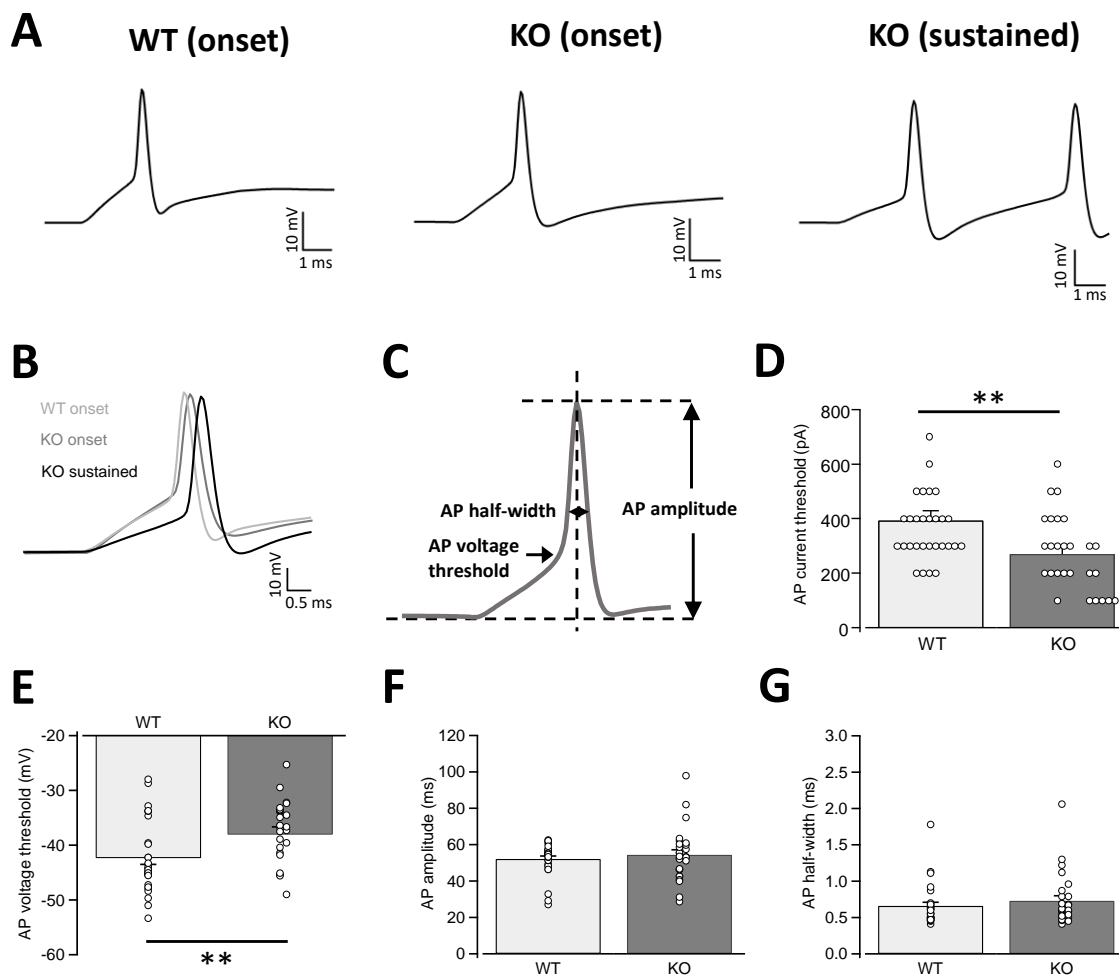


Figure 24: vNLL neurons between P22 OTOF^(+/+) (WT) and OTOF^(-/-) (KO) animals have different sets of firing patterns and resting membrane potentials. **A.** Representative voltage responses to hyperpolarizing and depolarizing current injections recorded in P22 WT (left) and KO (middle and right) animals. Depolarizing current injections elicited only onset-type (n=30) firing patterns in WT animals, whereas neurons in KO mice showed either onset (n=19) or sustained (n=8) firing patterns. **B.** Resting potential is significantly different between WT and KO animals. Values of sustained-firing neurons found in KO animals are shifted to the right for discrimination (also applied in C, D, and E). **C.** Peak (left) and steady-state (right) input resistance are measured at the peak and at steady state, respectively, of the voltage response to a current injection of -100 pA. No significant differences. **D.** I_h component. **E.** Membrane time constant shows no significant difference. A single-exponential function is fitted to the first few milliseconds of the voltage response to a current injection of -100 pA; tau is extracted.

All data sets were tested for normality and homogeneity of variance, and according to the result, statistical significance was determined by a non-parametric Kruskal-Wallis test followed by either a Tukey's or Games-Howell *post hoc* test. Significant difference is labeled with ** (P < 0.01).

Again, active intrinsic membrane properties were calculated at the first-suprathreshold voltage response trace (Figure 25A and B). The depolarizing current needed to elicit an action potential was significantly smaller in KO animals (current threshold; Figure 25C; Table 6) with sustained-firing neurons having the smallest current thresholds. Furthermore, voltage thresholds were significantly more depolarized in KO animals (Figure 25D; Table 6), suggesting a reduced excitability. In addition, the voltage threshold in KO animals behaved differently from those in P10 animals, leading to the assumption that the loss of otoferlin in the inner hair cells has an effect on the expression of voltage-gated ion channels that regulate firing behavior and biophysical characteristics in the vVNLL of KO mice. Additionally, action potential amplitudes and half-widths were similar in both genotypes (Figure 25E and F; Table 6). The correct development of these two properties in KO animals in comparison to P10 animals (see Table 6) suggests an independent developmental process from auditory-evoked activity.



← **Figure 25: Active firing properties differ between P22 OTOF^(+/+) (WT) and OTOF^(-/-) (KO) animals in their action potential current and voltage threshold.** **A.** Representative first-suprathreshold voltage traces recorded in neurons of P22 WT (left) and KO (middle and right) animals. **B.** Overlap of action potentials shown in A. **C.** Schematic diagram illustrating the analysis of the active membrane properties. The first action potential (AP) elicited by the lowest positive current injection is used for analysis. **D.** AP current threshold eliciting the first action potential or train of action potentials, respectively. Values of sustained firing neurons found in KO animals are shifted to the right for discrimination (also applied in E, F and G). **E.** AP voltage threshold. **F.** AP amplitude. **G.** AP half-width.

All data sets were tested for normality and homogeneity of variance, and according to the result, statistical significance was determined by a non-parametric Kruskal-Wallis test followed by either a Tukey's or Games-Howell *post hoc* test. Significant difference is labeled with ** ($P < 0.01$).

We conclude that vVNLL neurons of KO animals remain immature in terms of their firing patterns, as seen in P10 WT animals. Furthermore, a more depolarized voltage threshold leads to the assumption that vVNLL neurons of KO animals are less excitable.

6.3.8 Deafness impairs synaptic refinement

In the first section of Part 3 we demonstrated that the number of excitatory synaptic inputs is reduced during later development and that calyx-like inputs are found in the vVNLL. It has elsewhere been determined that the formation of the calyx of Held already occurs at P2 without sensory experience (Hoffpauir et al. 2006). We were interested in whether this reduction in the number of synaptic inputs and development of a calyx-like synapse depends on auditory-evoked activity. We therefore investigated the influence of congenital deafness on the development of synaptic formation. To measure the strength of synaptic inputs and calculate receptor rise and decay times, we stimulated in the fiber bundle about 50 μm ventral to the recorded neuron, and EPSCs were isolated pharmacologically. To estimate the number of fiber inputs, the stimulation intensity was gradually increased. We assume that each stepwise increase of EPSC amplitude as a response to a stimulation increment reflects the activation of additional synaptic inputs. Neurons of the vVNLL of KO animals were innervated by an estimated number of one to five fibers (Figure 26B1–B2 and D; Table 7), whereas WT animals had, according to their stepwise current responses, a maximum of estimated two excitatory inputs (Figure 26A1–A2 and D; Table 7). However, more than 50% of the recorded neurons in KO mice exhibited an all-or-none response with different maximal amplitudes ranging from 1 to 8 nA (Figure 26E; Table 7), while the remaining neurons displayed a stepwise increase of postsynaptic current with rising stimulation strengths. Additionally, the maximally evoked postsynaptic current was also significantly different in the two age groups, with KO animals having even smaller

maximal amplitudes than P10 WT animals (Figure 26E; Table 7). Moreover, 10–90% rise times but not tau decay times of EPSCs were significantly longer in KO than in WT animals (Figure 26F and G; Table 7), resembling P10 WT values.

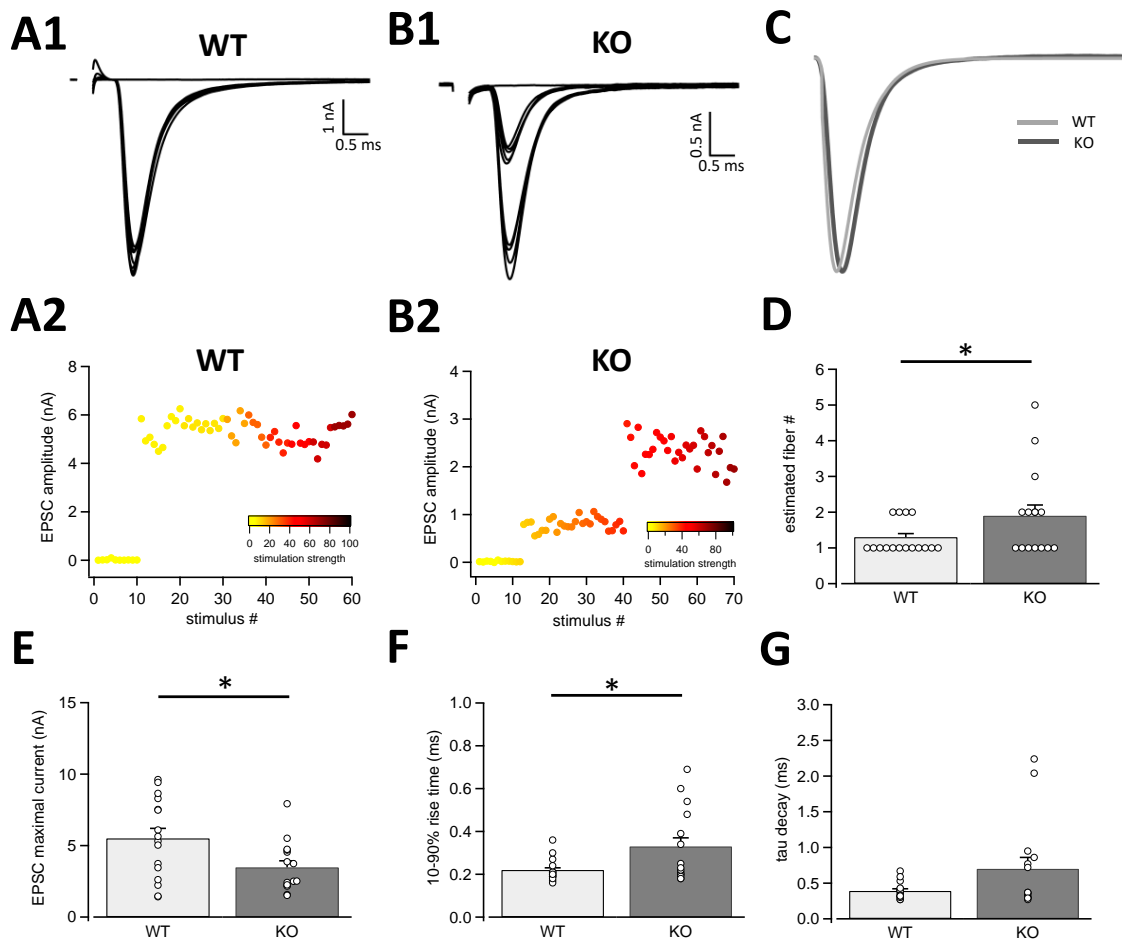


Figure 26: Excitatory postsynaptic currents (EPSC) of vNLL neurons are larger and faster in P22 OTOF^(+/+) (WT) than in P22 OTOF^(-/-) (KO) animals. **A1.** Average evoked current responses to increasing stimulation strengths of a representative P22 WT vNLL neuron. All traces represent the average of at least five consecutive recordings to the same stimulation strength. One distinct current step is visible. **A2.** EPSC amplitude as a function of stimulus number recorded from a P22 WT vNLL neuron shown in A1. The respective stimulation strength is color coded. **B1.** Average evoked current responses to increasing stimulation strengths of a representative P22 KO vNLL neuron. All traces represent the average of at least five consecutive recordings to the same stimulation strength. Two distinct current steps are visible. **B2.** EPSC amplitude as a function of stimulus number recorded from a P22 KO vNLL neuron shown in B1. The respective stimulation strength is color coded. **C.** Normalized maximal EPSC traces from P22 WT (light gray) and P22 KO (dark gray) as shown in A and B. **D.** Estimated number of EPSC steps evoked by an increasing stimulation strength in vNLL neurons of P22 WT and KO animals. KO animals have significantly more current steps. P22 WT: n=16; P22 KO: n=16. **E.** Maximal EPSC amplitude is significantly larger in P22 WT animals. Values referring to an estimated fiber number of three, four, and five are shifted slightly to the right to demonstrate their correlation with F and G. **F.** 10–90% rise time is measured by applying a minimal stimulation paradigm. P22 WT vNLL neurons rise significantly faster than P22 KO vNLL neurons. **G.** Tau decay is measured by applying a minimal stimulation paradigm. A single-exponential function is fitted to the decay of the current response; tau is extracted.

All data sets were tested for normality and homogeneity of variance, and according to the result, statistical significance was determined by a non-parametric Kruskal-Wallis test followed by a Games-Howell *post hoc* test. Significant differences are labeled with * ($P < 0.05$).

Neurons of KO animals exhibited a rather immature profile of synaptic EPSC characteristics, as seen P10 WT animals. Congenital deafness due to the loss of otoferlin apparently leads to an impairment of the typical development of synaptic refinement and synaptic strength.

6.3.9 Hyperactivity of vVNLL synapses in deaf mice

In the next steps of our analysis, we wanted to further dissect pre- and postsynaptic properties that are influenced by congenital deafness in mice. Therefore, we studied the spontaneous vesicle release and used these results for the analysis of short-term plasticity experiments.

While inhibitory receptors and voltage-gated sodium channels were pharmacologically blocked, mEPSCs were recorded for at least three minutes. Recordings of KO animals were generally shaky, reflected by a greater noise level, whereas in P22 animals, stable measurements were obtained (Figure 27A and B). All electrophysiological experiments in KO animals were affected by an unsteadiness of electrode patches on the membrane that might result from biophysical effects of the lack of otoferlin. Unfortunately, this phenomenon has not been described in literature. In spite of these experimental difficulties, mEPSC amplitudes and charges were similar in both genotypes (Figure 27 C and D; Table 8). The mEPSC charge reduction was similar in KO and control animals compared with P10 WT animals (see Table 8), suggesting a developmental process that is independent of auditory-evoked activity. However, the mEPSC frequency of KO animals was significantly larger than that of WT animals (Figure 27E; Table 8), leading to the conclusion that a controlled release of vesicles is missing. Moreover, 10–90% rise and tau decay times were both larger in KO; however, only the increase in decay time was statistically significant (Figure 27F and G; Table 8). Both values belonging to KO animals lay in between the values of P10 and P22 WT animals (see Table 8).

These results provide evidence that deafness not only alters postsynaptic receptor kinetics but also affects the presynaptic vesicle release.

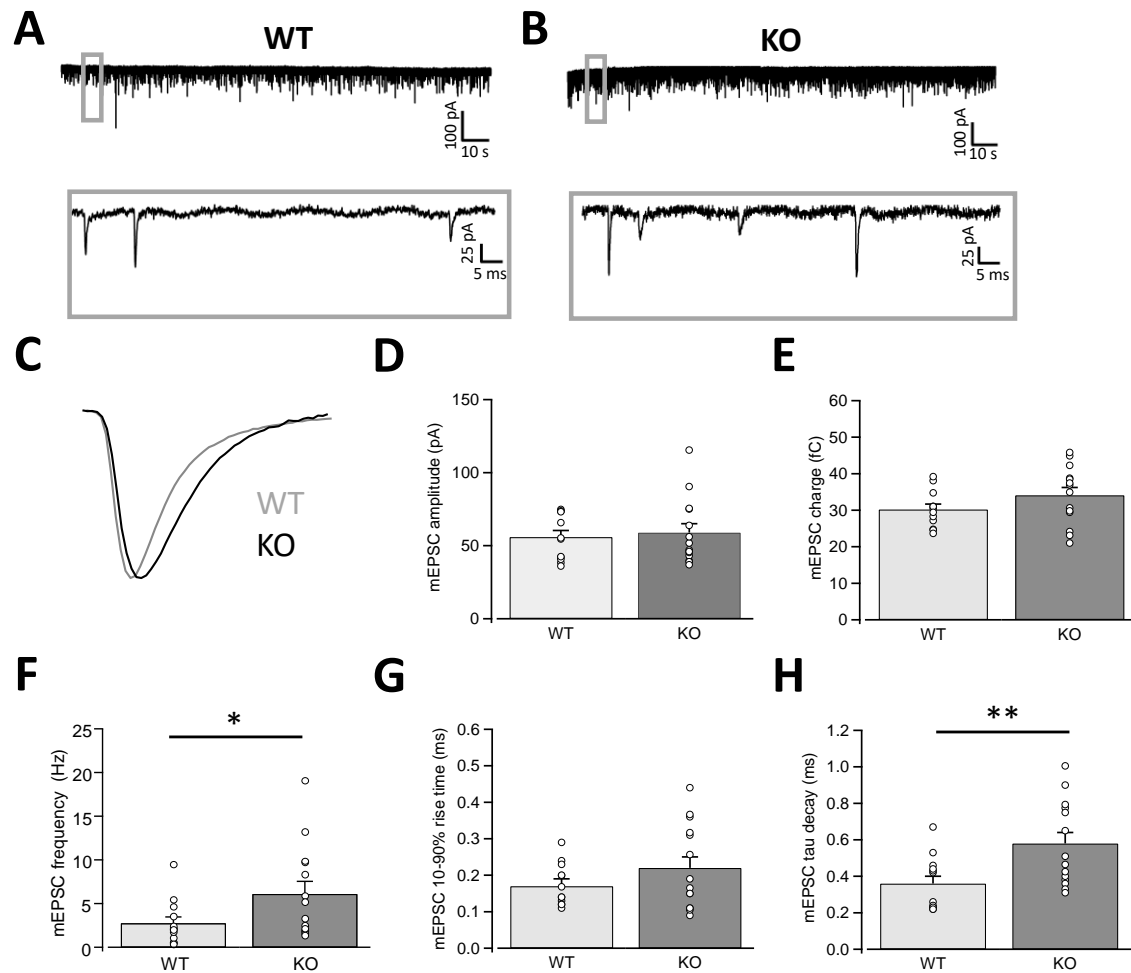


Figure 27: Miniature excitatory postsynaptic currents (mEPSC) of vNLL neurons have a larger frequency and decay more slowly in P22 $OTOF^{(-/-)}$ (KO) than in P22 $OTOF^{(+/+)}$ (WT) animals. **A.** Recording of a representative mEPSC of a P22 WT vNLL neuron (top). Enlargement of three single mEPSCs (bottom). **B.** Recording of a representative mEPSC of a P22 KO vNLL neuron (top). Enlargement of three single mEPSCs (bottom). **C.** Normalized average mEPSCs shown in A. **D.** Average mEPSC amplitudes of each neuron (P22 WT: n=13; P22 KO: n=14) are depicted as single circles. **E.** mEPSC charges. **F.** mEPSC frequency is larger in KO animals. **G.** mEPSC 10–90% rise time. **H.** mEPSC tau decay is measured by fitting a single-exponential function to the decay of the current response; tau is extracted. P22 WT vNLL neurons decay significantly faster than P22 KO vNLL neurons.

All data sets were tested for normality and homogeneity of variance, and according to the result, statistical significance was determined by a non-parametric Kruskal-Wallis test followed by either a Games-Howell or Tukey's *post hoc* test. Significant differences are labeled with * (P < 0.05) or ** (P < 0.01).

6.3.10 Depletion of the readily releasable pool remains unaffected in vVNLL synapses of deaf mice

We were also interested in examining other possible presynaptic developmental changes in otoferlin mice, such as depletion and replenishment of the RRP and its effects on the postsynaptic response strength to stimulation trains. Therefore, we investigated the short-term plasticity (STP) of excitatory inputs to vVNLL neurons in KO and WT mice (15 stimuli at 100 Hz).

All recorded neurons of both genotypes showed a substantial degree of short-term depression (Figure 28A–E). No significances were found regarding the overall (Figure 28C; Table 9), steady-state (Figure 28D; Table 9) or paired-pulse depression (Figure 28E; Table 9). Additionally, the overall depression from stimulus 2 to stimulus 15 was around 60% for both genotypes (Figure 28C; Table 9). Furthermore, all recorded KO neurons showed a paired-pulse depression in their first two EPSC amplitudes (Figure 28E; Table 9), and only one neuron in a P22 animal exhibited paired-pulse facilitation (Figure 28E; Table 9). Next, we were interested in how the RRP and its characteristics were shaped in mice without auditory nerve activity. Therefore, we applied the same procedure we used in the developmental study of otoferlin mice (see above). A representative Elmquist-Quastel plot is displayed in Figure 28F (dashed lines represent extrapolated RRP). From these calculations, we concluded that the RRP was similar in WT and KO animals (Figure 28G; Table 9). Furthermore, the release of the maximal response was exactly the same, and, plausibly, the ratio of the maximal response and the RRP also remained alike in both genotypes (Figure 28H and I; Table 9). It is worth noting that a cumulation of transmitted charges would have been more accurate in measurements with similar EPSC shapes as we found in KO and WT mice. However, since mEPSCs at early developmental stages had significantly longer time constants, we decided to also calculate the RRP and its properties with EPSC amplitudes for WT and KO mice to enable better comparability with P10 animals. Still, significances did not change with either method for KO and WT animals (results for calculation with EPSC charges not shown).

Taken together, our data suggest that congenital deafness has a large effect on the typical development of pre- and postsynaptic EPSC properties. In particular, the proper refinement of excitatory synaptic inputs together with receptor kinetics and the spontaneous release of

glutamatergic vesicles is altered in KO animals. However, STP and the RRP seem to develop typically in deaf mice.

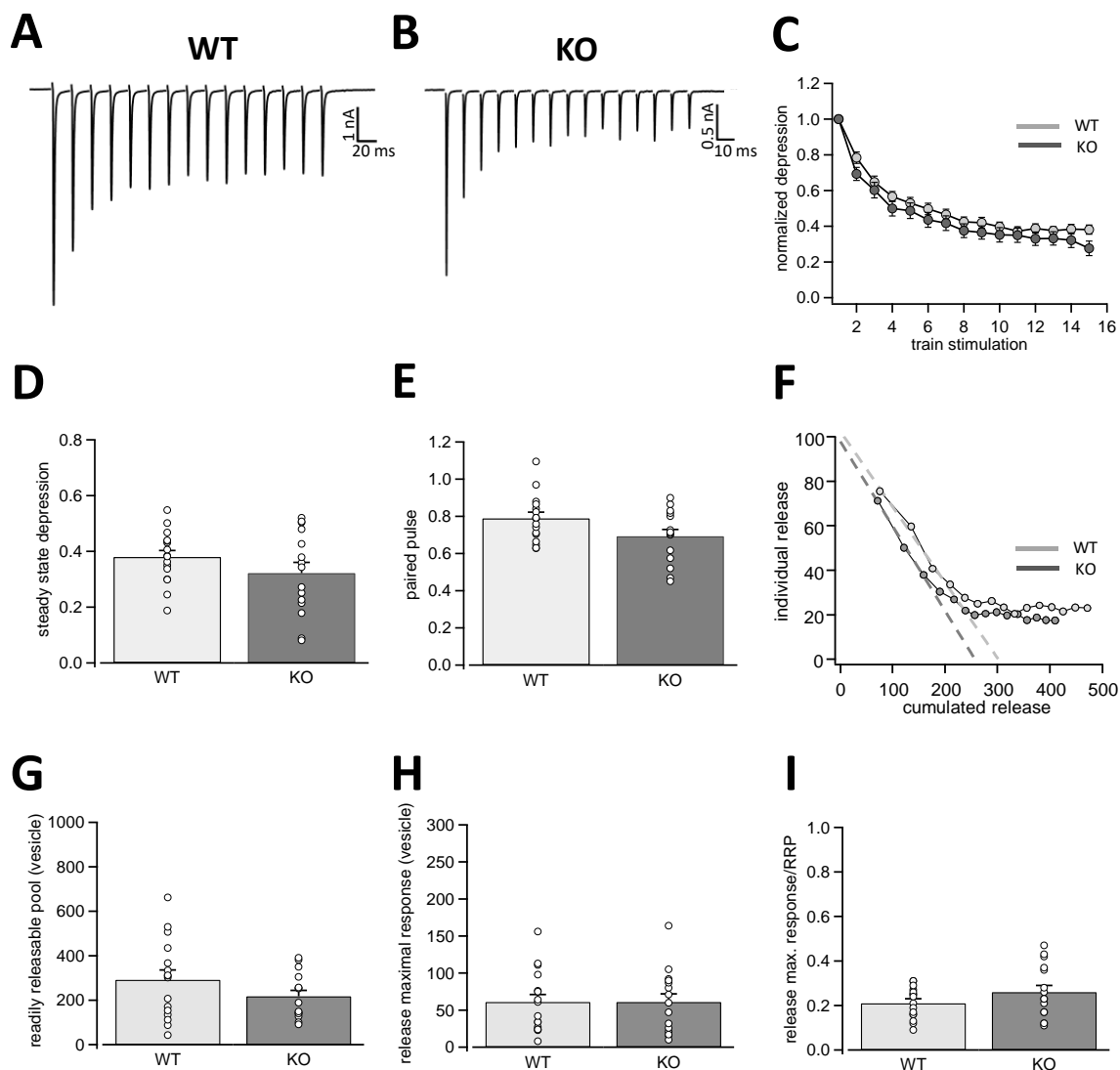


Figure 28: Synaptic short-term plasticity of excitatory inputs of vNLL neurons are similar in P22 OTOF^(+/+) (WT) and P22 OTOF^(-/-) (KO) animals. **A.** A representative EPSC trace in response to 15 stimulations at 100 Hz illustrating short-term plasticity in a vNLL neuron of a P22 WT animal. **B.** A representative EPSC trace in response to 15 stimulations at 100 Hz illustrating short-term plasticity in vNLL a neuron of a P22 KO animal. **C.** Normalized EPSC depression curve for all recorded vNLL neurons in P22 WT and KO animals (P22 WT: n=16; P22 KO: n=15). **D.** Steady-state depression is determined as the average of the last three amplitudes of the 100 Hz EPSC train divided by the first amplitude. **E.** Paired pulse is calculated as the second amplitude divided by first amplitude of the 100 Hz EPSC train. **F.** Elmquist-Quastel plot (EQ plot) - exemplary EQ plot to calculate the RRP from train stimulation data. Individual release of each current amplitude to each stimulus is calculated with the mEPSC amplitude from Figure 27D. Cumulated release is calculated as the cumulation of individual releases up to that specific stimulus. A linear regression is applied to the first three cumulative steps and extrapolated to the x-intercept. The x-intercept theoretically matches the RRP. **G.** RRP of all recorded vNLL neurons in P22 WT and KO animals. **H.** Release of the maximal response is determined by a maximal stimulation paradigm and calculated as the amplitude of the largest current response to a 100 Hz stimulation pulse divided by the amplitude of the average mEPSC (shown in Figure 27D). **I.** Ratio of the release at maximal response/readily releasable pool (RRP) is calculated from G and H. **(Continued on page 97)**

← Figure 28 continued:

All data sets were tested for normality and homogeneity of variance, and according to the result, statistical significance was determined by either a two-factor ANOVA followed by a Dunn's *post hoc* test, a single-factor ANOVA followed by a Scheffé's *post hoc* test or a non-parametric Kruskal-Wallis test followed by a Games-Howell *post hoc* test.

6.3.11 VGlut1 and calretinin distribution is similar in deaf and hearing mice

Our electrophysiological findings indicate impairments of pre- and postsynaptic characteristics in congenitally deaf animals. Therefore, we wanted to investigate the formation of calretinin in the presynaptic compartment of synapses innervating vVNLL neurons. To assure that we examined excitatory synapses, the distribution of VGlut1 was also studied (Figure 29). Here, WT animals showed a distribution pattern of perisomatic VGlut1-positive rings around numerous neurons (Figure 29A), and calretinin colocalized with the VGlut1-positive staining, showing the extents of the excitatory inputs (Figure 29B and C). Additionally, in the vVNLL of KO animals, a similar distinct perisomatic VGlut1-positive staining was found (Figure 29D) together with a similarly developed calretinin expression (Figure 29E). Altogether, these data suggest that the expression of the calcium-binding protein calretinin is independent of auditory-evoked activity and that large excitatory inputs to vVNLL neurons are present in both WT and KO animals (Figure 29C and F). However, the precise number of excitatory inputs cannot be derived from our immunohistochemical data.

Congenital deafness caused by a lack of otoferlin in the inner hair cells leads to an impairment of the typical development of intrinsic neuronal properties and reduced synaptic refinement. Additionally, some of the neuronal characteristics seem to be immature and resemble those of animals just around hearing onset. Interestingly, only a few neuronal and synaptic aspects seem to be unaffected by the lack of auditory-evoked activity. For instance, the activation of HCN channels for small negative current injections appears to be unaffected by the lack of sensory experience. Furthermore, the presynaptic RRP and its depletion are functionally unimpaired. However, a reduced excitability of vVNLL neurons could be found in a more depolarized action potential threshold, whereas an increased mEPSC frequency, by contrast, is a sign of an uncontrolled enhanced presynaptic activity. Our results indicate that auditory-evoked activity is essential for a typical development of spiking patterns and synaptic properties in neurons of the vVNLL in mice.

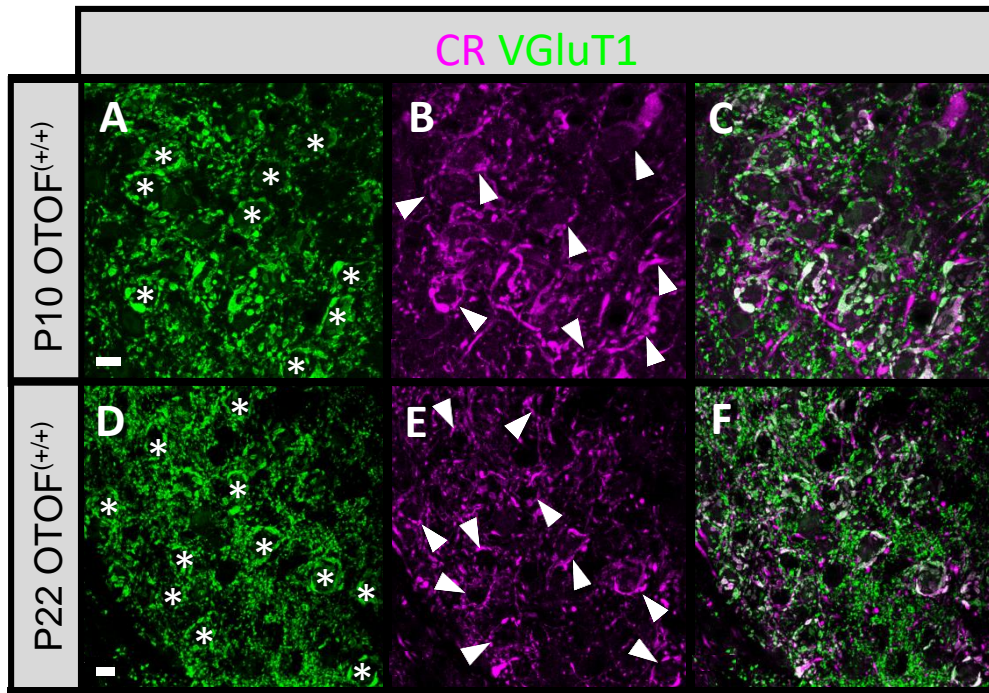


Figure 29: Immunolabelings to visualize excitatory inputs to vNLL neurons in P22 OTOF^(+/+) (WT) and P22 OTOF^(-/-) (KO) animals with antibodies against VGluT1 and calretinin (CR). **A.** A VGluT1-positive perisomatic staining of nine neurons (asterisks) of a maximal projection of the vNLL of a P22 WT animal. N=2. **B.** Calretinin labeling of a maximal projection of the vNLL of the P22 animal shown in A. Arrowheads point to CR-positive staining of synaptic inputs to eight neurons shown in A. **C.** Merged image of A and B. Colocalization of VGluT1 and CR appears white. Eight out of nine neurons with a perisomatic VGluT1 labeling have CR in their synaptic inputs. **D.** A VGluT1-positive perisomatic staining of 10 neurons (asterisks) of a maximal projection of the vNLL of a P22 KO animal. N=4. **E.** Calretinin labeling of a maximal projection of the vNLL of the P22 KO animal shown in D. Arrowheads point to CR-positive staining of synaptic inputs to 10 neurons shown in D. **F.** Merged image of D and E. Colocalization of VGluT1 and CR appears white. All 10 neurons with a perisomatic VGluT1 labeling have CR in their synaptic inputs. Scale bar: 10 μ m.

7 Discussion

7.1 Characterization of the VNLL

We characterized the VNLL of mice in a ventrodorsal orientation, since this has not been systematically done in previous studies. Furthermore, the margins of the VNLL were still unclear before we did this study, especially of the dorsal part that is argued to form a separate nucleus – the INLL (Saint Marie et al. 1997; Ito et al. 2011). We were particularly interested in the VNLL because it may play an important role in the analysis of acoustic temporal features (Aitkin et al. 1970; Covey and Casseday 1991; Recio-Spinoso and Joris 2014) and, therefore, speech perception. The first part of this thesis demonstrated several distinct subpopulations of neurons in the dorsal and ventral parts of the VNLL. One distinct subpopulation of neurons, located in the ventrolateral part of the VNLL, displayed an onset-type firing pattern and only little I_h . These neurons for the most part received one large calyx-like excitatory input and multiple large inhibitory inputs and were densely packed in a cluster lateral to the fiber bundle. A second cell type, located in the ventromedial part of the VNLL, was scattered within the fiber bundle. Although these neurons exhibited similar firing and intrinsic properties compared with ventrolateral neurons, they received several and much weaker excitatory inputs.

In the dVNLL, neurons with two different firing patterns are intermingled. Neurons showed either a single spike at the onset of the response or a sustained firing pattern. Moreover, all dorsal neurons exhibited large I_h . The onset-type firing neurons in the dorsal part clearly differed from the onset-type firing neurons in the ventral part of the VNLL in terms of their intrinsic properties. Ventromedial VNLL neurons that were intermingled within the lemniscal fiber tract had intrinsic properties similar to the ventrolateral neurons and synaptic properties that resembled those of neurons in the dVNLL. All neuron types in the dorsal and ventral VNLL depolarized by light stimulation in a VGAT-channelrhodopsin mouse model where channelrhodopsin is expressed under the promoter of VGAT (Zhao et al. 2011). Since in this mouse model only inhibitory neurons depolarize by light stimulation, our sample neurons were inhibitory and were part of the VNLL rather than the INLL (Saint Marie et al. 1997; Ito et al. 2011).

7.1.1 The ventral part of the VNLL contains a cluster of neurons with calyx-like synaptic inputs

Part 1 described a distinct population of neurons in the vVNLL with biophysical membrane properties that are very similar to those found in neurons of the MNTB (Brew and Forsythe 1995; Hassfurth et al. 2009). Both these neuron populations have a typical onset-type response pattern, little I_h and a lack of HCN1 immunoreactivity. Previously, similar onset-type firing neurons have been described in the ventral part of the rat VNLL that were correlated with a bushy cell-like morphology (Wu 1999; Zhao and Wu 2001). However, only around 25% of the neurons studied belonged to this neuron type. An explanation for this relatively low fraction of onset neurons might be the different developmental time frames studied, variations in recording sites (dorsal vs. ventral), and the different recording techniques employed. A recent study of gerbil VNLL neurons with calyx-like inputs demonstrated a developmental change from a sustained to an onset-type firing pattern within the first week after hearing onset (Berger et al. 2014; Franzen et al. 2015). However, neither the spatial distribution of neurons within the VNLL nor the existence of other cell types was discussed in that study.

Our data indicate that these neurons receive one large calyx-like excitatory input similar in amplitude and temporal properties to the calyx of Held synapse in the MNTB (Borst and Soria van Hoeve 2012). Moreover, these neurons are surrounded by a VGluT1- and calretinin-positive ring, which suggests that this input originates from octopus cells of the contralateral VCN (Adams 1997; Schofield and Cant 1997; Felix Ii et al. 2017). Similar calyx-like synaptic structures with comparable physiological characteristics were recently described in the gerbil VNLL (Berger et al. 2014). However, in that study VNLL neurons were usually contacted by two large excitatory synaptic inputs. Whether this is a species-specific adaptation or whether a further developmental reduction of inputs occurs after P12, when these gerbil experiments were performed, remains unexplored. Anatomical studies in other mammals have identified a subdivision within the ventral VNLL with densely arranged and fairly uniformly shaped neurons (Willard and Ryugo 1983; Vater and Feng 1990; Adams 1997; Schofield and Cant 1997; Benson and Cant 2008), which suggests that this neuron type is commonly found in all mammalian species. In fact, an anatomical study suggests that in humans this area is even hypertrophied (Adams 1997), which would support the theory that the VNLL is immensely important for the analysis of speech containing temporal patterns. Communication is widely spread among species of the animal

kingdom, but a controlled and unpredictable use of language is unique to humans. Interestingly, neurons in the ventral VNLL that were not located in this cluster but were intermingled within the fiber tract of the lateral lemniscus received several excitatory inputs with much smaller amplitudes similar to dVNLL neurons, while intrinsic properties were indistinguishable from the ventrolateral VNLL neurons. Further experiments are necessary to determine whether input origin and response properties of these neurons are more similar to ventrolateral or dorsal VNLL neurons.

7.1.2 Neurons in the dorsal part of the VNLL have two different firing patterns and large I_h

Dorsal VNLL neurons responded to depolarizing current injections with two different firing patterns. Whereas one population of neurons had the typical onset-type response similar to principal cells in the lateral and medial superior olive, with low input resistance and large I_h (Mathews et al. 2010; Walcher et al. 2011), the other neuronal population fired throughout the depolarizing stimulus and with increasing frequency for stronger depolarization. This suggests a differential distribution of potassium channels, especially the low-threshold potassium channels of the K_v1 family, that are usually abundant in neurons with an onset-type firing pattern (Barnes-Davies et al. 2004; Mathews et al. 2010). Morphologically, two different neuron types are present in the dVNLL. The most frequent type is the multipolar cells that are densely packed in the most dorsal part of the VNLL in most species (Schofield and Cant 1997; Benson and Cant 2008). Another less-frequent type is the giant cells (Schofield and Cant 1997; Benson and Cant 2008). Whether this morphological cell type corresponds to our onset- or sustained-firing type is unclear but could be determined by studying potassium channel distribution in the VNLL.

In the dVNLL, all neurons had relatively large I_h that was confirmed by an intensive immunostaining against the HCN1 channel. Among other HCN subtypes, the HCN1 subunit is the one with the fastest activation time constant and the most depolarized half-maximal activation of I_h (Wahl-Schott and Biel 2009). Therefore, neurons with large HCN1-mediated currents integrate excitatory and inhibitory inputs with a high temporal resolution and little summation (Khurana et al. 2012; Baumann et al. 2013). Consistently, most of the neurons received excitatory and inhibitory inputs with fast synaptic time constants. These fast synaptic currents together with the rapid membrane time constants

suggest that these neurons may contribute to temporal sound pattern analysis by integrating their inputs with high temporal precision, as has been suggested for VNLL neurons (Nayagam et al. 2005; Yavuzoglu et al. 2011; Recio-Spinoso and Joris 2014).

7.1.3 Dorsal and ventral VNLL neurons are inhibitory

Several studies have demonstrated that a population of neurons in the most dorsal VNLL differs from more ventral VNLL neurons in terms of input projection, binaurality, and neurotransmitter type. These dorsal VNLL neurons mostly express excitatory markers, whereas most neurons in ventral VNLL are either GABAergic, glycinergic, or co-express both inhibitory transmitters (Saint Marie et al. 1997; Riquelme et al. 2001; Ito et al. 2011). The very dorsal VNLL neurons also receive prominent projections from binaural nuclei of the superior olive (Kelly et al. 2009), which are mostly absent in the ventral VNLL. A number of studies have therefore defined this structure in the very dorsal VNLL as a distinct nucleus, named the intermediate nucleus of the lateral lemniscus (INLL). Nevertheless, the boundaries and extent of this structure are not clearly defined and show large species-specific differences (Zook and Casseday 1982b; Saint Marie et al. 1997; Kelly et al. 2009; Ito et al. 2011). Using a transgenic mouse model, which expresses channelrhodopsin-2 under the VGAT promoter and thus only in inhibitory, GABAergic, or glycinergic neurons (Zhao et al. 2011), we demonstrated that all our neurons in the dorsal VNLL are inhibitory and therefore presumably not part of the excitatory, binaural INLL structure. We also identified a population of small neurons that are located dorsal of our investigated neurons and may fulfill these criteria such as responding to binaural inputs and being excitatory.

7.1.4 Functional heterogeneity of VNLL neurons for sound processing

Part 1 revealed distinct variations in intrinsic and synaptic properties between the different populations in the ventral and dorsal VNLL. *In vivo* several response patterns to sounds, including onset, regular, sustained, and chopper cells have been recorded in several species, but with no clear correlation between response type and location within the VNLL (Batra and Fitzpatrick 1997; Nayagam et al. 2006; Zhang and Kelly 2006). One possible explanation for this discrepancy is that the *in vivo* response patterns are predominantly determined by the input properties, whereas the intrinsic and synaptic properties are less influential. A similar lack of position with binaural response type of VNLL neurons has

been observed in most species examined. In the rat and cat, most VNLL neurons are driven by contralateral stimulation, with more pronounced ipsilateral inhibitory inputs in the rat but only weak influence by ipsilateral stimulation in the cat (Nayagam et al. 2006; Zhang and Kelly 2006; Recio-Spinoso and Joris 2014). A similar weak input from the ipsilateral ear is present in the mouse VNLL (unpublished observation). It is therefore unlikely that the two different response types in the dVNLL correspond to different groups of binaurality. We observed inhibitory, glycinergic inputs with similar characteristics to all neuron types in all regions of the VNLL. Whether these inputs all derive from the previously characterized input of the ipsilateral MNTB (Kelly et al. 2009) or whether some of these inputs originate from other glycinergic nuclei such as, for example, the contralateral MNTB or the lateral nucleus of the trapezoid body, remains to be demonstrated.

Finally, human anatomical and physiological observations suggest that the VNLL is involved in various forms of temporal processing of sound patterns (Covey and Casseday 1991; Adams 1997; Oertel 1999; Nayagam et al. 2005). The bushy cell-like neurons in the vVNLL that receive calyx-like inputs have received particular attention in this context. In the mouse we have identified a cluster of neurons in the ventrolateral part of the VNLL that receives a single calyx-like input most likely originating from the octopus cells in the PVCN. Octopus cells preferably respond to broadband stimuli with precisely timed discharges (Rhode et al. 1983; Rouiller and Ryugo 1984). Similarly, VNLLc neurons in bats respond with exceptionally sharply timed spikes to the onset of sounds (Covey and Casseday 1991). Likewise, a population of VNLL neurons in other mammals shows precisely timed onset responses (Nayagam et al. 2005; Recio-Spinoso and Joris 2014). These neurons are monaural and respond with one spike with short latencies precisely locked to the stimulus onset, which makes these neurons well suited to accurately encode temporal information (Recio-Spinoso and Joris 2014). In accordance with this, ventrolateral VNLL neurons exhibit intrinsic properties that secure temporally precise information processing (Franzen et al. 2015). A recent model suggests that these neurons provide fast onset inhibition to neurons in other parts of the VNLL and the IC, thereby suppressing spectral splatter (Spencer et al. 2015). Indeed, a previous study has illustrated that a subpopulation of VNLL neurons receives a large preceding inhibition that strongly influences first spike latency (Nayagam et al. 2005; Spencer et al. 2015). The fast membrane and synaptic properties of the onset-type neurons of the dVNLL would be

ideally suited to precisely integrate the fast preceding inhibition with several excitatory inputs. Nevertheless, in none of our recordings from the dVNLL neurons were we able to detect an extremely large inhibitory input, as proposed in the model study (Spencer et al. 2015). It is possible that these large inhibitory inputs are received by a special type of neuron that is not preserved in the brain slice preparation. Alternatively, our stimulation method could be less effective in stimulating these inputs. Using a VGAT-channelrhodopsin mouse model could provide more information about this intrinsic inhibitory circuit.

We found distinct populations of neurons with different biophysical and synaptic properties in the dorsal and ventral parts of the VNLL. One neuron type in the ventrolateral VNLL displays onset-type response pattern and calyx-like excitatory input properties very similar to MNTB neurons. These properties make these neurons likely candidates for providing temporally precise and fast feed-forward inhibition to target cells within the VNLL and to the IC. By contrast, onset-type dVNLL neurons with large I_h and short membrane time constants might contribute to the analysis of temporal sound patterns by integrating excitatory and inhibitory inputs on a fast time scale.

7.2 Development of neuronal and synaptic features in the ventrolateral VNLL

Neurons located in the ventrolateral part of the VNLL receive calyx-like inputs that are comparable to the MNTB innervation (von Gersdorff and Borst 2002). Previously performed studies on the ventrolateral VNLL of rodents have focused on either intrinsic or synaptic specifics, but the developmental aspects of calyx formation and intrinsic properties have not been investigated (Berger et al. 2014; Franzen et al. 2015). Studies in the MNTB have indicated that calyx formation and refinement of synaptic inputs occur very early during development before hearing onset (Hoffpauir et al. 2006, 2010). Therefore, in Part 2 of this thesis, we aimed to investigate the development of the calyx-like input and intrinsic properties in vVNLL neurons based on Part 1 of this thesis to compare it to the developmental time course of the calyx of Held. The VNLL can be subdivided into at least two distinct regions in terms of their synaptic inputs and intrinsic firing properties. In the vVNLL, neurons of mature animals are innervated by one to maximally two excitatory

inputs. In order to elucidate the onset of calyx formation, we performed experiments on C57Bl/6 mice before, shortly after, and several days after hearing onset (P10, P13, and P22). As controls for an activity-dependence investigation we used otoferlin WT mice at P10 and P22 to further investigate intrinsic neuronal characteristics, calyx-formation, and short-term plasticity.

7.2.1 Neurons of the vVNLL become more homogeneous during development

Synaptic inputs were reduced to an average of one large input at P22. However, the synaptic strength of these large calyx-like inputs remained similar during development of OTOF WT mice, in contrast to the increase in synaptic strength in Bl6 mice. Along with these developments, time constants of AMPA receptors were also reduced substantially during that time. Moreover, short-term depression was largest in P10 (~78%) animals and was reduced during development to approximately 62%. Properties of the RRP were unchanged during development in WT mice.

Animals before hearing onset (P10) displayed several distinct neuronal subpopulations in the ventrolateral part of the VNLL. One distinct subpopulation of neurons displayed an onset-type firing pattern that was also found in mature P22 WT mice. A second cell type that was only found in immature mice was intermingled with onset-type firing neurons. These cells showed a sustained firing pattern and occurred in 26% of all recordings. Intrinsic properties remained relatively similar during development; only the resting membrane potential of P22 WT animals was shifted to a more hyperpolarized state. Action potential properties, however, apparently changed after hearing onset. While neurons of P10 animals had a current threshold of approximately 300 pA, neurons of older animals displayed an increased threshold of almost 400 pA. In addition, action potential shapes became briefer, suggesting a faster progression of action potentials in older animals. Intrinsic neuronal properties found in this study accord with findings in literature (Baumann and Koch 2017), where authors have recently focused on developmental changes of vVNLL neurons under the influence of nicotine and compared their results to untreated C57Bl/6 mice. Although these experiments were performed in even younger animals (P8), their results resemble those of this study and show the power of reproducibility. Another study compared VNLL neurons of gerbils in P9 and P25 animals (Franzen et al. 2015), finding decreases in membrane time constants and input resistances and authors claiming

these substantial reductions on a significant decrease of cell size. The cell size determines the capacitance of a neuron and strongly influences the speed with which the membrane is charged (Franzen et al. 2015). Furthermore, a reduction of cell size is caused by a reduction of dendritic arborization (Rogowski and Feng 1981; Sanes et al. 1992; Rietzel and Friauf 1998; Rautenberg et al. 2009). A significant reduction of cell size and thus capacitance has not been observed in vVNLL neurons of mice (Baumann and Koch 2017).

Recent studies on the VNLL of gerbils have demonstrated that neurons with calyx-like inputs undergo a developmental change from a sustained to an onset-type firing pattern within the first week after hearing onset (Berger et al. 2014; Franzen et al. 2015). Moreover, MNTB principal neurons also undergo a similar developmental pattern. At prenatal day E17, almost two thirds of the neurons show sustained firing (Hoffpauir et al. 2010). This percentage increases until the age P1 (95%), and only after that does a transition from sustained to onset occur. Interestingly, this transition in firing patterns happens at the onset of calyx growth (Hoffpauir et al. 2010). Long before hearing onset at P6, 95% of the neurons exhibit an onset firing pattern (Hoffpauir et al. 2010). It has been demonstrated for many auditory brainstem nuclei that a change of passive and active membrane properties occurs during development and that a reduction of input resistances and membrane time constants leads to a faster generation of action potentials that, in turn, results in the fast and precise transmission of auditory signals (Wu and Oertel 1987; Kandler and Friauf 1995; Ahuja and Wu 2000; Kuba et al. 2002; Scott et al. 2005; Ammer et al. 2012). Modifications in action potential shapes influence the ability to code certain auditory information; for example, a neuron with narrower action potentials will be able to follow fast signals, as found during auditory processing.

7.2.2 Low-voltage-activated potassium channels might trigger fast and precise onset firing

In addition to passive properties influencing the neuronal ability to generate action potentials and follow auditory stimuli with a high temporal precision, the interplay of intrinsic passive with active properties also determines the firing behavior and rates of cells (Fricker and Miles 2000; Kuba et al. 2002; Axmacher and Miles 2004; Gittelman and Tempel 2006; Berntson and Walmsley 2008; Ammer et al. 2012). Moreover, intrinsic membrane properties are greatly affected by the biophysical properties of embedded ion channels (Fricker and Miles 2000; Gittelman and Tempel 2006; Berntson and Walmsley

2008; Johnston et al. 2010) and cell morphology (Mainen and Sejnowski 1996). Potassium channels in particular are known for their role in modifying firing patterns and neuronal excitability (Garden et al. 2008; Oertel et al. 2008; Hassfurth et al. 2009). Voltage-gated potassium channels that are activated around resting potential, such as K_v1 , and HCN channels influence the resting potential and synaptic integration, especially in the auditory brainstem (Garden et al. 2008; Oertel et al. 2008; Hassfurth et al. 2009). Some authors have demonstrated that K_v1 , K_v4 , and K_v7 are low-voltage-activated potassium channels opening on small depolarizations around the resting potential and provide a powerful instrument to regulate action potential number (Coetzee et al. 1999; Brew et al. 2003, 2007; Brown and Passmore 2009). The K_v1 channels are known to contribute to the firing threshold and action potential amplitude, and the low-voltage-activated potassium channel $K_v1.2$ in particular determines action potential properties in the auditory brainstem nucleus MNTB (Brew and Forsythe 1995; Dodson et al. 2002; Klug and Trussell 2006). Neurons of the MNTB fire exclusively with one spike at the onset, although the postsynaptic current is large enough to trigger more. According to Dodson et al. (2002), neurons of the MNTB show a more depolarized action potential threshold and a smaller peak amplitude in recordings with active $K_v1.2$ channels in comparison with measurements where these channels were blocked.

In accordance with the study of Dodson et al. (2002), other studies on MNTB neurons have found a shortening of action potentials under the influence of $K_v1.2$ channels. A blockage of these channels results in a more hyperpolarized resting potential and a growth in action potential amplitude (Leao et al. 2004a; Klug and Trussell 2006). It has been argued that a lack of $K_v1.2$ prevents a complete repolarization of action potentials and elicits additional firing due to the presence of residual synaptic current from the large excitatory synaptic inputs to the MNTB (Leao et al. 2004a). The ventrolateral part of the VNLL is similar to neurons of the MNTB in terms of firing patterns, the ability to fire at high rates, action potential precision, and inputs. The size of the synaptic input charges the membrane very quickly and brings it rapidly to its threshold (Johnston et al. 2009).

In addition, principal neurons in the LSO show an interesting distribution of $K_v1.1$ (Barnes-Davies et al. 2004). There, 70% of the principal neurons located in the lateral LSO exhibit an onset firing pattern, whereas for neurons closer to the medial region, more than 90% display a sustained firing pattern. Interestingly, a morphological study in the publication from Barnes-Davies et al. (2004) shows a correlation with the $K_v1.1$ distribution. The

lateral LSO displays a much larger degree of fluorescent intensity. Furthermore, other morphological studies confirm the expression of $K_v1.1$ and $K_v1.2$ in other brainstem nuclei of mice (Wang et al. 1994; Grigg et al. 2000). Other authors linked the activity of high-voltage-activated potassium channels such as K_v3 with the rapid action potential repolarization and firing of numerous action potentials (Wang et al. 1998a; Rudy and McBain 2001).

These results indicate that mature VNLL neurons may have an enhanced expression of K_v1 channels, whereas younger animals still exhibit neurons with a larger K_v3 expression. Whether this change is evoked by auditory activity is evaluated in Section 7.3 below.

7.2.3 Synaptic refinement of calyx-like inputs in the vVNLL occurs much later around hearing onset than of the calyces of Held in the MNTB

Synaptic activity can be divided into two separate systems – evoked and spontaneous (Lu et al. 2007). Here, postsynaptic responses are described that resulted from artificial fiber stimulation to imitate either spontaneous or evoked (only in animals after hearing onset) action potential transmission. Although the calyx of Held is already formed at P2 (Hoffpauir et al. 2006), it still undergoes pruning during early development between prenatal day E17 and postnatal day P1 (Morest 1968; Kandler and Friauf 1993; Rodriguez-Contreras et al. 2008; Hoffpauir et al. 2010). Neurons of the vVNLL undergo refinement of excitatory synaptic inputs much later than those of the MNTB. At P10, an average of 3.38 excitatory fibers innervates one vVNLL neuron, whereas only three days later synaptic pruning is finished and not further altered. Furthermore, the increase of synaptic strength also occurs much earlier in MNTB neurons, between P3 and P4 (Hoffpauir et al. 2010), whereas in vVNLL neurons a significant increase is found only after hearing onset. Rise and decay times are similarly reduced both in MNTB and vVNLL neurons of mice (Hoffpauir et al. 2010).

A recent study on the VNLL of gerbils implies that VNLL neurons are generally innervated by two excitatory inputs (Berger et al. 2014). While in that study experiments were performed in gerbils just before hearing onset at P9–11, we examined the developmental reduction of VNLL inputs in mice at P10, P13, and P22. Our electrophysiological results in mice indicate a synaptic refinement to mainly one large excitatory input in adult mice. Whether there is further decrease of excitatory inputs in the gerbil VNLL was not

investigated by Berger et al. (2014) and remains unclear. Older studies, though, support the assumption of two presynaptic terminals innervating the VNLL (Covey and Casseday 1986; Vater and Feng 1990; Adams 1997; Schofield and Cant 1997). Berger et al. (2014) claim that the activation of both inputs is necessary in order to trigger a postsynaptic response (Berger et al. 2014). In the vVNLL of mice, however, it has been demonstrated that stimulations of calyx-like inputs generate action potentials at a high precision rate (Baumann and Koch 2017). Here, we showed that stimulations of single fibers resulted in large postsynaptic responses that accord with the results of the study performed by Baumann and Koch (2017). The mechanisms by which these redundant inputs are downregulated are still not entirely understood. A theory by Rusu and Borst (2011) proposed that a spike-time dependent plasticity influences both the formation of the calyx synapse and the postsynaptic area that corresponds to the release sites of the calyx. There, the postsynaptic membrane develops a decreased input resistance and accelerated kinetics of postsynaptic receptors that in turn strengthen the bond of calyx synapse and postsynaptic membrane and may indirectly prime the downregulation of inputs that cause only subthreshold responses (Rusu and Borst 2011).

We conclude that either sound-evoked activity is crucial for calyx formation in the VNLL or a coincidental development of synaptic refinement during hearing onset takes place. This issue required further investigation with hearing-impaired animals, which I performed in Part 3 of this thesis and discuss below.

7.2.4 Strain-specific synaptic refinement of excitatory inputs to the vVNLL

The EPSCs of otoferlin WT animals were slightly different than the those in the EPSC developmental study performed in C57Bl/6 mice. Rise and decay times were also slower in otoferlin mice, and they also differed from time constants found in mice and rats (Futai et al. 2001; Yamashita et al. 2003; Fernández-Chacón et al. 2004). It has been demonstrated that different mouse strains may develop a variance of different phenotypes – for example, hereditary hearing loss (Ralls 1967; Turner and Willott 1998; Willott et al. 1998; Willott and Turner 1999; Zheng et al. 1999; Turner et al. 2005; Rivera and Tessarollo 2008). Furthermore, after 20 generations of inbreeding, genetically former relatives develop a genetic distance that can result in morphological and physiological differences (Beck et al.

2000). We conclude, therefore, that both mouse strains exhibit different morphological and physiological peculiarities that result from a genetic distance. Nevertheless, a reduced number of synaptic inputs and a decrease of time constants was observed in both mouse strains.

7.2.5 Downregulation of NMDA receptor-mediated currents is accompanied by postsynaptic AMPA receptor acceleration

Fast glutamatergic synaptic transmission is mediated by ionotropic glutamate receptors, of which three groups are known in the brain – AMPA, NMDA, and kainate receptors (Dingledine et al. 1999). The AMPA receptors mediate the majority of the fast neurotransmission in the central nervous system and are expressed by nearly all neurons of the CNS (Borges and Dingledine 1998; Michaelis 1998), including the auditory VNLL (Wu and Kelly 1996).

In this present study, blocking AMPA and NMDA receptor-mediated currents resulted in a baseline with only really small residual currents, indicating that AMPA and NMDA receptors were primarily responsible for glutamatergic synaptic transmission in the VNLL. Maturation and pruning of synaptic inputs in vVNLL neurons have been observed at P13. It has been demonstrated that type, number, and distribution of receptors largely determine postsynaptic responses to transmitter release (Rubio et al. 2017). Although synaptic refinement is complete by P13, an increase of excitatory postsynaptic current was found in P22 animals. The increase of AMPA receptor-mediated currents may be a reflection of more vesicle release sites in the presynapse, a change of release probability, or an increase of postsynaptic receptor density (Joshi and Wang 2002; Baumann and Koch 2017). The kinetics of AMPA receptors also decrease significantly in the MNTB (Futai et al. 2001; Joshi and Wang 2002) and the VNLL, and they can be influenced by subunit gating kinetics, desensitization (Jones and Westbrook, 1996), and by asynchronous release of vesicles from the presynaptic membrane (Chuhma and Ohmori 1998).

The EPSC decay time at large somatic synapses is largely determined by postsynaptic factors (Berger et al. 2014) and accelerates during development (Taschenberger and von Gersdorff 2000; Joshi and Wang 2002; Joshi et al. 2004). In accordance with the findings of other studies, tau decay is reduced to 0.3 ms in mice and rats at P20 (Futai et al. 2001; Yamashita et al. 2003; Fernández-Chacón et al. 2004). In particular, a developmental

switch to the GluR4 subunit containing AMPA receptors mediated a fast and precise synaptic transmission in rat and chick auditory synapses (Geiger et al. 1995; Otis et al. 1995; Zhou et al. 1995; Wang et al. 1998b; Caicedo and Eybalin 1999; Ravindranathan et al. 2000). Receptor subunits, their molecular organization, and pharmacological and biophysical characteristics differ and greatly determine their receptor properties through a combination of different AMPA receptor subunits (Rubio et al. 2017). Furthermore, it has been suggested that the developmental reduction of AMPA receptor kinetics is responsible for an increased temporal precision of action potential generation, since the summation of synaptic current is reduced (Futai et al. 2001).

Interestingly, a developmental change in calcium-binding proteins was also observed. While mature mice expressed large amounts of calretinin, mice before hearing onset showed much less. Calretinin has been shown to have a strong affinity for calcium and reduces the time that calcium mediates transmitter release, in turn increasing the temporal resolution to follow auditory signaling (Maruyama et al. 1984). Additionally, the developmental reduction of AMPA-receptor kinetics has also been observed in MNTB neurons and may be caused by a larger density of functional postsynaptic receptors or/and a switch of AMPA-receptor subunits (Joshi and Wang 2002). Moreover, Tarusawa et al., (2009) have revealed that a higher density of postsynaptic receptors affects the amplitude of the postsynaptic response. During the same time that AMPA receptor-mediated currents increased, NMDA receptor-mediated currents decreased. This has also been demonstrated for the MNTB (Futai et al. 2001; Joshi and Wang 2002). Indeed, NMDA receptor-mediated currents increase until ear canal opening, after which they decline rapidly to a point of being almost absent (Joshi and Wang 2002). This reverse development of NMDA and AMPA receptor-mediated currents has not been observed in other central synapses than the VNLL and MNTB synapses.

The calyx of Held synapse in the MNTB also undergoes drastic changes in the second postnatal week after the onset of sensory experience (Kikuchi and Hilding 1965; Mikaelian and Ruben 1965). During this time, the calyx of Held reshapes from a spoon to a finger-like profile and synaptic precision is perfected. It has been demonstrated that an activity-dependent downregulation of NMDA receptor expression is responsible for these changes (Futai et al. 2001; Joshi and Wang 2002). It has been reported that NMDA-receptor kinetics speed up during maturation, which has also been confirmed in studies of other synapses

due to an alteration of NMDA subunits (Carmignoto and Vicini 1992; Hestrin 1992; Takahashi et al. 1996; Flint et al. 1997; Cathala et al. 2000).

But why are NMDA receptors expressed in the first place? The NMDA receptor-mediated currents are particularly important for synaptic plasticity, short- and long-term potentiation, and memory formation (Willard and Koochekpour 2013). However, it is unclear whether plasticity in the VNLL is activity-dependent of NMDA receptors, since they are downregulated early during development. It has been shown that also NMDA receptor-mediated currents are essential for a proper synaptic formation and synapse migration during the very early days of ontogeny (Komuro and Rakic 1993; Farrant et al. 1994; Durand et al. 1996) and may, therefore, play a critical role in the formation and refinement of calyx-like synapses in the VNLL. Interestingly, a recent study on vVNLL neurons of mice has revealed a reduction of nicotinic acetylcholine receptors during the development of the calyx-synapse (Baumann and Koch 2017) that may also affect synaptic refinement. A deletion of the $\alpha 9$ acetylcholinic subunit impairs synaptic refinement in an auditory brainstem projection before hearing onset (Clause et al. 2014). Taken together, both the downregulation of NMDA receptor- and acetylcholine receptor-mediated currents could promote calyx-formation in the VNLL.

Spontaneous synaptic activity occurs without sound stimulation and can be action potential-dependent or independent (Lu et al. 2007). Action potential-independent spontaneous activity can be measured after pharmacological blockade of voltage-gated sodium channels with TTX (Lu et al., 2007) and are called spontaneous or miniature EPSCs. Miniature EPSCs are mostly very small and result from the release of a single transmitter-filled vesicle that may be stored in different vesicle pools than vesicles for evoked transmitter release (Frerking et al. 1997; Sara et al. 2005). Amplitudes and frequencies were not changed after P10 in vVNLL WT neurons, whereas mEPSC shapes became significantly briefer, since time constants decreased considerably during development. In contrast to the results obtained from our vVNLL experiments, it has been demonstrated that the development of mEPSC frequencies is increased in SOC nuclei (MNTB: Taschenberger and von Gersdorff, 2000; MSO: Magnusson et al., 2005) and the AVCN of mice (Lu et al. 2007). However, our findings accord with a recently published vVNLL study in mice (Baumann and Koch 2017). It was proposed that mEPSC frequencies change during development when the overall size of synaptic inputs increases and is accompanied by a growing number of release sites (Lu et al. 2007). Logically, the more

release sites that are available, the higher the probability of spontaneous vesicle release. Since our immunohistochemical stainings of the dominant glutamatergic marker VGluT1 in vVNLL neurons did not show any obvious differences in synaptic extents, we conclude that the overall size – not number – of synaptic inputs remains similar.

7.2.6 Short-term depression is reduced in neurons of mature mice

When presynaptic axons were stimulated at 100 Hz, AMPA receptor-mediated currents showed a robust short-term depression in vVNLL neurons of both age groups. However, short-term depression exhibited a strong age dependence from ~80% in P10 to ~60% in P22 otoferlin WT mice. A repetitive stimulation of the calyx of Held also resulted in a robust depression (Borst et al. 1995; von Gersdorff et al. 1997; Wang and Kaczmarek 1998). Theoretically, short-term depression can be dependent on various pre- and postsynaptic factors. These factors include, for instance, depletion of the RRP and postsynaptic receptor inactivation and desensitization (von Gersdorff et al. 1997; Forsythe et al. 1998; Schneggenburger et al. 1999; Weis et al. 1999). Properties of the RRP remained similar with only slight changes during development in WT animals. The size of the RRP and its depletion can be calculated based on various assumptions discussed below.

7.2.7 Assumption I: Only presynaptic factors contribute to short-term depression

Older studies on the MNTB synapse have shown that the depletion of the RRP is accountable for short-term depression (von Gersdorff et al. 1997; Wang and Kaczmarek 1998). Only a few studies have calculated the RRP under this assumption and obtained values between 600 and 800 in the MNTB (Schneggenburger et al. 1999; Bollmann et al. 2000), which is quite comparable with the results found in vVNLL neurons in this study. The RRP pool is calculated from train stimulation data that are stepwise cumulated. Usually, train stimulations reach steady state, and authors using this method assume that the amplitudes of the EPSCs at steady state result from vesicles that are exclusively freshly replenished, and neither postsynaptic desensitization nor a presynaptic mixture of old and new vesicles are depleted (Neher 2015). In the Schneggenburger approach, a linear regression is fitted through the last three cumulated amplitudes and is extrapolated backwards (Schneggenburger et al. 1999). The hypothetical value this regression reaches

theoretically matches the RRP under the assumption of presynaptic predominance. Although these data were similar to our findings, we used a different approach, taking pre- and postsynaptic factors into account.

7.2.8 Assumption II: Both pre- and postsynaptic factors contribute to short-term depression

Previously it was widely accepted that presynaptic factors determine short-term depression, until some authors expressed well-founded doubts about the methodical approach discussed in the previous Section 7.2.7. These researchers claim that depression is the result of presynaptic pool properties and postsynaptic desensitization (Scheuss et al. 2002; Wong et al. 2003). Elmquist and Quastel already in 1965 developed a method to take postsynaptic desensitization into account. While the Schneggenburger approach focuses on the last amplitudes of a train stimulation, the Elmquist-Quastel approach emphasizes the first amplitudes during the first few milliseconds that represent depletion of the RRP, and desensitization of postsynaptic receptors is not as crucial (Neher 2015). The individual release is plotted as a function of the cumulated release, and a linear regression is fitted through the first three amplitudes (Elmquist and Quastel 1965). The x-intercept corresponds to the RRP. This approach was used in our analysis.

A study in the calyx of Held with a prolonged stimulation of the presynaptic terminal resulted in large postsynaptic responses of 10 nA. A vesicle release of approximately 3000 vesicles was estimated (Sakaba and Neher 2001), an amount that strongly exceeds the vesicle number found in vVNLL neurons of this study (292 vesicles in P22 animals). One reason for such a large difference in vesicle release may lie in the significantly larger size of calyces of Held compared with calyces in the VNLL. Morphological reconstructions estimate the calyces of Held to be twice as large as calyces in the VNLL (Berger et al. 2014). Still, this does not fully explain these large differences.

Other methods that directly measure the RRP are electron microscopy studies (Sätzler et al. 2002; Taschenberger et al. 2002) and measurements of capacitance changes of the presynaptic membrane during vesicle fusion (Berger et al. 2014; Wölfel and Schneggenburger 2003; Wu et al. 2007). Berger et al. (2014) performed experiments on the VNLL of gerbils and determined the number of vesicles that were released from the calyx-like synapse in the VNLL and calyx of Held in the MNTB. In their experiments, they

measured presynaptic changes in capacitance during transmitter release as a response to a large calcium influx and compared it to the change of capacitance produced by one vesicle (Wu et al. 2007). This method produced very large numbers. The mean vesicle release in the VNLL amounted to 4076, whereas in the MNTB it was almost double (~7500; Berger et al., 2014). However, taking the size differences into account, the calyx of the VNLL is simply a scaled-down version of the calyx of Held. A much smaller number was calculated for the MNTB with the same methodical approach (4000 vesicles; Wölfel and Schneggenburger, 2003). Furthermore, two electron microscopy studies in the MNTB estimated a RRP of 1100–2800 vesicles (Sätzler et al. 2002; Taschenberger et al. 2002). Unfortunately, data on VNLL synapses are unavailable. Comparison of the presented studies illustrates the large diversity of experimental outcomes and complicates relating these results to our own findings. Although we applied a different method, we expected a similar number in the VNLL of mice. However, a 10-fold decrease of readily releasable vesicles in the mouse VNLL is indicated by our data, with only a 2-fold decrease in synapse size. Perhaps not only the synaptic extent but also the distribution of release sites that could greatly increase the RRP is important.

Calyx-like synapses in the vVNLL are smaller and transmit smaller postsynaptic responses than those found in the MNTB. Synapses of the MNTB contain many active zones with an excess supply in vesicles that serve as potential backup for assuring a fast and precise synaptic transmission (Berger et al. 2014; Franzen et al. 2015). This functional insurance is not developed in VNLL synapses.

7.2.9 AMPA receptor subunit switch might be responsible for reduction of short-term depression

It is recognized that AMPA receptor subunits exist in different conformations – flip and flop – both resulting from alternative splicing variants (Mosbacher et al. 1994; Geiger et al. 1995; Koike-Tani et al. 2005). Mosbacher et al. (1994) also demonstrated that GluR4 AMPA receptor subunits spliced in the flop variant displayed a faster desensitization. The variety of subunit compositions and its splicing variants result in diverse functional characteristics of AMPA receptors (Borges and Dingledine 1998; Wenthold and Roche 1998). Furthermore, subunit composition is under developmental control (Wenthold et al. 1996), and the postsynaptic AMPA receptor density is regulated by synaptic activity

(Mosbacher et al. 1994). Moreover, neurons of the auditory system undergo a rapid desensitization (Raman et al. 1994; Gardner et al. 1999), seen, for instance, in MNTB neurons. It has been demonstrated that cyclothiazide only affects synaptic depression of MNTB neurons of young animals (Joshi and Wang, 2002). Wang and Kaczmarek (1998) also showed that depression is unaffected by desensitization of postsynaptic receptors in mice after hearing onset. Thus, the larger depression found in young mice before hearing onset may at least partially result from desensitization of postsynaptic AMPA receptors. A change of calyx formation may also lead to a reduction of depression in mature animals (Taschenberger et al. 2002, 2005), since the fenestration of mature calyces of Held allow a faster diffusion of glutamate from the synaptic cleft (Renden et al. 2005). Generally speaking, a rapid deactivation and desensitization of receptors is interpreted as an important adaptation for fast auditory signaling and essential for the preservation of timing information (Trussell 1999).

To summarize, firing patterns depend largely on the expression of low-voltage-activated potassium channel expression, and $K_v1.1$ and $K_v1.2$ in particular are strongly expressed during late postnatal development, influencing and regulating the onset firing found in the vVNLL neurons of mature animals. Furthermore, depletion is likely the main mechanism underlying postsynaptic short-term depression in older animals, whereas differences of depression in younger animals may result from faster desensitization of postsynaptic AMPA receptors. The first three postnatal weeks are a critical period during which synapse pruning and formation occur, postsynaptic glutamatergic receptors are modified, and hearing onset takes place. The NMDA receptor currents are essential for the proper formation of mature synaptic innervation, and its reduction is, in turn, necessary for fast and precise synaptic transmission in mature hearing mice.

7.3 Deafness impairs the typical neuronal and synaptic development

The previous chapter revealed that both synaptic refinement and intrinsic neuronal properties in vVNLL neurons occur during hearing onset, but it is unclear whether this temporal co-development is regulated by sound-evoked activity or rather arises coincidentally at that time. In order to test the influence of sensory experience, we performed

experiments on hearing and deaf mice. Congenitally deaf mice were used where exons 14 and 15 had been deleted from the otoferlin gene (Roux et al. 2006; Reisinger et al. 2011). Otoferlin is a protein necessary for vesicle fusion and therefore exocytosis of neurotransmitter in inner hair cells of the cochlea (Roux et al. 2006). While signal transmission is interrupted in the inner hair cells, the auditory nerve remains intact (Roux et al. 2006). Breeding of heterozygous animals produced hearing (WT: OTOF^(+/+)) and deaf (KO: OTOF^(-/-)) littermates.

7.3.1 Auditory-evoked activity is essential for a typical neuronal and synaptic development

By comparing mature deaf mice with hearing P10 and P22 mice as controls, we attempted to elucidate intrinsic or environmental factors that are involved in neuronal and synaptic maturation. Intrinsic neuronal properties were in some ways similar to mice before hearing onset and in other ways similar to adult mice. For instance, firing patterns of KO mice resembled those found in P10 WT mice with almost exactly the same ratio of onset- and sustained-firing neurons (P10 WT: onset 74%, sustained 26%; P22 KO: onset 70%, sustained 26%). While the resting membrane potentials and current thresholds of deaf mice remained similar to P10 WT animals, other properties such as I_h component and action potential shapes were unaffected by deafness and developed typically. Although membrane time constants were not significantly different between either experimental group, large variabilities were generally detected in P10 WT and P22 KO mice. Not only is this variability reflected in our results, but experimental difficulties were also observed, especially in KO mice. Patching of KO neurons was always very difficult, and stable measurements were hard to obtain. This has not been described in the literature.

However, it has been discussed that otoferlin is expressed not only in the ribbon synapse of inner hair cells but also in the brainstem, inferior and superior colliculus, hippocampus, and cortex (Schug et al. 2006). In that study of Schug et al. (2006), authors suggest that otoferlin not only mediates exocytosis but also plays an important role in membrane recycling in the Golgi apparatus and other yet-unknown roles, since it is also found in the cytoplasm located in the vicinity of the nucleus. Therefore, a lack of otoferlin leads to deafness but may also influence the biochemical construction of the lipid bilayer that, in

turn, causes difficulties patching. These biochemical effects on the membrane must still be unraveled.

The number of synaptic inputs and time constants of postsynaptic receptors of deaf mice are similar to young WT animals. Interestingly, the frequency of spontaneous EPSCs (mEPSCs) was increased in KO compared with WT mice, while time constants of spontaneous and evoked EPSCs resembled those found in immature mice. Short-term plasticity and properties of the RRP were unaffected by congenital hearing loss.

7.3.2 Spontaneous activity is not involved in synaptic refinement of vVNLL synapses

The activity of the cochlea of rodents begins at around P1 and occurs with an increased frequency until hearing onset (Tritsch and Bergles 2010). During spontaneous activity, hair cells are depolarized by ATP that is released by nearby supporting cells (Tritsch et al. 2007). The depolarization leads to a calcium influx that mediates exocytosis of transmitter into the synaptic cleft (Johnson et al. 2005; Tritsch et al. 2007). Neurons of the MNTB also show an increased bursting activity *in vivo* around P1 (Tritsch et al. 2010). This cochlea output may be suited to promoting calyx formation and MNTB maturation (Hoffpauir et al. 2010). Mice with hearing disorders and defects in hair cells still develop calyces and undergo typical MNTB maturation (Erazo-Fischer et al. 2007; Youssoufian et al. 2008; Noh et al. 2010). The development of the calyx of Held occurs before hearing onset, whereas a modification of the calyx shape takes place only after hearing onset (Hoffpauir et al. 2006; Ford et al. 2009). During this developmental fenestration of the calyx of Held, Ford and colleagues (2009) found out that neurons located in the medially oriented part of the MNTB that respond to high frequencies develop the calyx fenestration earlier than those in the lateral part. Deaf animals without auditory-evoked activity did not develop such a temporal developmental gradient (Ford et al., 2009).

Deaf deafwaddler mice that have a mutation in the plasma membrane calcium ATPase (Penheiter et al. 2001) have larger mEPSC and EPSC amplitudes (Weatherstone et al. 2017), whereas EPSC amplitudes were smaller in the VNLL of KO mice. The decrease of excitatory postsynaptic currents may affect the ability to follow firing rates and decrease the temporal precision of neurons (Weatherstone et al. 2017). Additionally, the typical development of tonotopy in MNTB neurons is altered in these mice (Weatherstone et al.

2017). In the absence of auditory-evoked activity, spontaneous cochlear activity could be sufficient to induce and regulate calyx formation and neuronal development. Spontaneous activity is found in otoferlin KO mice before hearing onset (Beurg et al. 2010). Synaptic refinement in the vVNLL, however, takes place around hearing onset after P11 and is disturbed in KO mice, indicating that spontaneous activity is not sufficient for a typical synaptic development.

Deafness resulting from cochlea ablation is a different methodical approach than the genetic mutations previously presented. Cochleae are destroyed, and transmission of sound-evoked activity is prevented (Lu et al. 2007). Postsynaptic responses and spontaneous activity are increased in a study of cochlea ablated mice (Sumner et al. 2005). These effects may be a result of growing nerve endings and a co-development of more release sites, because the frequency of spontaneous EPSCs seems to be correlated with the number of auditory inputs (Lu et al. 2007). This could also explain the increase of spontaneous EPSCs in otoferlin KO mice, and the lack of sound-evoked activity may have generated an increase in release sites as a compensatory mechanism (Lu et al. 2007). The increased spontaneous activity of vVNLL synapses in otoferlin KO mice may likely be a compensatory mechanism for the lack of sound-evoked activity (Weatherstone et al. 2017). In addition, synaptic inputs that have degenerated as a consequence of deafness were replaced by either nearby terminals (Gentshev and Sotelo 1973) or synaptogenesis (Benson et al. 1997).

In the previous Section 7.2.5 on the development of calyx-like inputs to the vVNLL, we demonstrated that NMDA receptor-mediated currents almost entirely diminish during development. This decrease co-occurs with synaptic refinement in the vVNLL. In a study where mice had been cochlea-ablated at P7, slice recordings of NMDA receptor-mediated currents in the MNTB were performed between P14 and P16 (Futai et al. 2001). The NMDA receptor-mediated current amplitudes of deafened mice match recordings done in animals before hearing onset. Furthermore, a downregulation of NMDA-receptor expression of subunit NR2 is missing, whereas a reduction of subunit NR1 behaves the same as in untreated animals (Futai et al. 2001). Both subunits are essential for the activity of a functional NMDA receptor, and a developmental loss or decrease of one subunit could explain functional loss of the NMDA receptor (Meguro et al. 1992; Boeckman and Aizenman 1994; Kutsuwada et al. 1996). A missing downregulation of NMDA-receptor

functionality in the postsynaptic membrane may, at least partially, cause a disturbed synaptic refinement in vVNLL neurons.

The MNTB is a nucleus involved in sound localization (Boudreau and Tsuchitani 1968; Cant 1984), whereas the VNLL is considered to play a critical role in the analysis of temporal sound patterns (Aitkin et al. 1970; Covey and Casseday 1991; Recio-Spinoso and Joris 2014). These differing functional fates of the two nuclei could account for their diverse requirements for sensory experience, assuming the VNLL requires “language” as a promoter for mature synaptic formation.

7.3.3 Sound-evoked experience is necessary for determining firing patterns through ion channel modulation

It has been demonstrated that MNTB neurons of hearing-impaired animals undergo a typical developmental reduction of input resistances and modulation to onset firing patterns (Noh et al., 2010). However, the reduced cochlea activity in mice with hearing disorders affects the tonotopy and expression of voltage-gated ion channels (Leao et al. 2006). Furthermore, auditory-evoked activity leads to a higher expression of low-voltage-activated potassium channels (Leao et al. 2004a). Leao et al. (2004) show that deaf animals have smaller low-voltage-activated potassium currents near the resting membrane potential, consequently causing neurons to display sustained firing patterns. It has been also suggested that, at least in the AVCN, synaptic and intrinsic conductances are under activity-dependent control (Oleskevich and Walmsley 2002). A study performed on deafwaddler mice revealed that sound-evoked activity also greatly affects the ion channel expression in MNTB neurons (Leão et al. 2010). Neurons responding to high frequencies display an increased expression of the high-voltage-activated potassium channel $K_v3.1$ (Leão et al. 2010) that is thought to minimize action potential duration (Wang et al. 1998a).

Another study on the deaf mouse model *dn/dn*, with a mutation of the transmembrane cochlear expressed gene 1 (Leao et al. 2004a; Youssoufian et al. 2008) that occurs naturally in humans (Kurima et al. 2003), indicates that a reduction of low-voltage-activated potassium channels leads to an augmented firing of action potentials (Leao et al. 2004a). A firing of numerous action potentials disrupts the ability of these cells to precisely follow high frequencies (Leao et al., 2004). In addition, deaf animals show smaller low-voltage-activated potassium currents near the resting potential (Leao et al., 2004). Leao and

colleagues (2004) used dendrotoxin to block low-voltage-gated potassium channels in order to investigate effects on firing patterns. Interestingly, pharmacological blockade of low-voltage-gated potassium channels results in a firing of numerous action potentials (Leao et al., 2004). These results may also explain the existence of sustained-firing neurons in P10 WT and P22 KO mice in our study. A developmental increase of low-voltage-gated potassium channels controlled by auditory-evoked activity downregulates sustained firing of neurons in the vVNLL. We conclude that sensory experience is necessary for ion channel modulation and regulation.

In summary, it can now be stated convincingly that auditory-evoked activity is essential for ion channel modulation and expression, which determine the maturation of firing patterns in the vVNLL and all other auditory nuclei investigated.

7.4 Concluding remarks and outlook

As mentioned previously, the VNLL is a nucleus considered to play an important role in the analysis of speech and the transmission of speech containing temporal specifics to the IC and thence upstream to the cortex. The rapid signal transmission from the auditory nerve to octopus cells in the PVCN, then to the VNLL, and from there to higher auditory centers provides the fundamental basis for comprehending, for example, sophisticated language like that of humans. Synaptic refinement and the development of an exclusively onset firing pattern are disturbed in deaf mice lacking the protein otoferlin, indicating that spontaneous activity is not sufficient but rather auditory-evoked activity is essential for typically functional neuronal development in the VNLL. That, however, is contradictory to our expectations that the calyx formation in the VNLL behaves similarly to the formation of the calyx of Held. A lack of auditory information leads to the inability of the brain to analyze speech components, which, in fact, makes sense. Only auditory experience will trigger neuronal modifications in the VNLL that, in turn, reliably and accurately transmit relevant temporal information to higher auditory centers.

These results may contribute to the understanding of deafness-related mutations in humans. Indeed, to predict the outcome of treatments of, for instance, cochlear implant patients, it is immensely important to understand central auditory pathways and whether deafness has

an incurable impact on neuronal structures. Our results imply a meaningful consequence for humans with hearing loss, since the lack of sensory experience alters the synaptic and biophysical development of the VNLL. The clinical utilization of cochlear implants, however, may cure through experience the neuronal defects obtained by this mutation, at least in the VNLL, by providing auditory-nerve activity. Consequently, our results encourage the use of cochlear implants in patients with an otoferlin-related deafness.

8 References

- Adams JC.** Ascending projections to the inferior colliculus. *J Comp Neurol* 183: 519–538, 1979.
- Adams JC.** Projections from octopus cells of the posteroventral cochlear nucleus to the ventral nucleus of the lateral lemniscus in cat and human. *Auditory Neuroscience* 3: 335–350, 1997.
- Adams JC, Mugnaini E.** Dorsal nucleus of the lateral lemniscus: a nucleus of GABAergic projection neurons. *Brain Res Bull* 13: 585–590, 1984.
- Adesnik H, Nicoll RA.** Conservation of glutamate receptor 2-containing AMPA receptors during long-term potentiation. *J Neurosci* 27: 4598–4602, 2007.
- Ahuja TK, Wu SH.** Developmental changes in physiological properties in the rat's dorsal nucleus of the lateral lemniscus. *Hearing Research* 149: 33–45, 2000.
- Aitkin LM, Anderson DJ, Brugge JF.** Tonotopic organization and discharge characteristics of single neurons in nuclei of the lateral lemniscus of the cat. *Journal of Neurophysiology* 33: 421–440, 1970.
- Akil O, Oursler AE, Fan K, Lustig LR.** Mouse Auditory Brainstem Response Testing. *Bio Protoc* 6, 2016.
- Alberts B, Johnson A, Lewis J, Raff M, Roberts K, Walter P.** Ion Channels and the Electrical Properties of Membranes [Online]. *Molecular Biology of the Cell*. 4th edition. <https://www.ncbi.nlm.nih.gov/books/NBK26910/> [26 Sep. 2018].
- Ammer JJ, Grothe B, Felmy F.** Late postnatal development of intrinsic and synaptic properties promotes fast and precise signaling in the dorsal nucleus of the lateral lemniscus. *J Neurophysiol* 107: 1172–1185, 2012.
- Atherton JF, Kitano K, Baufreton J, Fan K, Wokosin D, Tkatch T, Shigemoto R, Surmeier DJ, Bevan MD.** Selective participation of somatodendritic HCN channels in inhibitory but not excitatory synaptic integration in neurons of the subthalamic nucleus. *J Neurosci* 30: 16025–16040, 2010.
- Axmacher N, Miles R.** Intrinsic cellular currents and the temporal precision of EPSP-action potential coupling in CA1 pyramidal cells. *J Physiol (Lond)* 555: 713–725, 2004.
- Bagal SK, Marron BE, Owen RM, Storer RI, Swain NA.** Voltage gated sodium channels as drug discovery targets. *Channels (Austin)* 9: 360–366, 2015.
- Bak LK, Schousboe A, Waagepetersen HS.** The glutamate/GABA-glutamine cycle: aspects of transport, neurotransmitter homeostasis and ammonia transfer. *J Neurochem* 98: 641–653, 2006.
- Barnes-Davies M, Barker MC, Osmani F, Forsythe ID.** Kv1 currents mediate a gradient of principal neuron excitability across the tonotopic axis in the rat lateral superior olive. *European Journal of Neuroscience* 19: 325–333, 2004.
- Batra R, Fitzpatrick DC.** Neurons Sensitive to Interaural Temporal Disparities in the Medial Part of the Ventral Nucleus of the Lateral Lemniscus. *Journal of Neurophysiology* 78: 511–515, 1997.

- Batra R, Fitzpatrick DC.** Monaural and binaural processing in the ventral nucleus of the lateral lemniscus: a major source of inhibition to the inferior colliculus. *Hearing Research* 168: 90–97, 2002.
- Baumann V, Lehnert S, Leibold C, Koch U.** Tonotopic organization of the hyperpolarization-activated current (I_h) in the mammalian medial superior olive. *Front Neural Circuits* 7: 117, 2013.
- Baumann VJ, Koch U.** Perinatal nicotine exposure impairs the maturation of glutamatergic inputs in the auditory brainstem. *J Physiol* 595: 3573–3590, 2017.
- Baydyuk M, Xu J, Wu L-G.** The Calyx of Held in the auditory system: structure, function, and development. *Hear Res* 338: 22–31, 2016.
- Bear MF, Connors BW, Paradiso MA.** *Neuroscience*. Lippincott Williams & Wilkins, 2007.
- Beck JA, Lloyd S, Hafezparast M, Lennon-Pierce M, Eppig JT, Festing MF, Fisher EM.** Genealogies of mouse inbred strains. *Nat Genet* 24: 23–25, 2000.
- Bekesy GV.** Neural inhibitory units of the eye and skin. Quantitative description of contrast phenomena. *J Opt Soc Am* 50: 1060–1070, 1960.
- Békésy GV.** *Experiments in Hearing*. McGraw, 1960.
- Benson CG, Cant NB.** The ventral nucleus of the lateral lemniscus of the gerbil (*Meriones unguiculatus*): Organization of connections with the cochlear nucleus and the inferior colliculus. *The Journal of Comparative Neurology* 510: 673–690, 2008.
- Benson CG, Gross JS, Suneja SK, Potashner SJ.** Synaptophysin immunoreactivity in the cochlear nucleus after unilateral cochlear or ossicular removal. *Synapse* 25: 243–257, 1997.
- Berger C, Meyer EMM, Ammer JJ, Felmy F.** Large Somatic Synapses on Neurons in the Ventral Lateral Lemniscus Work in Pairs. *J Neurosci* 34: 3237–3246, 2014.
- Bernstein J.** *Electrobiologie*. Braunschweig: Vieweg, 1912.
- Berntson AK, Walmsley B.** Characterization of a potassium-based leak conductance in the medial nucleus of the trapezoid body. *Hear Res* 244: 98–106, 2008.
- Bertoli A, Moran O, Conti F.** Activation and deactivation properties of rat brain K⁺ channels of the Shaker-related subfamily. *Eur Biophys J* 23: 379–384, 1994.
- Betts JG, Desaix P, Johnson E, Johnson JE, Korol O, Kruse D, Poe B, Wise JA, Womble M, Young KA.** *Anatomy and Physiology*. 1 edition. OpenStax, 2013.
- Beurg M, Michalski N, Safieddine S, Bouleau Y, Schneggenburger R, Chapman ER, Petit C, Dulon D.** Control of Exocytosis by Synaptotagmins and Otoferlin in Auditory Hair Cells. *J Neurosci* 30: 13281–13290, 2010.
- Bezánilla F.** Ion Channels: From Conductance to Structure. *Neuron* 60: 456–468, 2008.
- Bliss TV, Collingridge GL.** A synaptic model of memory: long-term potentiation in the hippocampus. *Nature* 361: 31–39, 1993.
- Bock GR, Frank MP, Steel KP.** Preservation of central auditory function in the deafness mouse. *Brain Res* 239: 608–612, 1982.

- Boeckman FA, Aizenman E.** Stable transfection of the NR1 subunit in Chinese hamster ovary cells fails to produce a functional N-methyl-D-aspartate receptor. *Neurosci Lett* 173: 189–192, 1994.
- Bollmann JH, Sakmann B, Borst JG.** Calcium sensitivity of glutamate release in a calyx-type terminal. *Science* 289: 953–957, 2000.
- Borges K, Dingledine R.** AMPA receptors: molecular and functional diversity. *Prog Brain Res* 116: 153–170, 1998.
- Borst JG, Helmchen F, Sakmann B.** Pre- and postsynaptic whole-cell recordings in the medial nucleus of the trapezoid body of the rat. *J Physiol (Lond)* 489 (Pt 3): 825–840, 1995.
- Borst JGG, Soria van Hoeve J.** The Calyx of Held Synapse: From Model Synapse to Auditory Relay. *Annual Review of Physiology* 74: 199–224, 2012.
- Boudreau JC, Tsuchitani C.** Binaural interaction in the cat superior olive S segment. *J Neurophysiol* 31: 442–454, 1968.
- Bowman CL, Baglioni A.** Application of the Goldman-Hodgkin-Katz current equation to membrane current-voltage data. *J Theor Biol* 108: 1–29, 1984.
- Brew HM, Forsythe ID.** Two Voltage-Dependent K⁺ Conductances with Complementary Functions in Postsynaptic Integration at a Central Auditory Synapse. *J Neurosci* 15: 8011–8022, 1995.
- Brew HM, Gittelman JX, Silverstein RS, Hanks TD, Demas VP, Robinson LC, Robbins CA, McKee-Johnson J, Chiu SY, Messing A, Tempel BL.** Seizures and reduced life span in mice lacking the potassium channel subunit Kv1.2, but hypoexcitability and enlarged Kv1 currents in auditory neurons. *J Neurophysiol* 98: 1501–1525, 2007.
- Brew HM, Hallows JL, Tempel BL.** Hyperexcitability and reduced low threshold potassium currents in auditory neurons of mice lacking the channel subunit Kv1.1. *J Physiol (Lond)* 548: 1–20, 2003.
- Brown DA, Passmore GM.** Neural KCNQ (Kv7) channels. *Br J Pharmacol* 156: 1185–1195, 2009.
- Brown SDM, Hardisty-Hughes RE, Mburu P.** Quiet as a mouse: dissecting the molecular and genetic basis of hearing. *Nat Rev Genet* 9: 277–290, 2008.
- Brunso-Bechtold JK, Thompson GC, Masterton RB.** HRP study of the organization of auditory afferents ascending to central nucleus of inferior colliculus in cat. *J Comp Neurol* 197: 705–722, 1981.
- Burnashev N, Rozov A.** Presynaptic Ca²⁺ dynamics, Ca²⁺ buffers and synaptic efficacy. *Cell Calcium* 37: 489–495, 2005.
- Caicedo A, d'Aldin C, Eybalin M, Puel JL.** Temporary sensory deprivation changes calcium-binding proteins levels in the auditory brainstem. *J Comp Neurol* 378: 1–15, 1997.
- Caicedo A, Eybalin M.** Glutamate receptor phenotypes in the auditory brainstem and mid-brain of the developing rat. *European Journal of Neuroscience* 11: 51–74, 1999.

- Cant NB.** The fine structure of the lateral superior olivary nucleus of the cat. *J Comp Neurol* 227: 63–77, 1984.
- Cant NB, Benson CG.** Parallel auditory pathways: projection patterns of the different neuronal populations in the dorsal and ventral cochlear nuclei. *Brain Research Bulletin* 60: 457–474, 2003.
- Cant NB, Casseday JH.** Projections from the anteroventral cochlear nucleus to the lateral and medial superior olivary nuclei. *J Comp Neurol* 247: 457–476, 1986.
- Cant NB, Hyson RL.** Projections from the lateral nucleus of the trapezoid body to the medial superior olivary nucleus in the gerbil. *Hearing Research* 58: 26–34, 1992.
- Carmignoto G, Vicini S.** Activity-dependent decrease in NMDA receptor responses during development of the visual cortex. *Science* 258: 1007–1011, 1992.
- Carvalho TP, Buonomano DV.** Differential effects of excitatory and inhibitory plasticity on synaptically-driven neuronal Input-Output functions. *Neuron* 61: 774–785, 2009.
- Caspari F, Baumann VJ, Garcia-Pino E, Koch U.** Heterogeneity of Intrinsic and Synaptic Properties of Neurons in the Ventral and Dorsal Parts of the Ventral Nucleus of the Lateral Lemniscus. *Front Neural Circuits* 9: 74, 2015.
- Cathala L, Misra C, Cull-Candy S.** Developmental profile of the changing properties of NMDA receptors at cerebellar mossy fiber-granule cell synapses. *J Neurosci* 20: 5899–5905, 2000.
- Chase SM, Young ED.** First-spike latency information in single neurons increases when referenced to population onset. *PNAS* 104: 5175–5180, 2007.
- Chen C, Blitz DM, Regehr WG.** Contributions of receptor desensitization and saturation to plasticity at the retinogeniculate synapse. *Neuron* 33: 779–788, 2002.
- Chi XX, Nicol GD.** Manipulation of the potassium channel Kv1.1 and its effect on neuronal excitability in rat sensory neurons. *J Neurophysiol* 98: 2683–2692, 2007.
- Christie MJ, Adelman JP, Douglass J, North RA.** Expression of a cloned rat brain potassium channel in *Xenopus* oocytes. *Science* 244: 221–224, 1989.
- Chuhma N, Ohmori H.** Postnatal development of phase-locked high-fidelity synaptic transmission in the medial nucleus of the trapezoid body of the rat. *J Neurosci* 18: 512–520, 1998.
- Chung S, Li X, Nelson SB.** Short-term depression at thalamocortical synapses contributes to rapid adaptation of cortical sensory responses in vivo. *Neuron* 34: 437–446, 2002.
- Clark GM.** Vesicle shape versus type of synapse in the nerve endings of the cat medial superior olive. *Brain Res* 15: 548–551, 1969.
- Clause A, Kim G, Sonntag M, Weisz CJC, Vetter DE, Rübbsamen R, Kandler K.** The Precise Temporal Pattern of Prehearing Spontaneous Activity Is Necessary for Tonotopic Map Refinement. *Neuron* 82: 822–835, 2014.
- Clements JD.** Transmitter timecourse in the synaptic cleft: its role in central synaptic function. *Trends Neurosci* 19: 163–171, 1996.
- Coetzee WA, Amarillo Y, Chiu J, Chow A, Lau D, McCormack T, Moreno H, Nadal MS, Ozaita A, Pountney D, Saganich M, Vega-Saenz de Miera E, Rudy B.** Molecular diversity of K⁺ channels. *Ann N Y Acad Sci* 868: 233–285, 1999.

- Collingridge GL, Olsen RW, Peters J, Spedding M.** A nomenclature for ligand-gated ion channels. *Neuropharmacology* 56: 2–5, 2009.
- Collingridge GL, Volianskis A, Bannister N, France G, Hanna L, Mercier M, Tidball P, Fang G, Irvine MW, Costa BM, Monaghan DT, Bortolotto ZA, Molnár E, Lodge D, Jane DE.** The NMDA receptor as a target for cognitive enhancement. *Neuropharmacology* 64: 13–26, 2013.
- Colquhoun D, Jonas P, Sakmann B.** Action of brief pulses of glutamate on AMPA/kainate receptors in patches from different neurones of rat hippocampal slices. *J Physiol (Lond)* 458: 261–287, 1992.
- Covey E, Casseday JH.** Connectional basis for frequency representation in the nuclei of the lateral lemniscus of the bat *Eptesicus fuscus*. *J Neurosci* 6: 2926–2940, 1986.
- Covey E, Casseday JH.** The monaural nuclei of the lateral lemniscus in an echolocating bat: parallel pathways for analyzing temporal features of sound. *J Neurosci* 11: 3456–3470, 1991.
- Covey E, Casseday JH.** The Lower Brainstem Auditory Pathways. In: *Hearing by Bats*. Springer, New York, NY, p. 235–295.
- Crompton AW, Parker P.** Evolution of the mammalian masticatory apparatus. *Am Sci* 66: 192–201, 1978.
- Cull-Candy S, Brickley S, Farrant M.** NMDA receptor subunits: diversity, development and disease. *Curr Opin Neurobiol* 11: 327–335, 2001.
- Dabrowski KM, Castaño DJ, Tartar JL.** Basic Neuron Model Electrical Equivalent Circuit: An Undergraduate Laboratory Exercise. *J Undergrad Neurosci Educ* 12: A49–A52, 2013.
- D’Adamo MC, Imbrici P, Sponcichetti F, Pessia M.** Mutations in the KCNA1 gene associated with episodic ataxia type-1 syndrome impair heteromeric voltage-gated K(+) channel function. *FASEB J* 13: 1335–1345, 1999.
- DeCoursey TE, Chandy KG, Gupta S, Cahalan MD.** Voltage-dependent ion channels in T-lymphocytes. *J Neuroimmunol* 10: 71–95, 1985.
- Derkach VA, Oh MC, Guire ES, Soderling TR.** Regulatory mechanisms of AMPA receptors in synaptic plasticity. *Nat Rev Neurosci* 8: 101–113, 2007.
- DiFrancesco D.** Pacemaker mechanisms in cardiac tissue. *Annu Rev Physiol* 55: 455–472, 1993.
- Dingledine R, Borges K, Bowie D, Traynelis SF.** The glutamate receptor ion channels. *Pharmacol Rev* 51: 7–61, 1999.
- Dodson PD, Barker MC, Forsythe ID.** Two heteromeric Kv1 potassium channels differentially regulate action potential firing. *J Neurosci* 22: 6953–6961, 2002.
- Dror AA, Avraham KB.** Hearing impairment: a panoply of genes and functions. *Neuron* 68: 293–308, 2010.
- Durand GM, Kovalchuk Y, Konnerth A.** Long-term potentiation and functional synapse induction in developing hippocampus. *Nature* 381: 71–75, 1996.
- Egri C, Ruben PC.** Action Potentials: Generation and Propagation. In: *eLS*, edited by John Wiley & Sons, Ltd. John Wiley & Sons, Ltd., 2012.

- Elmqvist D, Quastel DM.** A quantitative study of end-plate potentials in isolated human muscle. *J Physiol (Lond)* 178: 505–529, 1965.
- Elzouki AY,** editor. *Textbook of clinical pediatrics*. 2nd ed. Berlin: Springer, 2012.
- Erazo-Fischer E, Striessnig J, Taschenberger H.** The role of physiological afferent nerve activity during in vivo maturation of the calyx of Held synapse. *J Neurosci* 27: 1725–1737, 2007.
- Farrant M, Feldmeyer D, Takahashi T, Cull-Candy SG.** NMDA-receptor channel diversity in the developing cerebellum. *Nature* 368: 335–339, 1994.
- Felix Ii RA, Gourévitch B, Gómez-Álvarez M, Leijon SCM, Saldaña E, Magnusson AK.** Octopus Cells in the Posteroventral Cochlear Nucleus Provide the Main Excitatory Input to the Superior Paraolivary Nucleus. *Front Neural Circuits* 11: 37, 2017.
- Felmy F, Schneggenburger R.** Developmental expression of the Ca²⁺-binding proteins calretinin and parvalbumin at the calyx of Held of rats and mice. *Eur J Neurosci* 20: 1473–1482, 2004.
- Fernandez FR, Morales E, Rashid AJ, Dunn RJ, Turner RW.** Inactivation of Kv3.3 potassium channels in heterologous expression systems. *J Biol Chem* 278: 40890–40898, 2003.
- Fernández-Chacón R, Wölfel M, Nishimune H, Tabares L, Schmitz F, Castellano-Muñoz M, Rosenmund C, Montesinos ML, Sanes JR, Schneggenburger R, Südhof TC.** The synaptic vesicle protein CSP alpha prevents presynaptic degeneration. *Neuron* 42: 237–251, 2004.
- Flint AC, Maisch US, Weishaupt JH, Kriegstein AR, Monyer H.** NR2A subunit expression shortens NMDA receptor synaptic currents in developing neocortex. *J Neurosci* 17: 2469–2476, 1997.
- Fogelson AL, Zucker RS.** Presynaptic calcium diffusion from various arrays of single channels. Implications for transmitter release and synaptic facilitation. *Biophys J* 48: 1003–1017, 1985.
- Ford MC, Grothe B, Klug A.** Fenestration of the calyx of held occurs sequentially along the tonotopic axis, is influenced by afferent activity, and facilitates glutamate clearance. *J Comp Neurol* 514: 92–106, 2009.
- Forsythe ID, Tsujimoto T, Barnes-Davies M, Cuttle MF, Takahashi T.** Inactivation of presynaptic calcium current contributes to synaptic depression at a fast central synapse. *Neuron* 20: 797–807, 1998.
- Foster KA, Kreitzer AC, Regehr WG.** Interaction of postsynaptic receptor saturation with presynaptic mechanisms produces a reliable synapse. *Neuron* 36: 1115–1126, 2002.
- Francotte P, de Tullio P, Fraikin P, Counerotte S, Goffin E, Pirotte B.** In search of novel AMPA potentiators. *Recent Pat CNS Drug Discov* 1: 239–246, 2006.
- Franzen DL, Gleiss SA, Berger C, Kümpfbeck FS, Ammer JJ, Felmy F.** Development and modulation of intrinsic membrane properties control the temporal precision of auditory brain stem neurons. *Journal of Neurophysiology* 113: 524–536, 2015.
- Frerking M, Borges S, Wilson M.** Are some minis multiquantal? *J Neurophysiol* 78: 1293–1304, 1997.

- Friauf E, Ostwald J.** Divergent projections of physiologically characterized rat ventral cochlear nucleus neurons as shown by intra-axonal injection of horseradish peroxidase. *Exp Brain Res* 73: 263–284, 1988.
- Fricker D, Miles R.** EPSP amplification and the precision of spike timing in hippocampal neurons. *Neuron* 28: 559–569, 2000.
- Futai K, Okada M, Matsuyama K, Takahashi T.** High-Fidelity Transmission Acquired via a Developmental Decrease in NMDA Receptor Expression at an Auditory Synapse. *The Journal of Neuroscience* 21: 3342–3349, 2001.
- Gandhi SP, Stevens CF.** Three modes of synaptic vesicular recycling revealed by single-vesicle imaging. *Nature* 423: 607–613, 2003.
- Garden DLF, Dodson PD, O'Donnell C, White MD, Nolan MF.** Tuning of Synaptic Integration in the Medial Entorhinal Cortex to the Organization of Grid Cell Firing Fields. *Neuron* 60: 875–889, 2008.
- Gardner SM, Trussell LO, Oertel D.** Time course and permeation of synaptic AMPA receptors in cochlear nuclear neurons correlate with input. *J Neurosci* 19: 8721–8729, 1999.
- Gasnier B.** The SLC32 transporter, a key protein for the synaptic release of inhibitory amino acids. *Pflugers Arch* 447: 756–759, 2004.
- Gebauer M, Isbrandt D, Sauter K, Callsen B, Nolting A, Pongs O, Bähring R.** N-type inactivation features of Kv4.2 channel gating. *Biophys J* 86: 210–223, 2004.
- Geiger JR, Melcher T, Koh DS, Sakmann B, Seeburg PH, Jonas P, Monyer H.** Relative abundance of subunit mRNAs determines gating and Ca²⁺ permeability of AMPA receptors in principal neurons and interneurons in rat CNS. *Neuron* 15: 193–204, 1995.
- Gentschev T, Sotelo C.** Degenerative patterns in the ventral cochlear nucleus of the rat after primary deafferentation. An ultra-structural study. *Brain Res* 62: 37–60, 1973.
- von Gersdorff H, Borst JGG.** Short-term plasticity at the calyx of Held. *Nat Rev Neurosci* 3: 53–64, 2002.
- von Gersdorff H, Matthews G.** Depletion and replenishment of vesicle pools at a ribbon-type synaptic terminal. *J Neurosci* 17: 1919–1927, 1997.
- von Gersdorff H, Schneggenburger R, Weis S, Neher E.** Presynaptic depression at a calyx synapse: the small contribution of metabotropic glutamate receptors. *J Neurosci* 17: 8137–8146, 1997.
- Gittelmann JX, Tempel BL.** Kv1.1-containing channels are critical for temporal precision during spike initiation. *J Neurophysiol* 96: 1203–1214, 2006.
- Glendenning KK, Brusno-Bechtold JK, Thompson GC, Masterton RB.** Ascending auditory afferents to the nuclei of the lateral lemniscus. *J Comp Neurol* 197: 673–703, 1981.
- Glowatzki E, Fuchs PA.** Transmitter release at the hair cell ribbon synapse. *Nat Neurosci* 5: 147–154, 2002.
- Goda Y, Stevens CF.** Two components of transmitter release at a central synapse. *Proc Natl Acad Sci U S A* 91: 12942–12946, 1994.

Goldberg EM, Clark BD, Zagha E, Nahmani M, Erisir A, Rudy B. K⁺ channels at the axon initial segment dampen near-threshold excitability of neocortical fast-spiking GABAergic interneurons. *Neuron* 58: 387–400, 2008.

Goldberg JM, Brown PB. Response of Binaural Neurons of Dog Superior Olivary Complex to Dichotic Tonal Stimuli: Some Physiological Mechanisms of Sound Localization. *J Neurophysiol* 32: 613–636, 1969.

Golding NL, Robertson D, Oertel D. Recordings from Slices Indicate That Octopus Cells of the Cochlear Nucleus Detect Coincident Firing of Auditory Nerve Fibers with Temporal Precision. *J Neurosci* 15: 3138–3153, 1995.

Goldman-Rakic PS. Cellular basis of working memory. *Neuron* 14: 477–485, 1995.

Golowasch J, Thomas G, Taylor AL, Patel A, Pineda A, Khalil C, Nadim F. Membrane Capacitance Measurements Revisited: Dependence of Capacitance Value on Measurement Method in Nonisopotential Neurons. *J Neurophysiol* 102: 2161–2175, 2009.

Goutman JD. Transmitter release from cochlear hair cells is phase locked to cyclic stimuli of different intensities and frequencies. *J Neurosci* 32: 17025–17035a, 2012.

Gratton MA, Vázquez AE. Age-related hearing loss: current research. *Curr Opin Otolaryngol Head Neck Surg* 11: 367–371, 2003.

Griffin DR, Galambos R. The sensory basis of obstacle avoidance by flying bats. *J Exp Zool* 86: 481–506, 1941.

Grigg JJ, Brew HM, Tempel BL. Differential expression of voltage-gated potassium channel genes in auditory nuclei of the mouse brainstem. *Hear Res* 140: 77–90, 2000.

Grothe B, Pecka M, McAlpine D. Mechanisms of sound localization in mammals. *Physiol Rev* 90: 983–1012, 2010.

Grothe B, Sanes DH. Synaptic inhibition influences the temporal coding properties of medial superior olivary neurons: an in vitro study. *J Neurosci* 14: 1701–1709, 1994.

Guan D, Lee JCF, Higgs MH, Spain WJ, Foehring RC. Functional roles of Kv1 channels in neocortical pyramidal neurons. *J Neurophysiol* 97: 1931–1940, 2007.

Guastella J, Brecha N, Weigmann C, Lester HA, Davidson N. Cloning, expression, and localization of a rat brain high-affinity glycine transporter. *Proc Natl Acad Sci USA* 89: 7189–7193, 1992.

Hassfurth B, Magnusson AK, Grothe B, Koch U. Sensory deprivation regulates the development of the hyperpolarization-activated current in auditory brainstem neurons. *European Journal of Neuroscience* 30: 1227–1238, 2009.

Hemilä S, Nummela S, Reuter T. Anatomy and physics of the exceptional sensitivity of dolphin hearing (Odontoceti: Cetacea). *J Comp Physiol A* 196: 165–179, 2010.

Hestrin S. Developmental regulation of NMDA receptor-mediated synaptic currents at a central synapse. *Nature* 357: 686–689, 1992.

Höber R. Über den Einfluss der Salze auf den Ruhestrom des Froschmuskels. *Pflüger, Arch* 106: 599–635, 1905.

- Hodgkin AL.** The Ionic Basis of Electrical Activity in Nerve and Muscle. *Biological Reviews* 26: 339–409, 1951.
- Hodgkin AL, Huxley AF.** A quantitative description of membrane current and its application to conduction and excitation in nerve. *J Physiol (Lond)* 117: 500–544, 1952.
- Hodgkin AL, Katz B.** The effect of sodium ions on the electrical activity of the giant axon of the squid. *J Physiol* 108: 37–77, 1949.
- Hoffpauir BK, Grimes JL, Mathers PH, Spirou GA.** Synaptogenesis of the calyx of Held: rapid onset of function and one-to-one morphological innervation. *J Neurosci* 26: 5511–5523, 2006.
- Hoffpauir BK, Kolson DR, Mathers PH, Spirou GA.** Maturation of synaptic partners: functional phenotype and synaptic organization tuned in synchrony. *Journal of Physiology* 588: 4365–4385, 2010.
- Hori T, Takahashi T.** Kinetics of Synaptic Vesicle Refilling with Neurotransmitter Glutamate. *Neuron* 76: 511–517, 2012.
- Hruskova B, Trojanova J, Kulik A, Kralikova M, Pysanenko K, Bures Z, Syka J, Trussell LO, Turecek R.** Differential Distribution of Glycine Receptor Subtypes at the Rat Calyx of Held Synapse. *Journal of Neuroscience* 32: 17012–17024, 2012.
- Huffman RF, Covey E.** Origin of ascending projections to the nuclei of the lateral lemniscus in the big brown bat, *Eptesicus fuscus*. *J Comp Neurol* 357: 532–545, 1995.
- Indig FE, Diaz-Gonzalez F, Ginsberg MH.** Analysis of the tetraspanin CD9-integrin alphaIIb beta3 (GPIIb-IIIa) complex in platelet membranes and transfected cells. *Biochem J* 327: 291–298, 1997.
- Irfan N, Zhang H, Wu SH.** Synaptic transmission mediated by ionotropic glutamate, glycine and GABA receptors in the rat's ventral nucleus of the lateral lemniscus. *Hearing Research* 203: 159–171, 2005.
- Isaac JTR, Ashby MC, McBain CJ.** The role of the GluR2 subunit in AMPA receptor function and synaptic plasticity. *Neuron* 54: 859–871, 2007.
- Ishii TM, Takano M, Xie LH, Noma A, Ohmori H.** Molecular characterization of the hyperpolarization-activated cation channel in rabbit heart sinoatrial node. *J Biol Chem* 274: 12835–12839, 1999.
- Ito T, Bishop DC, Oliver DL.** Expression of glutamate and inhibitory amino acid vesicular transporters in the rodent auditory brainstem. *J Comp Neurol* 519: 316–340, 2011.
- Iwasaki S, Takahashi T.** Developmental changes in calcium channel types mediating synaptic transmission in rat auditory brainstem. *J Physiol (Lond)* 509 (Pt 2): 419–423, 1998.
- Jacob TC, Moss SJ, Jurd R.** GABA(A) receptor trafficking and its role in the dynamic modulation of neuronal inhibition. *Nat Rev Neurosci* 9: 331–343, 2008.
- Jahn R, Lang T, Südhof TC.** Membrane fusion. *Cell* 112: 519–533, 2003.
- Jahr CE, Lester RA.** Synaptic excitation mediated by glutamate-gated ion channels. *Curr Opin Neurobiol* 2: 270–274, 1992.

- Jensen HS, Grunnet M, Olesen S-P.** Inactivation as a New Regulatory Mechanism for Neuronal Kv7 Channels. *Biophysical Journal* 92: 2747–2756, 2007.
- Johnson KL, Nicol TG, Kraus N.** Brain Stem Response to Speech: A Biological Marker of Auditory Processing. [Review]. *Ear & Hearing* 26: 424–434, 2005.
- Johnston J, Forsythe ID, Kopp-Scheinflug C.** Going native: voltage-gated potassium channels controlling neuronal excitability. *J Physiol* 588: 3187–3200, 2010.
- Johnston J, Griffin SJ, Baker C, Skrzypiec A, Chernova T, Forsythe ID.** Initial segment Kv2.2 channels mediate a slow delayed rectifier and maintain high frequency action potential firing in medial nucleus of the trapezoid body neurons. *J Physiol (Lond)* 586: 3493–3509, 2008.
- Johnston J, Postlethwaite M, Forsythe ID.** The impact of synaptic conductance on action potential waveform: evoking realistic action potentials with a simulated synaptic conductance. *J Neurosci Methods* 183: 158–164, 2009.
- de Jong APH, Verhage M.** Presynaptic signal transduction pathways that modulate synaptic transmission. *Curr Opin Neurobiol* 19: 245–253, 2009.
- Joshi I, Shokralla S, Titis P, Wang L-Y.** The role of AMPA receptor gating in the development of high-fidelity neurotransmission at the calyx of Held synapse. *J Neurosci* 24: 183–196, 2004.
- Joshi I, Wang L-Y.** Developmental profiles of glutamate receptors and synaptic transmission at a single synapse in the mouse auditory brainstem. *J Physiol* 540: 861–873, 2002.
- Kandler K, Friauf E.** Pre- and postnatal development of efferent connections of the cochlear nucleus in the rat. *J Comp Neurol* 328: 161–184, 1993.
- Kandler K, Friauf E.** Development of glycinergic and glutamatergic synaptic transmission in the auditory brainstem of perinatal rats. *J Neurosci* 15: 6890–6904, 1995.
- Keats BJ, Berlin CI.** Genomics and hearing impairment. *Genome Res* 9: 7–16, 1999.
- Kelly JB, van Adel BA, Ito M.** Anatomical projections of the nuclei of the lateral lemniscus in the albino rat (*rattus norvegicus*). *J Comp Neurol* 512: 573–593, 2009.
- Khurana S, Liu Z, Lewis AS, Rosa K, Chetkovich D, Golding NL.** An Essential Role for Modulation of Hyperpolarization-Activated Current in the Development of Binaural Temporal Precision. *J Neurosci* 32: 2814–2823, 2012.
- Kikuchi K, Hilding D.** The development of the organ of Corti in the mouse. *Acta Otolaryngol* 60: 207–222, 1965.
- Kim G, Kandler K.** Elimination and strengthening of glycinergic/GABAergic connections during tonotopic map formation. *Nat Neurosci* 6: 282–290, 2003.
- Kinoshita M, Matsuoka Y, Suzuki T, Mirrieles J, Yang J.** Sigma-1 receptor alters the kinetics of Kv1.3 voltage gated potassium channels but not the sensitivity to receptor ligands. *Brain Res* 1452: 1–9, 2012.
- Klemic KG, Kirsch GE, Jones SW.** U-type inactivation of Kv3.1 and Shaker potassium channels. *Biophys J* 81: 814–826, 2001.
- Klug A, Trussell LO.** Activation and deactivation of voltage-dependent K⁺ channels during synaptically driven action potentials in the MNTB. *J Neurophysiol* 96: 1547–1555, 2006.

- Koch C, Rapp M, Segev I.** A brief history of time (constants). *Cereb Cortex* 6: 93–101, 1996.
- Kochubey O, Babai N, Schneggenburger R.** A Synaptotagmin Isoform Switch during the Development of an Identified CNS Synapse. *Neuron* 90: 984–999, 2016.
- Koike-Tani M, Saitoh N, Takahashi T.** Mechanisms underlying developmental speeding in AMPA-EPSC decay time at the calyx of Held. *J Neurosci* 25: 199–207, 2005.
- Kole MHP, Letzkus JJ, Stuart GJ.** Axon initial segment Kv1 channels control axonal action potential waveform and synaptic efficacy. *Neuron* 55: 633–647, 2007.
- Komuro H, Rakic P.** Modulation of neuronal migration by NMDA receptors. *Science* 260: 95–97, 1993.
- Kozel PJ, Friedman RA, Erway LC, Yamoah EN, Liu LH, Riddle T, Duffy JJ, Doetschman T, Miller ML, Cardell EL, Shull GE.** Balance and hearing deficits in mice with a null mutation in the gene encoding plasma membrane Ca²⁺-ATPase isoform 2. *J Biol Chem* 273: 18693–18696, 1998.
- Kuba H, Koyano K, Ohmori H.** Synaptic depression improves coincidence detection in the nucleus laminaris in brainstem slices of the chick embryo. *European Journal of Neuroscience* 15: 984–990, 2002.
- Kupper J.** Functional expression of GFP-tagged Kv1.3 and Kv1.4 channels in HEK 293 cells. *Eur J Neurosci* 10: 3908–3912, 1998.
- Kurima K, Peters LM, Yang Y, Riazuddin S, Ahmed ZM, Naz S, Arnaud D, Drury S, Mo J, Makishima T, Ghosh M, Menon PSN, Deshmukh D, Oddoux C, Ostrer H, Khan S, Riazuddin S, Deininger PL, Hampton LL, Sullivan SL, Battey JF, Keats BJB, Wilcox ER, Friedman TB, Griffith AJ.** Dominant and recessive deafness caused by mutations of a novel gene, TMC1, required for cochlear hair-cell function. *Nat Genet* 30: 277–284, 2002.
- Kurima K, Yang Y, Sorber K, Griffith AJ.** Characterization of the transmembrane channel-like (TMC) gene family: functional clues from hearing loss and epidermodysplasia verruciformis. *Genomics* 82: 300–308, 2003.
- Kutsuwada T, Sakimura K, Manabe T, Takayama C, Katakura N, Kushiya E, Natsume R, Watanabe M, Inoue Y, Yagi T, Aizawa S, Arakawa M, Takahashi T, Nakamura Y, Mori H, Mishina M.** Impairment of suckling response, trigeminal neuronal pattern formation, and hippocampal LTD in NMDA receptor epsilon 2 subunit mutant mice. *Neuron* 16: 333–344, 1996.
- Kuwabara N, DiCaprio RA, Zook JM.** Afferents to the medial nucleus of the trapezoid body and their collateral projections. *J Comp Neurol* 314: 684–706, 1991.
- Kuwabara N, Zook JM.** Projections to the medial superior olive from the medial and lateral nuclei of the trapezoid body in rodents and bats. *J Comp Neurol* 324: 522–538, 1992.
- Lau CG, Zukin RS.** NMDA receptor trafficking in synaptic plasticity and neuropsychiatric disorders. *Nat Rev Neurosci* 8: 413–426, 2007.
- Leão KE, Leão RN, Deardorff AS, Garrett A, Fyffe R, Walmsley B.** Sound stimulation modulates high-threshold K(+) currents in mouse auditory brainstem neurons. *Eur J Neurosci* 32: 1658–1667, 2010.

Leao RN, Berntson A, Forsythe ID, Walmsley B. Reduced low-voltage activated K⁺ conductances and enhanced central excitability in a congenitally deaf (dn/dn) mouse. *J Physiol (Lond)* 559: 25–33, 2004a.

Leao RN, Oleskevich S, Sun H, Bautista M, Fyffe REW, Walmsley B. Differences in glycinergic mIPSCs in the auditory brain stem of normal and congenitally deaf neonatal mice. *J Neurophysiol* 91: 1006–1012, 2004b.

Leao RN, Sun H, Svahn K, Berntson A, Youssoufian M, Paolini AG, Fyffe REW, Walmsley B. Topographic organization in the auditory brainstem of juvenile mice is disrupted in congenital deafness. *J Physiol* 571: 563–578, 2006.

Legendre P. The glycinergic inhibitory synapse. *Cell Mol Life Sci* 58: 760–793, 2001.

Lek A, Lek M, North KN, Cooper ST. Phylogenetic analysis of ferlin genes reveals ancient eukaryotic origins. *BMC Evol Biol* 10: 231, 2010.

Lenzi D, Runyeon JW, Crum J, Ellisman MH, Roberts WM. Synaptic vesicle populations in saccular hair cells reconstructed by electron tomography. *J Neurosci* 19: 119–132, 1999.

Li G-L, Cho S, von Gersdorff H. Phase-locking precision is enhanced by multiquantal release at an auditory hair cell ribbon synapse. *Neuron* 83: 1404–1417, 2014.

Lieberman MC. Central projections of auditory-nerve fibers of differing spontaneous rate. I. Anteroventral cochlear nucleus. *J Comp Neurol* 313: 240–258, 1991.

Liu QR, López-Corcuera B, Mandiyan S, Nelson H, Nelson N. Cloning and expression of a spinal cord- and brain-specific glycine transporter with novel structural features. *J Biol Chem* 268: 22802–22808, 1993.

Liu Y, Zhang J. Recent development in NMDA receptors. *Chin Med J* 113: 948–956, 2000.

Llinás R, Sugimori M, Simon SM. Transmission by presynaptic spike-like depolarization in the squid giant synapse. *Proc Natl Acad Sci USA* 79: 2415–2419, 1982.

Lodish H, Berk A, Zipursky SL, Matsudaira P, Baltimore D, Darnell J. *Molecular Cell Biology*. 4th ed. W. H. Freeman, 2000.

Lu U, Roach SM, Song D, Berger TW. Nonlinear dynamic modeling of neuron action potential threshold during synaptically driven broadband intracellular activity. *IEEE Trans Biomed Eng* 59: 706–716, 2012.

Lu Y, Harris JA, Rubel EW. Development of spontaneous miniature EPSCs in mouse AVCN neurons over a critical period of afferent-dependent neuron survival. *J Neurophysiol* 97: 635–646, 2007.

Ludwig A, Zong X, Jeglitsch M, Hofmann F, Biel M. A family of hyperpolarization-activated mammalian cation channels. *Nature* 393: 587–591, 1998.

Lumpkin EA, Hudspeth AJ. Regulation of free Ca²⁺ concentration in hair-cell stereocilia. *J Neurosci* 18: 6300–6318, 1998.

Lüscher B, Keller CA. Regulation of GABA_A receptor trafficking, channel activity, and functional plasticity of inhibitory synapses. *Pharmacol Ther* 102: 195–221, 2004.

- Madara JL.** Regulation of the movement of solutes across tight junctions. *Annu Rev Physiol* 60: 143–159, 1998.
- Magnusson AK, Kapfer C, Grothe B, Koch U.** Maturation of glycinergic inhibition in the gerbil medial superior olive after hearing onset. *J Physiol (Lond)* 568: 497–512, 2005.
- Mainen ZF, Sejnowski TJ.** Influence of dendritic structure on firing pattern in model neocortical neurons. *Nature* 382: 363–366, 1996.
- Manley GA, Köppl C.** Phylogenetic development of the cochlea and its innervation. *Curr Opin Neurobiol* 8: 468–474, 1998.
- Maruyama K, Mikawa T, Ebashi S.** Detection of calcium binding proteins by ⁴⁵Ca autoradiography on nitrocellulose membrane after sodium dodecyl sulfate gel electrophoresis. *J Biochem* 95: 511–519, 1984.
- Mathews PJ, Jercog PE, Rinzel J, Scott LL, Golding NL.** Control of submillisecond synaptic timing in binaural coincidence detectors by Kv1 channels. *Nature Neuroscience* 13: 601–609, 2010.
- Matveev V, Zucker RS, Sherman A.** Facilitation through buffer saturation: constraints on endogenous buffering properties. *Biophys J* 86: 2691–2709, 2004.
- McIntire SL, Reimer RJ, Schuske K, Edwards RH, Jorgensen EM.** Identification and characterization of the vesicular GABA transporter. *Nature* 389: 870–876, 1997.
- Meguro H, Mori H, Araki K, Kushiya E, Kutsuwada T, Yamazaki M, Kumanishi T, Arakawa M, Sakimura K, Mishina M.** Functional characterization of a heteromeric NMDA receptor channel expressed from cloned cDNAs. *Nature* 357: 70–74, 1992.
- Metzner W, Radtke-Schuller S.** The nuclei of the lateral lemniscus in the rufous horseshoe bat, *Rhinolophus rouxi*. A neurophysiological approach. *J Comp Physiol A* 160: 395–411, 1987.
- Michaelis EK.** Molecular biology of glutamate receptors in the central nervous system and their role in excitotoxicity, oxidative stress and aging. *Prog Neurobiol* 54: 369–415, 1998.
- Mikaelian D, Ruben RJ.** Development of Hearing in the Normal Cba-J Mouse: Correlation of Physiological Observations with Behavioral Responses and with Cochlear Anatomy. *Acta Oto-Laryngologica* 59: 451–461, 1965.
- Moore BCJ.** *An Introduction to the Psychology of Hearing*. BRILL, 2012.
- Moore JK, Moore RY.** Glutamic acid decarboxylase-like immunoreactivity in brainstem auditory nuclei of the rat. *J Comp Neurol* 260: 157–174, 1987.
- Moore MJ, Caspary DM.** Strychnine blocks binaural inhibition in lateral superior olivary neurons. *J Neurosci* 3: 237–242, 1983.
- Morest DK.** The growth of synaptic endings in the mammalian brain: a study of the calyces of the trapezoid body. *Z Anat Entwicklungsgesch* 127: 201–220, 1968.
- Mosbacher J, Schoepfer R, Monyer H, Burnashev N, Seeburg PH, Ruppersberg JP.** A molecular determinant for submillisecond desensitization in glutamate receptors. *Science* 266: 1059–1062, 1994.

Moser T, Beutner D. Kinetics of exocytosis and endocytosis at the cochlear inner hair cell afferent synapse of the mouse. *Proc Natl Acad Sci USA* 97: 883–888, 2000.

Nakamura PA, Cramer KS. Formation and maturation of the calyx of Held. *Hearing Research* 276: 70–78, 2011.

Nayagam DAX, Clarey JC, Paolini AG. Powerful, Onset Inhibition in the Ventral Nucleus of the Lateral Lemniscus. *J Neurophysiol* 94: 1651–1654, 2005.

Nayagam DAX, Clarey JC, Paolini AG. Intracellular responses and morphology of rat ventral complex of the lateral lemniscus neurons in vivo. *J Comp Neurol* 498: 295–315, 2006.

Neher E. Vesicle pools and Ca²⁺ microdomains: new tools for understanding their roles in neurotransmitter release. *Neuron* 20: 389–399, 1998.

Neher E. Merits and Limitations of Vesicle Pool Models in View of Heterogeneous Populations of Synaptic Vesicles. *Neuron* 87: 1131–1142, 2015.

Neher E, Sakaba T. Multiple roles of calcium ions in the regulation of neurotransmitter release. *Neuron* 59: 861–872, 2008.

Neuweiler G, Heldmaier G. Vergleichende Tierphysiologie: Neuro- und Sinnesphysiologie. Band 1. Springer-Verlag. Berlin, Heidelberg, Deutschland, 2003.

Newman J. Electric Current and Cell Membranes. In: *Physics of the Life Sciences*. Springer New York, p. 1–30.

Niciu MJ, Kelmendi B, Sanacora G. Overview of Glutamatergic Neurotransmission in the Nervous System. *Pharmacol Biochem Behav* 100: 656–664, 2012.

Nishio S-Y, Hattori M, Moteki H, Tsukada K, Miyagawa M, Naito T, Yoshimura H, Iwasa Y-I, Mori K, Shima Y, Sakuma N, Usami S-I. Gene expression profiles of the cochlea and vestibular endorgans: localization and function of genes causing deafness. *Ann Otol Rhinol Laryngol* 124 Suppl 1: 6S-48S, 2015.

Nobili R, Mammano F, Ashmore J. How well do we understand the cochlea? *Trends Neurosci* 21: 159–167, 1998.

Noh J, Seal RP, Garver JA, Edwards RH, Kandler K. Glutamate co-release at GABA/glycinergic synapses is crucial for the refinement of an inhibitory map. *Nature Neuroscience* 13: 232–238, 2010.

Nowak L, Bregestovski P, Ascher P, Herbert A, Prochiantz A. Magnesium gates glutamate-activated channels in mouse central neurones. *Nature* 307: 462–465, 1984.

Oertel D. The Role of Timing in the Brain Stem Auditory Nuclei of Vertebrates. *Annual Review of Physiology* 61: 497–519, 1999.

Oertel D. Importance of Timing for Understanding Speech. Focus on “Perceptual Consequences of Disrupted Auditory Nerve Activity.” *Journal of Neurophysiology* 93: 3044–3045, 2005.

Oertel D, Shatadal S, Cao X-J. In the ventral cochlear nucleus Kv1.1 and subunits of HCN1 are colocalized at surfaces of neurons that have low-voltage-activated and hyperpolarization-activated conductances. *Neuroscience* 154: 77–86, 2008.

- Oleskevich S, Walmsley B.** Synaptic transmission in the auditory brainstem of normal and congenitally deaf mice. *J Physiol* 540: 447–455, 2002.
- Olo C, Schwartz IR.** The superior olivary complex in C57BL/6 mice. *Am J Anat* 155: 349–373, 1979.
- O’Shea RD.** Roles and regulation of glutamate transporters in the central nervous system. *Clin Exp Pharmacol Physiol* 29: 1018–1023, 2002.
- Otis TS, Raman IM, Trussell LO.** AMPA receptors with high Ca²⁺ permeability mediate synaptic transmission in the avian auditory pathway. *J Physiol (Lond)* 482 (Pt 2): 309–315, 1995.
- Palmer AR, Russell IJ.** Phase-locking in the cochlear nerve of the guinea-pig and its relation to the receptor potential of inner hair-cells. *Hear Res* 24: 1–15, 1986.
- Pang ZP, Südhof TC.** Cell biology of Ca²⁺-triggered exocytosis. *Curr Opin Cell Biol* 22: 496–505, 2010.
- Pangršič T, Reisinger E, Moser T.** Otoferlin: a multi-C2 domain protein essential for hearing. *Trends Neurosci* 35: 671–680, 2012.
- Paoletti P, Neyton J.** NMDA receptor subunits: function and pharmacology. *Current Opinion in Pharmacology* 7: 39–47, 2007.
- Paolini AG, Clarey JC, Needham K, Clark GM.** Fast inhibition alters first spike timing in auditory brainstem neurons. *J Neurophysiol* 92: 2615–2621, 2004.
- Pape HC.** Queer current and pacemaker: the hyperpolarization-activated cation current in neurons. *Annu Rev Physiol* 58: 299–327, 1996.
- Parsons CG, Hartmann S, Spielmanns P.** Budipine is a low affinity, N-methyl-D-aspartate receptor antagonist: patch clamp studies in cultured striatal, hippocampal, cortical and superior colliculus neurones. *Neuropharmacology* 37: 719–727, 1998.
- Pasic TR, Rubel EW.** Rapid changes in cochlear nucleus cell size following blockade of auditory nerve electrical activity in gerbils. *J Comp Neurol* 283: 474–480, 1989.
- Payne KB, Langbauer WR, Thomas EM.** Infrasonic calls of the Asian elephant *Elephas maximus*. *Behav Ecol Sociobiol* 18: 297–301, 1986.
- Penheiter AR, Filoteo AG, Croy CL, Penniston JT.** Characterization of the deafwaddler mutant of the rat plasma membrane calcium-ATPase 2. *Hearing Research* 162: 19–28, 2001.
- Perkins RE.** An electron microscopic study of synaptic organization in the medial superior olive of normal and experimental chinchillas. *J Comp Neurol* 148: 387–415, 1973.
- Peters S, Koh J, Choi DW.** Zinc selectively blocks the action of N-methyl-D-aspartate on cortical neurons. *Science* 236: 589–593, 1987.
- Pickles JO.** *An Introduction to the Physiology of Hearing, Third Edition.* 3 edition. London: Academic Press, 2008.
- Platkiewicz J, Brette R.** A threshold equation for action potential initiation. *PLoS Comput Biol* 6: e1000850, 2010.

- Pollak GD, Gittelman JX, Li N, Xie R.** Inhibitory projections from the ventral nucleus of the lateral lemniscus and superior paraolivary nucleus create directional selectivity of frequency modulations in the inferior colliculus: A comparison of bats with other mammals. *Hearing Research* 273: 134–144, 2011.
- Poole JH, Payne K, Langbauer WR, Moss CJ.** The social contexts of some very low frequency calls of African elephants. *Behav Ecol Sociobiol* 22: 385–392, 1988.
- Popoli M, Yan Z, McEwen BS, Sanacora G.** The stressed synapse: the impact of stress and glucocorticoids on glutamate transmission. *Nat Rev Neurosci* 13: 22–37, 2011.
- Prather JF.** Auditory signal processing in communication: Perception and performance of vocal sounds. *Hearing Research* 305: 144–155, 2013.
- Purves D.** *Neuroscience*. 2nd ed. Sunderland, Mass: Sinauer Associates, 2001.
- Purves D, Augustine GJ, Fitzpatrick D, Katz LC, LaMantia A-S, McNamara JO, Williams SM.** In: *The Middle Ear*. Sunderland, Mass: Sinauer Associates, 2001.
- Ralls K.** Auditory sensitivity in mice, *Peromyscus* and *Mus musculus*. *Anim Behav* 15: 123–128, 1967.
- Raman IM, Zhang S, Trussell LO.** Pathway-specific variants of AMPA receptors and their contribution to neuronal signaling. *J Neurosci* 14: 4998–5010, 1994.
- Rautenberg PL, Grothe B, Felmy F.** Quantification of the three-dimensional morphology of coincidence detector neurons in the medial superior olive of gerbils during late postnatal development. *J Comp Neurol* 517: 385–396, 2009.
- Ravindranathan A, Donevan SD, Sugden SG, Greig A, Rao MS, Parks TN.** Contrasting molecular composition and channel properties of AMPA receptors on chick auditory and brainstem motor neurons. *J Physiol (Lond)* 523 Pt 3: 667–684, 2000.
- Raviv D, Dror AA, Avraham KB.** Hearing loss: a common disorder caused by many rare alleles. *Ann N Y Acad Sci* 1214: 168–179, 2010.
- Recio-Spinoso A, Joris PX.** Temporal properties of responses to sound in the ventral nucleus of the lateral lemniscus. *J Neurophysiol* 111: 817–835, 2014.
- Regehr WG.** Short-Term Presynaptic Plasticity. *Cold Spring Harb Perspect Biol* 4: a005702, 2012.
- Reisinger E, Bresee C, Neef J, Nair R, Reuter K, Bulankina A, Nouvian R, Koch M, Bückers J, Kastrup L, Roux I, Petit C, Hell SW, Brose N, Rhee J-S, Kügler S, Brigande JV, Moser T.** Probing the functional equivalence of otoferlin and synaptotagmin 1 in exocytosis. *J Neurosci* 31: 4886–4895, 2011.
- Renden R, Taschenberger H, Puente N, Rusakov DA, Duvoisin R, Wang L-Y, Lehre KP, von Gersdorff H.** Glutamate transporter studies reveal the pruning of metabotropic glutamate receptors and absence of AMPA receptor desensitization at mature calyx of Held synapses. *J Neurosci* 25: 8482–8497, 2005.
- Rhode WS.** Neural encoding of single-formant stimuli in the ventral cochlear nucleus of the chinchilla. *Hearing Research* 117: 39–56, 1998.

- Rhode WS, Greenberg S.** Encoding of amplitude modulation in the cochlear nucleus of the cat. *Journal of Neurophysiology* 71: 1797–1825, 1994.
- Rhode WS, Oertel D, Smith PH.** Physiological response properties of cells labeled intracellularly with horseradish peroxidase in cat ventral cochlear nucleus. *J Comp Neurol* 213: 448–463, 1983.
- Rietzel HJ, Friauf E.** Neuron types in the rat lateral superior olive and developmental changes in the complexity of their dendritic arbors. *J Comp Neurol* 390: 20–40, 1998.
- Riquelme R, Saldaña E, Osen KK, Ottersen OP, Merchán MA.** Colocalization of GABA and glycine in the ventral nucleus of the lateral lemniscus in rat: An in situ hybridization and semiquantitative immunocytochemical study. *J Comp Neurol* 432: 409–424, 2001.
- Rivera J, Tessarollo L.** Genetic Background and the Dilemma of Translating Mouse Studies to Humans. *Immunity* 28: 1–4, 2008.
- Roberts WM.** Spatial calcium buffering in saccular hair cells. *Nature* 363: 74–76, 1993.
- Robinson RB, Siegelbaum SA.** Hyperpolarization-activated cation currents: from molecules to physiological function. *Annu Rev Physiol* 65: 453–480, 2003.
- Rodriguez-Contreras A, Lv P, Zhu J, Kim HJ, Yamoah EN.** Effects of strontium on the permeation and gating phenotype of calcium channels in hair cells. *J Neurophysiol* 100: 2115–2124, 2008.
- Rogowski BA, Feng AS.** Normal postnatal development of medial superior olivary neurons in the albino rat: a Golgi and Nissl study. *J Comp Neurol* 196: 85–97, 1981.
- Rouiller EM, Ryugo DK.** Intracellular marking of physiologically characterized cells in the ventral cochlear nucleus of the cat. *J Comp Neurol* 225: 167–186, 1984.
- Roux I, Safieddine S, Nouvian R, Grati M, Simmler M-C, Bahloul A, Perfettini I, Le Gall M, Rostaing P, Hamard G, Triller A, Avan P, Moser T, Petit C.** Otoferlin, Defective in a Human Deafness Form, Is Essential for Exocytosis at the Auditory Ribbon Synapse. *Cell* 127: 277–289, 2006.
- Rubel EW, Fritzsche B.** AUDITORY SYSTEM DEVELOPMENT: Primary Auditory Neurons and Their Targets. *Annual Review of Neuroscience* 25: 51–101, 2002.
- Rubio ME, Matsui K, Fukazawa Y, Kamasawa N, Harada H, Itakura M, Molnár E, Abe M, Sakimura K, Shigemoto R.** The number and distribution of AMPA receptor channels containing fast kinetic GluA3 and GluA4 subunits at auditory nerve synapses depend on the target cells. *Brain Struct Funct* 222: 3375–3393, 2017.
- Rudy B, McBain CJ.** Kv3 channels: voltage-gated K⁺ channels designed for high-frequency repetitive firing. *Trends Neurosci* 24: 517–526, 2001.
- Rusu SI, Borst JGG.** Developmental changes in intrinsic excitability of principal neurons in the rat medial nucleus of the trapezoid body. *Dev Neurobiol* 71: 284–295, 2011.
- Ryugo DK, Sento S.** Synaptic connections of the auditory nerve in cats: relationship between endbulbs of held and spherical bushy cells. *J Comp Neurol* 305: 35–48, 1991.
- Ryugo DK, Spirou GA.** Auditory System: Giant Synaptic Terminals, Endbulbs, and Calyces. In: *Encyclopedia of Neuroscience*. Elsevier, p. 759–770, 2009.

Sabatini BL, Regehr WG. Timing of synaptic transmission. *Annu Rev Physiol* 61: 521–542, 1999.

Safieddine S, Wenthold RJ. SNARE complex at the ribbon synapses of cochlear hair cells: analysis of synaptic vesicle- and synaptic membrane-associated proteins. *Eur J Neurosci* 11: 803–812, 1999.

Sagné C, El Mestikawy S, Isambert MF, Hamon M, Henry JP, Giros B, Gasnier B. Cloning of a functional vesicular GABA and glycine transporter by screening of genome databases. *FEBS Lett* 417: 177–183, 1997.

Saint Marie RL, Baker RA. Neurotransmitter-specific uptake and retrograde transport of [3H]glycine from the inferior colliculus by ipsilateral projections of the superior olivary complex and nuclei of the lateral lemniscus. *Brain Research* 524: 244–253, 1990.

Saint Marie RL, Shneiderman A, Stanforth DA. Patterns of gamma-aminobutyric acid and glycine immunoreactivities reflect structural and functional differences of the cat lateral lemniscal nuclei. *J Comp Neurol* 389: 264–276, 1997.

Sakaba T, Neher E. Quantitative relationship between transmitter release and calcium current at the calyx of held synapse. *J Neurosci* 21: 462–476, 2001.

Samson JE, Mooney TA, Gussekloo SWS, Hanlon RT. A Brief Review of Cephalopod Behavioral Responses to Sound. *Adv Exp Med Biol* 875: 969–975, 2016.

Sanes DH, Song J, Tyson J. Refinement of dendritic arbors along the tonotopic axis of the gerbil lateral superior olive. *Brain Res Dev Brain Res* 67: 47–55, 1992.

Sankaranarayanan K, Varshney A, Mathew MK. N type rapid inactivation in human Kv1.4 channels: functional role of a putative C-terminal helix. *Mol Membr Biol* 22: 389–400, 2005.

Santoro B, Liu DT, Yao H, Bartsch D, Kandel ER, Siegelbaum SA, Tibbs GR. Identification of a gene encoding a hyperpolarization-activated pacemaker channel of brain. *Cell* 93: 717–729, 1998.

Sara Y, Virmani T, Deák F, Liu X, Kavalali ET. An isolated pool of vesicles recycles at rest and drives spontaneous neurotransmission. *Neuron* 45: 563–573, 2005.

Sätzler K, Söhl LF, Bollmann JH, Borst JGG, Frotscher M, Sakmann B, Lübke JHR. Three-dimensional reconstruction of a calyx of Held and its postsynaptic principal neuron in the medial nucleus of the trapezoid body. *J Neurosci* 22: 10567–10579, 2002.

Schacter, Gilbert DT, Wegner DM. *Psychology (2nd Edition)*. New York: Worth, 2011.

Scheuss V, Schneggenburger R, Neher E. Separation of presynaptic and postsynaptic contributions to depression by covariance analysis of successive EPSCs at the calyx of Held synapse. *J Neurosci* 22: 728–739, 2002.

Schneggenburger R, Forsythe ID. The calyx of Held. *Cell Tissue Res* 326: 311–337, 2006.

Schneggenburger R, Meyer AC, Neher E. Released fraction and total size of a pool of immediately available transmitter quanta at a calyx synapse. *Neuron* 23: 399–409, 1999.

Schneggenburger R, Neher E. Presynaptic calcium and control of vesicle fusion. *Curr Opin Neurobiol* 15: 266–274, 2005.

- Schneggenburger R, Rosenmund C.** Molecular mechanisms governing Ca(2+) regulation of evoked and spontaneous release. *Nat Neurosci* 18: 935–941, 2015.
- Schnitzler H-U, Moss CF, Denzinger A.** From spatial orientation to food acquisition in echolocating bats. *Trends in Ecology & Evolution* 18: 386–394, 2003.
- Schnupp J, Nelken I, King A.** *Auditory Neuroscience: Making Sense of Sound*. MIT Press, 2011.
- Schofield BR, Cant NB.** Ventral nucleus of the lateral lemniscus in guinea pigs: Cytoarchitecture and inputs from the cochlear nucleus. *J Comp Neurol* 379: 363–385, 1997.
- Schug N, Braig C, Zimmermann U, Engel J, Winter H, Ruth P, Blin N, Pfister M, Kalbacher H, Knipper M.** Differential expression of otoferlin in brain, vestibular system, immature and mature cochlea of the rat. *Eur J Neurosci* 24: 3372–3380, 2006.
- Schwaller B, Meyer M, Schiffmann S.** ‘New’ functions for ‘old’ proteins: The role of the calcium-binding proteins calbindin D-28k, calretinin and parvalbumin, in cerebellar physiology. Studies with knockout mice. *Cerebellum* 1: 241–258, 2002.
- Schwartzkopff J.** Auditory communication in lower animals: role of auditory physiology. *Annu Rev Psychol* 28: 61–84, 1977.
- Scott LL, Mathews PJ, Golding NL.** Posthearing developmental refinement of temporal processing in principal neurons of the medial superior olive. *J Neurosci* 25: 7887–7895, 2005.
- Seifert R, Scholten A, Gauss R, Mincheva A, Lichter P, Kaupp UB.** Molecular characterization of a slowly gating human hyperpolarization-activated channel predominantly expressed in thalamus, heart, and testis. *Proc Natl Acad Sci USA* 96: 9391–9396, 1999.
- Shneiderman A, Oliver DL, Henkel CK.** Connections of the dorsal nucleus of the lateral lemniscus: an inhibitory parallel pathway in the ascending auditory system? *J Comp Neurol* 276: 188–208, 1988.
- Shu Y, Yu Y, Yang J, McCormick DA.** Selective control of cortical axonal spikes by a slowly inactivating K⁺ current. *Proc Natl Acad Sci USA* 104: 11453–11458, 2007.
- Silver RA, Traynelis SF, Cull-Candy SG.** Rapid-time-course miniature and evoked excitatory currents at cerebellar synapses in situ. *Nature* 355: 163–166, 1992.
- Simon SM, Llinás RR.** Compartmentalization of the submembrane calcium activity during calcium influx and its significance in transmitter release. *Biophys J* 48: 485–498, 1985.
- Smith AJ, Owens S, Forsythe ID.** Characterisation of inhibitory and excitatory postsynaptic currents of the rat medial superior olive. *J Physiol (Lond)* 529 Pt 3: 681–698, 2000.
- Smith PH.** Structural and functional differences distinguish principal from nonprincipal cells in the guinea pig MSO slice. *J Neurophysiol* 73: 1653–1667, 1995.
- Smith PH, Joris PX, Carney LH, Yin TC.** Projections of physiologically characterized globular bushy cell axons from the cochlear nucleus of the cat. *J Comp Neurol* 304: 387–407, 1991.
- Smith PH, Joris PX, Yin TCT.** Projections of physiologically characterized spherical bushy cell axons from the cochlear nucleus of the cat: Evidence for delay lines to the medial superior olive. *J Comp Neurol* 331: 245–260, 1993.

Smith PH, Massie A, Joris PX. Acoustic stria: Anatomy of physiologically characterized cells and their axonal projection patterns. *J Comp Neurol* 482: 349–371, 2005.

Snyders DJ, Tamkun MM, Bennett PB. A rapidly activating and slowly inactivating potassium channel cloned from human heart. Functional analysis after stable mammalian cell culture expression. *J Gen Physiol* 101: 513–543, 1993.

Sonntag M, Englitz B, Kopp-Scheinflug C, RübSamen R. Early postnatal development of spontaneous and acoustically evoked discharge activity of principal cells of the medial nucleus of the trapezoid body: an in vivo study in mice. *J Neurosci* 29: 9510–9520, 2009.

Spencer MJ, Nayagam DAX, Clarey JC, Paolini AG, Meffin H, Burkitt AN, Grayden DB. Broadband Onset Inhibition Can Suppress Spectral Splatter in the Auditory Brainstem. *PLoS ONE* 10: e0126500, 2015.

Spencer RH, Sokolov Y, Li H, Takenaka B, Milici AJ, Aiyar J, Nguyen A, Park H, Jap BK, Hall JE, Gutman GA, Chandy KG. Purification, visualization, and biophysical characterization of Kv1.3 tetramers. *J Biol Chem* 272: 2389–2395, 1997.

Sprunger LK, Stewig NJ, O’Grady SM. Effects of charybdotoxin on K⁺ channel (KV1.2) deactivation and inactivation kinetics. *Eur J Pharmacol* 314: 357–364, 1996.

Spruston N, Johnston D. Perforated patch-clamp analysis of the passive membrane properties of three classes of hippocampal neurons. *Journal of Neurophysiology* 67: 508–529, 1992.

Street VA, McKee-Johnson JW, Fonseca RC, Tempel BL, Noben-Trauth K. Mutations in a plasma membrane Ca²⁺-ATPase gene cause deafness in deafwaddler mice. *Nat Genet* 19: 390–394, 1998.

Street VA, Robinson LC, Erford SK, Tempel BL. Molecular genetic analysis of distal mouse chromosome 6 defines gene order and positions of the deafwaddler and opisthotonos mutations. *Genomics* 29: 123–130, 1995.

Stühmer W, Ruppersberg JP, Schröter KH, Sakmann B, Stocker M, Giese KP, Perschke A, Baumann A, Pongs O. Molecular basis of functional diversity of voltage-gated potassium channels in mammalian brain. *EMBO J* 8: 3235–3244, 1989.

Südhof TC. Neurotransmitter release: the last millisecond in the life of a synaptic vesicle. *Neuron* 80: 675–690, 2013.

Südhof TC, Rothman JE. Membrane fusion: grappling with SNARE and SM proteins. *Science* 323: 474–477, 2009.

Sumner CJ, Tucci DL, Shore SE. Responses of ventral cochlear nucleus neurons to contralateral sound after conductive hearing loss. *J Neurophysiol* 94: 4234–4243, 2005.

Takahashi T, Feldmeyer D, Suzuki N, Onodera K, Cull-Candy SG, Sakimura K, Mishina M. Functional correlation of NMDA receptor epsilon subunits expression with the properties of single-channel and synaptic currents in the developing cerebellum. *J Neurosci* 16: 4376–4382, 1996.

Takamori S. VGLUTs: “exciting” times for glutamatergic research? *Neurosci Res* 55: 343–351, 2006.

Tarusawa E, Matsui K, Budisantoso T, Molnár E, Watanabe M, Matsui M, Fukazawa Y, Shigemoto R. Input-specific intrasynaptic arrangements of ionotropic glutamate receptors and their impact on postsynaptic responses. *J Neurosci* 29: 12896–12908, 2009.

Taschenberger H, von Gersdorff H. Fine-tuning an auditory synapse for speed and fidelity: developmental changes in presynaptic waveform, EPSC kinetics, and synaptic plasticity. *J Neurosci* 20: 9162–9173, 2000.

Taschenberger H, Leão RM, Rowland KC, Spirou GA, von Gersdorff H. Optimizing synaptic architecture and efficiency for high-frequency transmission. *Neuron* 36: 1127–1143, 2002.

Taschenberger H, Scheuss V, Neher E. Release kinetics, quantal parameters and their modulation during short-term depression at a developing synapse in the rat CNS. *J Physiol (Lond)* 568: 513–537, 2005.

Tomczak AP, Fernández-Trillo J, Bharill S, Papp F, Panyi G, Stühmer W, Isacoff EY, Pardo LA. A new mechanism of voltage-dependent gating exposed by KV10.1 channels interrupted between voltage sensor and pore. *J Gen Physiol* 149: 577–593, 2017.

Tour O, Parnas H, Parnas I. Depolarization increases the single-channel conductance and the open probability of crayfish glutamate channels. *Biophys J* 74: 1767–1778, 1998.

Traynelis SF, Wollmuth LP, McBain CJ, Menniti FS, Vance KM, Ogden KK, Hansen KB, Yuan H, Myers SJ, Dingledine R. Glutamate receptor ion channels: structure, regulation, and function. *Pharmacol Rev* 62: 405–496, 2010.

Tripathi ON, Ravens U, Sanguinetti MC. *Heart Rate and Rhythm: Molecular Basis, Pharmacological Modulation and Clinical Implications.* Springer Science & Business Media, 2011.

Tritsch NX, Bergles DE. Developmental regulation of spontaneous activity in the Mammalian cochlea. *J Neurosci* 30: 1539–1550, 2010.

Tritsch NX, Rodríguez-Contreras A, Crins TTH, Wang HC, Borst JGG, Bergles DE. Calcium action potentials in hair cells pattern auditory neuron activity before hearing onset. *Nat Neurosci* 13: 1050–1052, 2010.

Tritsch NX, Yi E, Gale JE, Glowatzki E, Bergles DE. The origin of spontaneous activity in the developing auditory system. *Nature* 450: 50–55, 2007.

Trussell LO. Synaptic Mechanisms for Coding Timing in Auditory Neurons. *Annual Review of Physiology* 61: 477–496, 1999.

Trussell LO, Zhang S, Raman IM. Desensitization of AMPA receptors upon multiquantal neurotransmitter release. *Neuron* 10: 1185–1196, 1993.

Tucker T, Fettiplace R. Confocal imaging of calcium microdomains and calcium extrusion in turtle hair cells. *Neuron* 15: 1323–1335, 1995.

Turner JG, Parrish JL, Hughes LF, Toth LA, Caspary DM. Hearing in Laboratory Animals: Strain Differences and Nonauditory Effects of Noise. *Comp Med* 55: 12–23, 2005.

Turner JG, Willott JF. Exposure to an augmented acoustic environment alters auditory function in hearing-impaired DBA/2J mice. *Hear Res* 118: 101–113, 1998.

- Vater M, Covey E, Casseday JH.** The columnar region of the ventral nucleus of the lateral lemniscus in the big brown bat (*Eptesicus fuscus*): synaptic arrangements and structural correlates of feedforward inhibitory function. *Cell Tissue Res* 289: 223–233, 1997.
- Vater M, Feng AS.** Functional organization of ascending and descending connections of the cochlear nucleus of horseshoe bats. *J Comp Neurol* 292: 373–395, 1990.
- Wadiche JI, Jahr CE.** Multivesicular release at climbing fiber-Purkinje cell synapses. *Neuron* 32: 301–313, 2001.
- Wahl-Schott C, Biel M.** HCN channels: Structure, cellular regulation and physiological function. *Cellular and Molecular Life Sciences* 66: 470–494, 2009.
- Walcher J, Hassfurth B, Grothe B, Koch U.** Comparative posthearing development of inhibitory inputs to the lateral superior olive in gerbils and mice. *Journal of Neurophysiology* 106: 1443–1453, 2011.
- Wang H, Kunkel DD, Schwartzkroin PA, Tempel BL.** Localization of Kv1.1 and Kv1.2, two K channel proteins, to synaptic terminals, somata, and dendrites in the mouse brain. *J Neurosci* 14: 4588–4599, 1994.
- Wang L-Y, Augustine GJ.** Presynaptic nanodomains: a tale of two synapses. *Front Cell Neurosci* 8: 455, 2014.
- Wang L-Y, Gan L, Forsythe ID, Kaczmarek LK.** Contribution of the Kv3.1 potassium channel to high-frequency firing in mouse auditory neurones. *J Physiol* 509: 183–194, 1998a.
- Wang LY, Kaczmarek LK.** High-frequency firing helps replenish the readily releasable pool of synaptic vesicles. *Nature* 394: 384–388, 1998.
- Wang YX, Wenthold RJ, Ottersen OP, Petralia RS.** Endbulb synapses in the anteroventral cochlear nucleus express a specific subset of AMPA-type glutamate receptor subunits. *J Neurosci* 18: 1148–1160, 1998b.
- Weatherstone JH, Kopp-Scheinflug C, Pilati N, Wang Y, Forsythe ID, Rubel EW, Tempel BL.** Maintenance of neuronal size gradient in MNTB requires sound-evoked activity. *J Neurophysiol* 117: 756–766, 2017.
- Weis S, Schneggenburger R, Neher E.** Properties of a model of Ca⁺⁺-dependent vesicle pool dynamics and short term synaptic depression. *Biophys J* 77: 2418–2429, 1999.
- Wenthold RJ, Petralia RS, Blahos J II, Niedzielski AS.** Evidence for multiple AMPA receptor complexes in hippocampal CA1/CA2 neurons. *J Neurosci* 16: 1982–1989, 1996.
- Wenthold RJ, Roche KW.** The organization and regulation of non-NMDA receptors in neurons. *Prog Brain Res* 116: 133–152, 1998.
- Willard FH, Ryugo DK.** Anatomy of the central auditory system. In: *The auditory psychobiology of the mouse*. Charles C Thomas Pub Ltd, 1983, p. 201–304.
- Willard SS, Koochekpour S.** Glutamate, glutamate receptors, and downstream signaling pathways. *Int J Biol Sci* 9: 948–959, 2013.
- Willott JF, Turner JG.** Prolonged exposure to an augmented acoustic environment ameliorates age-related auditory changes in C57BL/6J and DBA/2J mice. *Hear Res* 135: 78–88, 1999.

- Willott JF, Turner JG, Carlson S, Ding D, Seegers Bross L, Falls WA.** The BALB/c mouse as an animal model for progressive sensorineural hearing loss. *Hear Res* 115: 162–174, 1998.
- Wimmer VC, Horstmann H, Groh A, Kuner T.** Donut-Like Topology of Synaptic Vesicles with a Central Cluster of Mitochondria Wrapped into Membrane Protrusions: A Novel Structure–Function Module of the Adult Calyx of Held. *J Neurosci* 26: 109–116, 2006.
- Wölfel M, Schneggenburger R.** Presynaptic capacitance measurements and Ca²⁺ uncaging reveal submillisecond exocytosis kinetics and characterize the Ca²⁺ sensitivity of vesicle pool depletion at a fast CNS synapse. *J Neurosci* 23: 7059–7068, 2003.
- Wong AYC, Graham BP, Billups B, Forsythe ID.** Distinguishing between presynaptic and postsynaptic mechanisms of short-term depression during action potential trains. *J Neurosci* 23: 4868–4877, 2003.
- Wu SH.** Physiological Properties of Neurons in the Ventral Nucleus of the Lateral Lemniscus of the Rat: Intrinsic Membrane Properties and Synaptic Responses. *J Neurophysiol* 81: 2862–2874, 1999.
- Wu SH, Kelly JB.** In vitro brain slice studies of the rat's dorsal nucleus of the lateral lemniscus. III. synaptic pharmacology. *J Neurophysiol* 75: 1271–1282, 1996.
- Wu SH, Oertel D.** Maturation of synapses and electrical properties of cells in the cochlear nuclei. *Hear Res* 30: 99–110, 1987.
- Wu X-S, Xue L, Mohan R, Paradiso K, Gillis KD, Wu L-G.** The origin of quantal size variation: vesicular glutamate concentration plays a significant role. *J Neurosci* 27: 3046–3056, 2007.
- Xiao L, Michalski N, Kronander E, Gjoni E, Genoud C, Knott G, Schneggenburger R.** BMP signaling specifies the development of a large and fast CNS synapse. *Nature Neuroscience* 16: 856–864, 2013.
- Xu-Friedman MA, Regehr WG.** Structural contributions to short-term synaptic plasticity. *Physiol Rev* 84: 69–85, 2004.
- Yamashita T, Ishikawa T, Takahashi T.** Developmental increase in vesicular glutamate content does not cause saturation of AMPA receptors at the calyx of Held synapse. *J Neurosci* 23: 3633–3638, 2003.
- Yamoah EN, Lumpkin EA, Dumont RA, Smith PJ, Hudspeth AJ, Gillespie PG.** Plasma membrane Ca²⁺-ATPase extrudes Ca²⁺ from hair cell stereocilia. *J Neurosci* 18: 610–624, 1998.
- Yang Y-M, Wang L-Y.** Amplitude and kinetics of action potential-evoked Ca²⁺ current and its efficacy in triggering transmitter release at the developing calyx of Held synapse. *J Neurosci* 26: 5698–5708, 2006.
- Yasunaga S, Grati M, Cohen-Salmon M, El-Amraoui A, Mustapha M, Salem N, El-Zir E, Loiselet J, Petit C.** A mutation in OTOF, encoding otoferlin, a FER-1-like protein, causes DFNB9, a nonsyndromic form of deafness. *Nat Genet* 21: 363–369, 1999.
- Yavuzoglu A, Schofield BR, Wenstrup JJ.** Circuitry Underlying Spectrotemporal Integration in the Auditory Midbrain. *J Neurosci* 31: 14424–14435, 2011.
- Yorgason JG, Fayad JN, Kalinec F.** Understanding drug ototoxicity: molecular insights for prevention and clinical management. *Expert Opin Drug Saf* 5: 383–399, 2006.

- Youssoufian M, Couchman K, Shivdasani MN, Paolini AG, Walmsley B.** Maturation of auditory brainstem projections and calyces in the congenitally deaf (dn/dn) mouse. *J Comp Neurol* 506: 442–451, 2008.
- Youssoufian M, Oleskevich S, Walmsley B.** Development of a Robust Central Auditory Synapse in Congenital Deafness. *Journal of Neurophysiology* 94: 3168–3180, 2005.
- Zenner H-P.** *Hören*. Stuttgart: Thieme, Stuttgart, 1994.
- Zhang H, Kelly JB.** Responses of Neurons in the Rat's Ventral Nucleus of the Lateral Lemniscus to Amplitude-Modulated Tones. *Journal of Neurophysiology* 96: 2905–2914, 2006.
- Zhao M, Wu SH.** Morphology and physiology of neurons in the ventral nucleus of the lateral lemniscus in rat brain slices. *The Journal of Comparative Neurology* 433: 255–271, 2001.
- Zhao S, Ting JT, Atallah HE, Qiu L, Tan J, Gloss B, Augustine GJ, Deisseroth K, Luo M, Graybiel AM, Feng G.** Cell type-specific channelrhodopsin-2 transgenic mice for optogenetic dissection of neural circuitry function. *Nat Meth* 8: 745–752, 2011.
- Zheng QY, Johnson KR, Erway LC.** Assessment of hearing in 80 inbred strains of mice by ABR threshold analyses. *Hear Res* 130: 94–107, 1999.
- Zhou N, Taylor DA, Parks TN.** Cobalt-permeable non-NMDA receptors in developing chick brainstem auditory nuclei. *Neuroreport* 6: 2273–2276, 1995.
- Zook JM, Casseday JH.** Origin of ascending projections to inferior colliculus in the mustache bat, *Pteronotus parnellii*. *J Comp Neurol* 207: 14–28, 1982a.
- Zook JM, Casseday JH.** Cytoarchitecture of auditory system in lower brainstem of the mustache bat, *Pteronotus parnellii*. *J Comp Neurol* 207: 1–13, 1982b.

9 Abbreviations

ACSF	artificial cerebrospinal fluid
AHP	afterhyperpolarization
AMPA	α -amino-3-hydroxy-5-methyl-4-isoxazolepropionic acid
AMPA	α -amino-3-hydroxy-5-methyl-4-isoxazolepropionic acid receptor
AP	action potential
AVCN	anteroventral cochlear nucleus
BDA	Biotinylated dextran amine
bp	base pairs
CaR	calcium receptor
CN	cochlear nucleus
CR	calretinin
DCN	dorsal cochlear nucleus
DFN	deafness
dfw	deafwaddler
DNA	deoxyribonucleic acid
DNLL	dorsal nucleus of the lateral lemniscus
DNQX	6,7-dinitroquinoxaline-2,3-dione
dVNLL	dorsal part of the ventral nucleus of the lateral lemniscus
Ex	prenatal day x
EAAT	excitatory amino acid transporter
EDTA	ethylenediaminetetraacetic acid
EPSC	excitatory postsynaptic current
EQ	Elmqvist-Quastel
EYFP	enhanced yellow fluorescent protein
FEM	Forschungseinrichtungen für Experimentelle Medizin
GABA	γ -aminobutyric acid
GAD	glutamic acid decarboxylase
GL	gene ladder
Gln	glutamine
Glu	glutamate
GluR	glutamate receptor
GlyTx	glycine transporter x
HCN	Hyperpolarization-activated cyclic nucleotide-gated channel
HRP	horseradish peroxidase
IC	inferior colliculus
I _h	HCN channel-mediated current
IHC	inner hair cell
IID	interaural intensity difference
INLL	intermediate nucleus of the lateral lemniscus
IPSC	inhibitory postsynaptic current

ITD	interaural time difference
KO	knock-out
K _v x	voltage-gated potassium channel x
LNTB	lateral nucleus of the trapezoid body
LSO	lateral superior olive
mEPSC	miniature excitatory postsynaptic current
mGluR	metabotropic glutamate receptor
MNTB	medial nucleus of the trapezoid body
MSO	medial superior olive
Na _v x	voltage-gated sodium channel x
NDS	normal donkey serum
NMDA	N-Methyl-D-aspartic acid
NMDAR	N-Methyl-D-aspartic acid receptor
NRx	NMDA receptor subunit x
OHC	outer hair cell
OTOF ^(-/-)	otofelin KO
OTOF ^(+/-)	heterozygous otoferlin expression
OTOF ^(+/+)	otofelin WT
Px	postnatal day x
PB	phosphate buffer
PBS	phosphate buffer saline
PCR	polymerase chain reaction
PFA	paraformaldehyde
PMCA	plasma membrane calcium ATPase
PSC	postsynaptic current
RRP	readily releasable pool
SEM	standard error of the mean
SNARE	soluble N-ethylmaleimide-sensitive-factor attachment receptor
SOC	superior olivary complex
STP	short-term plasticity
Syt1/Syt2	synaptotagmin I and II
PVCN	posteroventral cochlear nucleus
TBE	TRIS-Borat-EDTA buffer
tmc1	transmembrane channel-like protein 1
TRIS	Tris(hydroxymethyl)-aminomethan
TTX	tetrodotoxin
VCN	ventral cochlear nucleus
VGAT	vesicular GABA transporter
VGluTx	vesicular glutamate transporter x
VNLL	ventral nucleus of the lateral lemniscus
vVNLL	ventrolateral part of the ventral nucleus of the lateral lemniscus
WT	wild type
YFP	yellow fluorescent protein

10 List of figures

- Figure 1: The outer, middle and inner ear of humans.
- Figure 2: Schematic of the mammalian auditory pathway.
- Figure 3: Three large mammalian auditory synapses.
- Figure 4: Developmental refinement of the Calyx of Held in the MNTB.
- Figure 5: Glutamatergic synaptic transmission in the central nervous system.
- Figure 6: Inner hair cell of the cochlea and its functional composition of the ribbon synapse.
- Figure 7: Representative genotyping result.
- Figure 8: Elmquist-Quastel plot of a representative WT animal.
- Figure 9: Intrinsic properties differ between vVNLL and dVNLL neurons.
- Figure 10: Heterogeneous firing properties differ between neurons of the dVNLL and vVNLL.
- Figure 11: dVNLL neurons have large hyperpolarization-activated currents (I_h) and stronger HCN1 immunoreactivity.
- Figure 12: Excitatory postsynaptic currents (EPSCs) are larger and the excitatory inputs are stronger in vVNLL neurons.
- Figure 13: Inhibitory inputs are similar in vVNLL and dVNLL neurons.
- Figure 14: Synaptic short-term plasticity of excitatory and inhibitory inputs is similar in vVNLL and dVNLL neurons.
- Figure 15: Both vVNLL and dVNLL neurons are inhibitory.
- Figure 16: AMPA- and NMDA-current components undergo significant changes in size and time constants during development of vVNLL neurons in Bl6 mice.
- Figure 17: Excitatory postsynaptic currents (EPSCs) of vVNLL neurons in Bl6 mice at P10, P13 and P22. A reduction of synaptic input number and an increase of synaptic strength in combination with faster time constants is seen during development.
- Figure 18: vVNLL neurons have a different set of firing patterns and passive intrinsic membrane properties between P10 and P22 OTOF^(+/+) (WT) animals.
- Figure 19: Active firing properties differ between P10 and P22 OTOF^(+/+) (WT) animals in their action potential current threshold, amplitude and half-width.
- Figure 20: Excitatory postsynaptic currents (EPSCs) of vVNLL neurons rise and decay faster in P22 OTOF^(+/+) (WT) than in P10 and animals.

- Figure 21: Miniature excitatory postsynaptic currents (mEPSCs) of vVNLL neurons rise and decay faster in P22 OTOF^(+/+) (WT) than in P10 animals.
- Figure 22: Synaptic short-term plasticity of excitatory inputs of vVNLL neurons of P10 OTOF^(+/+) (WT) animals exhibits a higher degree of depression and a smaller paired pulse than P22 WT animals.
- Figure 23: Immunolabelings to visualize excitatory inputs to vVNLL neurons in P10 and P22 OTOF^(+/+) (WT) animals with antibodies against VGluT1 and calretinin (CR).
- Figure 24: vVNLL neurons of P22 OTOF^(+/+) (WT) and OTOF^(-/-) (KO) animals have a different set of firing patterns and resting membrane potentials.
- Figure 25: Active firing properties differ between P22 OTOF^(+/+) (WT) and OTOF^(-/-) (KO) animals in their action potential current and voltage thresholds.
- Figure 26: Excitatory postsynaptic currents (EPSCs) of vVNLL neurons are larger and faster in P22 OTOF^(+/+) (WT) than in P22 OTOF^(-/-) (KO) animals.
- Figure 27: Miniature excitatory postsynaptic currents (mEPSCs) of vVNLL neurons have a larger frequency and decay slower in P22 OTOF^(-/-) (KO) than in P22 OTOF^(+/+) (WT) animals.
- Figure 28: Synaptic short-term plasticity of excitatory inputs of vVNLL neurons are similar in P22 OTOF^(+/+) (WT) and P22 OTOF^(-/-) (KO) animals.
- Figure 29: Immunolabelings to visualize excitatory inputs to vVNLL neurons in P22 OTOF^(+/+) (WT) and P22 OTOF^(-/-) (KO) animals with antibodies against VGluT1 and calretinin (CR).

11 List of tables

- Table 1: List of primary and secondary antibodies used in the experiments.
- Table 2: Summary of membrane properties of dVNLL and vVNLL neurons.
- Table 3: Summary of synaptic properties of dVNLL and vVNLL neurons of C57Bl/6J mice.
- Table 4: Summary of AMPAR and NMDAR mediated currents of vVNLL neurons of P10, P13 and P22 Bl6 mice.
- Table 5: Summary of excitatory postsynaptic currents (EPSCs) of vVNLL neurons of P10, P13 and P22 Bl6 mice.
- Table 6: Summary of membrane properties of vVNLL neurons of P10 and P22 OTOF^(+/+) (WT) and P22 OTOF^(-/-) (KO) mice.
- Table 7: Summary of excitatory postsynaptic currents (EPSCs) of vVNLL neurons of P10 and P22 OTOF^(+/+) (WT) and P22 OTOF^(-/-) (KO) mice.
- Table 8: Summary of miniature excitatory postsynaptic currents (mEPSCs) of vVNLL neurons of P10 and P22 OTOF^(+/+) (WT) and P22 OTOF^(-/-) (KO) mice.
- Table 9: Summary of short-term plasticity of excitatory postsynaptic currents (EPSCs) of vVNLL neurons of P10 and P22 OTOF^(+/+) (WT) and P22 OTOF^(-/-) (KO) mice.

12 Publication

Caspari, F., Baumann, V. J., Garcia-Pino, E., & Koch, U. (2015). Heterogeneity of Intrinsic and Synaptic Properties of Neurons in the Ventral and Dorsal Parts of the Ventral Nucleus of the Lateral Lemniscus. *Frontiers in Neural Circuits*, 9, 74. <http://doi.org/10.3389/fncir.2015.00074>

13 Acknowledgements

First of all, I would like to sincerely thank Prof. Dr. Ursula Koch, without whom the realization of this work would not have been possible. I especially thank her for supporting me all these years and creating a very pleasant working environment. Honestly, it was great.

Moreover, I thank Dr. Daniela Vallentin for evaluating this thesis. I really appreciate that.

Also, I am grateful for Dr. Nicola Strenzke who sent us animals and provided information useful for this thesis.

Special thanks also go to Veronika, who has accompanied and guided me for the first three years of this work and who tried to teach me all her knowledge. You have been the best colleague imaginable and I am grateful for the wonderful years in the office and at "our" setup.

I thank Niko for the numerous private and professional conversations. Without you, I would have come to the point of desperation more often. In addition, you have shown me that perfectionism is the real deal and one can always improve it.

Victor, you are the creative one. Thanks for thinking out of the box and making our lives a little more purple.

I thank Eli and Julia for passing on their knowledge about immunohistochemistry and confocal imaging. This was not my favorite job to do, but with all your pieces of advice I survived.

I would like to thank our lab managing ladies, Conny, Fauve and Karin, for their diligence. You've shown me how to get results quickly and, yet, precise. Without you, I would not be here now.

Thank you, Peter, for taking care of the animals and for always having an open ear.

I would also like to thank Waltraud and Angelika, who kept the bureaucracy away, so that I could concentrate on my actual work.

I thank the SFB 665: "Developmental disturbances in the nervous system" for partially financing my projects.

Without the support of my family -Mama, Papa, Uli and Harry- I would have struggled a lot more, especially with taking care of my kids in times of need. Thank you so much!

Stephan, my love, you are the best. Thanks for being my rock and all you do for us.

14 Declaration of originality

I herewith declare that I have written the submitted dissertation independently and without any unauthorized external help. Furthermore, I assure that I did not use any other than the cited literature. Both the submitted electronic and printed versions are identical. This dissertation – as submitted here and in any other form – has not been submitted before as doctoral thesis to any university.

Date, signature

15 Curriculum vitæ

Der Lebenslauf ist in der Online-Version aus Gründen des Datenschutzes nicht enthalten.

*In Erinnerung an
Günter*